UNIVERSIDAD NACIONAL AUTÓNOMA DE MÉXICO
PROGRAMA DE MAESTRÍA Y DOCTORADO EN INGENIERÍA
INGENIERÍA ELÉCTRICA – SISTEMAS DE POTENCIA

ECONOMIC OPERATION OF AC/DC NETWORKS INCLUDING BATTERY ENERGY STORAGE SYSTEMS AND PHOTOVOLTAIC POWER PLANTS

TESIS
QUE PARA OPTAR POR EL GRADO DE:
DOCTOR EN INGENIERÍA

PRESENTA:
JUAN SEBASTIÁN GUZMÁN FERIA

TUTOR PRINCIPAL
DR. LUIS MIGUEL CASTRO GONZÁLEZ
FACULTAD DE INGENIERÍA, UNAM

CIUDAD UNIVERSITARIA, CIUDAD DE MÉXICO, JUNIO DE 2023

JURADO ASIGNADO:

Presidente:	Dr. Rafael Escarela Pérez
Secretario:	Dr. Frederic Trillaud
1 er. Vocal:	Dr. Luis Miguel Castro González
2 do. Vocal:	Dr. Rubén Tapia Olvera
3 er. Vocal:	Dr. José Horacio Tovar Hernández

La Tesis se realizó en la División de Posgrado de la Facultad de Ingeniería de la UNAM.

TUTOR DE TESIS:

Dr. Luis Miguel Castro González

FIRMA

Abstract

Electric power networks are critical infrastructure for the development of modern societies, with the economic operation being of utmost importance to guarantee that their associated assets are cost-effective. Nowadays, power systems face several glitches in their planning and operation processes due to the growth of renewable energy sources such as wind and photovoltaic (PV) power plants. Although the associated technical and economic challenges are being faced from several fronts. A case in point is that conventional transmission systems are being upgraded as AC/DC networks by power electronics equipment using High Voltage Direct Current links based on Voltage Source Converters (VSC-HVDC systems). This leading-edge technology allows to reduce the transmission power losses compared with conventional AC transmission systems, while simultaneously improving the overall system stability. This results in technical advantages from the point of view of flexibility and reliability of the power network operation. Similarly, Battery Energy Storage Systems (BESS) are also arising as leading energy storage technologies able to support the system operation, thus offering solutions to several grid code requirements that would take place in the future. Because of this, the study of the economic operation of AC/DC electrical networks incorporating BESS units and PV plants is fundamental for transmission system operators at system control centers.

It is in this context in which this thesis contributes new knowledge to the development of optimization models for the power system economic operation of VSC-based AC/DC networks including BESS with practical operational strategies and PV plants. Firstly, a Security-constrained Economic Dispatch (SCED) model considering BESS with load-following strategy and PV plants is presented. This is followed by the corrective Security-constrained Optimal Power Flow (SCOPF) model where hybrid AC/DC systems with power rescheduling by generation plants and VSC stations are addressed. This research work finalizes with a Unit Commitment (UC) model for AC/DC systems considering BESS with energy time-shifting strategy. The hallmark of these tree economic operation tools is the linear programming frameworks supported by piecewise linearization (PWL) of generation cost curves, PV generation, VSC and AC/DC power losses, thus enabling efficient solutions with adequate accuracy. The research area covered in this thesis bears true relevance to the real-time and offline economic operation of modern power grids.

Acknowledgments

Thank God! Without you, nothing is possible in life.

First of all, I want to dedicate this project to my beloved mother, Luz. Despite her early departure, there is not a single day I do not remember her. Thanks for your love, your guidance, and companionship. Someday I will see you again. I LOVE YOU, MOM. Likewise, this thesis is dedicated to the memory of my grandfather, Rude; I miss you too.

On the other hand, I want to dedicate this work to my family, especially my dad Héctor, my brother David, and my grandmother Rosa. Despite all the life obstacles, everything is possible when we go together.

Not less important are my friends, without which this project would have been impossible. Thanks a lot, Jorge for your help in Matlab coding doubts, Cristian for your support in English matters, and Julio and Elkin for your valuable comments and discussion about power systems.

I want to express my gratitude to Dr. Luis Miguel, without any doubt a brilliant mind of power systems; thanks to you for sharing with me your knowledge, I have certainly learned a lot from you.

Also, I want to render thanks to my classmates at UNAM, especially Jesus, who always gave me his hand in difficult moments, I really appreciate your support in México.

Finally, my gratitude to UNAM, it is an honor for me to be part of the best University in the region, a benchmark of excellence not only in México but in the world.

Contents

List of figures

List of tables

List of abbreviations and symbols

Abbreviations

AC	Alternating Current
AC/DC	Alternating Current/Direct Current
BESS	Battery Energy Storage System
DC	Direct Current
ED	Economic Dispatch
ESS	Energy Storage System
FACTS	Flexible Alternating Current Transmission System
HVDC	High Voltage Direct Current
LP	Linear Programming
MILP	Mixed Integer Linear Programming
MTDC	Multi Terminal Direct Current
MPPT	Maximum Power Point Tracking
OPF	Optimal Power Flow
PV	Photovoltaic generator
PWL	Piecewise Linearization
PWM	Pulse Width Modulation
SCED	Security Constrained Economic Dispatch
SCOPF	Security Constrained Optimal Power Flow
SCUC	Security Constrained Unit Commitment
TSO	Transmission System Operator
UC	Unit Commitment
VSC	Voltage Source Converter

Symbols

θ, V	Voltage phase angle and magnitude	E_{pv}	PV plant optimal voltage
P_{gk}, Q_{gk}	Active and reactive power generations at bus k	m_a	VSC modulation ratio
P_{dk}, Q_{dk}	Active and reactive power consumed by load at bus k	ϕ	VSC phase-shifting angle
P_k^{cal}, Q_k^{cal}	Active and reactive power injections at bus k	G_{sw}	Conductance representing commutation losses of VSC
ρ	Number of AC nodes	R, X	Resistance and reactance
$\mathbb{Z}_k$	Set of AC nodes connecting to bus k	G, B	Conductance and susceptance
$\mathbf{B}$	Susceptance matrix	I_{nom}	VSC nominal current
$\boldsymbol{\theta}$	Vector of nodal voltage phase angles	P_{pv}	Photovoltaic power
$\boldsymbol{\Gamma}$	Shift factor matrix	S_i	Solar irradiance
$\boldsymbol{Z_{ph}}$	VSC filter impedance	$m_{pv,\eta}$	η-*th* slope of the MPPT curve
$\boldsymbol{r_{ph}}$	VSC filter resistance	$P_{b(t)}$	BESS power at time t
$\boldsymbol{x_{ph}}$	VSC filter reactance	P_b^{min}	BESS minimum power limit
$\boldsymbol{Z_{tr}}$	VSC transformer impedance	P_b^{max}	BESS maximum power limit
$\boldsymbol{r_{tr}}$	VSC transformer resistance	CR	BESS charging rate
$\boldsymbol{x_{tr}}$	VSC transformer reactance	DR	BESS discharging rate
σ	Number of AC nodes	$W_{(t)}$	Stored energy at time t
$\mathbb{Z}_j$	Set of DC buses connecting to bus j	W^{min}	BESS minimum energy storage
ΔP	Nodal net power injections	W^{max}	BESS maximum energy storage
ns	Number of linear segments of generation cost curves	η_B	BESS round-trip efficiency
ls	Number of linear segments of transmission losses	IC	Investment, operation and maintenance costs of BESS
$\bar{P}_{g,i}$	i-*th* linear segment of the generated power	ξ	Cost per use of BESS
$m_{g,i}$	i-*th* slope of the generation cost curve	n_c	Number of cycles of BESS
$\bar{C}$	Linearized cost function	OC	Operation cost of BESS
B_{eq}	Equivalent shunt susceptance of VSC	$\mathbb{Z}_{la}$	Set of la transmission lines
C_{dc}	DC capacitor of the converter	RU	Generator ramp-up
E_{dc}	DC bus voltage	RD	Generator ramp-down
D	Damping of a generator	SR	Spinning reserve
R	Droop constant of a generator	s^{su}	Start-up costs
f	AC system frequency	s^{sd}	Shut-down costs
k_p	Coefficient of the frequency dependency of the load	$v_{k(t)}$	Binary variable indicating the on/off status of the k-*th* generation unit at time t
$\mathbb{Z}_\alpha$	Set of AC subsystems comprising an AC/DC system	$\tau_{k(t)}^{on}$	Binary variable indicating if the k-*th* generator turns on at time t
Δf	Frequency deviation	$\tau_{k(t)}^{off}$	Binary variable indicating if the k-*th* generator turns off at time t

Chapter 1

1. Introduction

The provision of electricity to all consumers, in a safe and reliable way, is a fundamental human activity that directly impacts on social mobility, national security, and economic growth of all nations worldwide. But nowadays, power systems face several challenges mostly driven by the increasing penetration of renewable energy sources in combination with electricity demand surge because of population growth. To solve this complicated problem, both transmission networks and energy matrix must be reinforced in time and manner. For instance, by moving into AC/DC systems using High Voltage Direct Current (HVDC) systems based on Voltage Source Converters (VSC), which can bring about technical and economic benefits such as reduction of transmission losses, improvement of the economic operation and system stability, among others [1 - 3]. In parallel with this technology, Energy Storage Systems (ESS) are being lately explored as part of the energy matrix since these enable energy storage during specific periods to be injected to the power grid later when required. This valuable characteristic offers flexibility to the system allowing both a smoother incorporation of renewables and increasing reliability to its operation [4 - 6], even though at the expense of making the system planning and operation more complex to achieve.

The primary concern of power grids is to satisfy the load consumption guaranteeing the best conditions, i.e., at minimum possible operation costs without violating network physical constraints. And these concerns must be always satisfied, that is, in a real-time operation basis. Hence, admitting that modern power systems are being recently upgraded by Battery Energy Storage Systems (BESS) incorporated to either conventional or hybrid AC/DC networks, fit-for-purpose optimization models for the economic operation must be formulated in advance to support the decision-making process by transmission system

operators (TSO) at system control centers. Indeed, this is the main goal pursued in this thesis as is customary in the arena of power system economic operation and analysis.

This chapter addresses the introduction of the doctoral project where the motivation of this research is firstly stated. The state-of-the-art is also presented focusing on the incorporation of BESS and PV plants within the Security-constrained Economic Dispatch (SCED) context, followed by the Security-constrained Optimal Power Flow (SCOPF) in hybrid AC/DC systems, and finalizing with the Unit Commitment (UC) problem for AC/DC grids and BESS facilities. Subsequently, the main hypothesis, objectives and contributions of this doctoral thesis are discussed in detail. Moreover, the papers derived from this research are listed, and a brief description of the remaining chapters is given.

1.1. Research motivation

In the last few decades, power systems characterized by AC transmission grids and conventional thermal and hydro generation units have been experiencing rapid changes due to the incorporation of new generation and transmission facilities. Such is the case of renewable energy projects, mostly solar and wind power plants, energy storage systems and transmission grid renewals using power electronic converters. These changes are expected to contribute to the system efficiency and reliability, while reducing carbon emissions. Notwithstanding the above, these new technologies imply new challenges from technical and economic standpoints, mainly related to the operation and planning, which are primarily driven by physical limitations of the network and the intermittent nature of renewable sources.

To address some of these overly complex problems, different technologies such as VSC-HVDC links and BESS have emerged in the power systems scene. In the case of the formers, VSC-HVDC systems are at the forefront of AC/DC grids due to the significant benefits these transmission links can bring about. Some remarkable examples are the reduction of transmission losses particularly when dealing with very long distances, the improvement of system stability and reliability performance, the coupling of AC power systems operating with different frequencies, and the creation of multi-terminal VSC-based AC/DC systems. As for the latter, storage systems of the BESS type also offer higher

degrees of system flexibility, particularly when used in combination with renewable resources, while employing practical operation strategies such as energy-time shift and load-following.

Because the high penetration level of renewable resources and the fast growth of energy consumption impose pressure on the power systems operation, it makes sense to look for solutions that can guarantee the correct performance, both technical- and economic-wise. And motivated by these concerns, this research focuses on studying the economic operation of AC/DC power grids considering the incorporation of BESS facilities and PV plants. This is carried out through the formulation of fit-for-purpose optimization models that enable the solution of the economic operation problems related to SCED, SCOPF and UC. The state-of-the-art of these topics are presented next in a separate manner to analyze them in detail.

1.2. State-of-the-art literature revision

As stated from the outset of this chapter, this thesis seeks to address the economic operation of VSC-based AC/DC systems considering BESS units. The first part of the present subsection aims to review relevant pieces of research about the inclusion of BESS facilities in the SCED model. The second part examines relevant works about the incorporation of VSC-HVDC technology forming AC/DC grids within SCOPF studies. While the third part of the state-of-the-art focuses on the inclusion of BESS units into VSC-based AC/DC grids placing emphasis on UC studies, i.e., day-ahead market analysis.

1.2.1. On security-constrained economic dispatch with BESS and PV plants

One of the main concerns of TSO at system control centers is the proper real-time power system operation performance. But due to the increasing penetration of wind and solar plants, its complexity has been increased even further [7, 8]. To address this challenge, BESS have been establishing recently as the preferred solutions by industrial and research parties. This equipment is an excellent option to enhance the system reliability when integrating renewable energy sources at a large-scale level [4 - 6]. In this vein, relevant research efforts have been conducted aiming to study the BESS integration in power systems, taking advantage of both their inherent technical benefits and recent decreasing investment costs [9, 10]. These aspects motivate the need for analyzing the BESS

performance in several contexts, starting with the SCED problem that considers the transmission grid and energy matrix, which is often run on a 5-min, 10-min, or 15-min look-ahead basis at energy control centers.

SCED studies are of utmost importance in the power system real-time operation because they enable the obtainment of the optimal generation dispatch while fulfilling the system security criteria [11]; for this reason, a suitable SCED modeling becomes indispensable. In this regard, valuable research has been conducted where some authors have proposed nonlinear SCED formulations aiming at obtaining accurate solution of the optimization problem. For instance, the SCED formulation with wind generators included was presented in [12], considering a system state selection through components outage probability. However, one of the biggest concerns for the control center operation is the SCED modeling and its computational execution times required to solve the optimization model. In this sense, authors in [13, 14] present a temporal decomposition strategy to resolve the nonlinear SCED to reduce both computational complexity and execution times. Based on similar concerns, a multi-area reserve-constrained ED model is presented in [15], considering a multiperiod analysis using a fireworks algorithm to solve the nonlinear problem.

As opposed to the above-mentioned techniques, linear modeling frameworks are lately imposing a trend on SCED modeling because of the reduced complexity and computational times compared with its nonlinear counterparts. For this, two approaches arise to represent the transmission network constraints in the SCED formulation. First, the classic one featured by bus bar angles representation [16 - 18] and the method using linear sensitivity factors commonly termed as shift factors [19 - 22]. Moreover, to obtain more accurate results upon the SCED solution, some authors have considered the inclusion of power transmission losses in linear SCED formulations [17, 18], but without using the Piecewise Linearization (PWL) technique employed in this doctoral thesis.

It should be also mentioned that the inclusion of the system frequency in the ED problem has been also proposed by including the primary frequency response of generators as constraint in the mathematical model, as this is a relevant problem for the power system operation [18, 21, 23]. Likewise, it is crucial to consider the inclusion of wind and PV

plants in SCED formulations, an increasing aspect due to environmental awareness. This is the case of [23] where the impact of renewable energy on the primary frequency response is analyzed. In line with this research, authors in [18] propose a multi-period SCED subject to N-1 contingency criteria and frequency stability constraints. Additionally, the incorporation of wind plants through HVDC links is analyzed in [24], where the nonlinear SCED model is solved through a robust optimization formulation. It is worth mentioning that additional research about the SCED problem has been carried out. For instance, in [25] real-time measurements from PMU units are considered in the SCED formulation, while in [26] the integration of natural gas and electrical systems with wind power is studied. And in this sense, a robust optimization model for SCED in AC/DC grids considering wind generation uncertainty was proposed in [27].

The previous literature review speaks to how important all related SCED aspects are to the power system community, particularly when considering the complexity of transmission networks and energy matrix. Regarding the incorporation of BESS (or ESS) in an optimal operation context, just a few research works have been conducted. For instance, on one hand, an emission-aware ED considering ESS is presented in [28], but one without paying specific attention to the ESS strategy per se. On the other hand, authors in [29] present a chance-constrained ED with renewables sources and ESS, whereas a distributed algorithm for dynamic ED with ESS was developed in [30]. Certainly, microgrids with ESS have also received research attention in line with ED studies using a semidefinite programming framework [31].

However, after carrying out a detailed revision of the open literature, the inclusion of PV plants and BESS operating with a load-following strategy within the SCED problem is not present in the open literature so far. In Chapter 3 of this doctoral thesis, a novel SCED model is addressed which features a linear programming framework improved by shift factors and piecewise linearization of generation cost curves, PV plant generation, and transmission power losses.

1.2.2. On security constrained OPF for AC/DC systems

One of the leading technologies in transmission systems renewal is the VSC-HVDC link. This power electronic equipment is the backbone of actual hybrid AC/DC power systems

which continue to capture the attention of power systems planners and TSO due to well identified technical and economic benefits [1]. But adequate control and operating strategies need to be defined a priori by carrying out sophisticated analysis through adequate optimization tools to guarantee the reliability and proper performance of the system [2]. Two remarkable examples are the generation/transmission expansion planning studies [32] and the SCOPF [33, 34]. As for the latter, these studies permit TSO to obtain optimal generation dispatches while observing transmission operating limits in face of critical contingencies.

In this regard, creditable research efforts have been conducted to address the SCOPF problem in conventional AC systems. Examples of these are the optimization of the system primary frequency response through a preventive SCOPF approach [35] and a distributed frequency control via the alternating direction method of multipliers [36]. Not far from these ideas, the inclusion of voltage and frequency responses was recently studied in [37]. On the other hand, a corrective SCOPF model was exploited in [38], which incorporates stochastic uncertainties in transmission lines outages. Besides, different researchers have focused on including risk-based constraints with probabilistic guarantees [39] and on an agent-based distributed SCOPF model useful for the massification of smart grids [40]. Certainly, the inclusion of ESS units has been also a matter of research in this context, where a reliability improvement is pursued by using a corrective SCOPF model [41]. Similarly, [42] presents a corrective SCOPF considering the optimization of power system discrete controllers such as tap changers and shunt capacitor banks, all this under selected contingencies.

It must be mentioned that all these SCOPF methods rely on a nonlinear power system modelling which often implies large computing times. Essentially, one of the main characteristics defining the SCOPF model is whether the optimization problem is formulated through linear [43] or nonlinear [42] equations. This feature directly impacts the model's applicability in terms of accuracy and computing requirements since nonlinear SCOPF formulations are not always suitable for fair-sized power grids because of the high execution times involved. Not surprisingly, linear formulations have continued to gain acceptance at system control centers because many simulations must be executed at the

real-time operation stage, requiring rapid execution times with acceptable precision [43 - 46].

The previous literature review has exposed the broad applicability of SCOPF studies to AC transmission systems. However, the reality is different for multi-terminal VSC-based AC/DC systems as just a few research works have been reported in the open literature. One of the first attempts to include VSC-HVDC system models within the SCOPF problem was carried out in [47], developing a probabilistic formulation considering wind generation uncertainty. Soon after, authors in [48] developed a SCOPF model based on a differential evolution algorithm considering the N-1 security criteria, even though both AC and DC grids were analyzed separately. Similarly, the same problem related to VSC-HVDC grids was addressed in [49] comprising corrective actions by the VSC stations. In this sense, [50] presented a hierarchical SCOPF formulation for AC/DC grids with wind generators, while in [51] a multi-objective SCOPF for AC/DC systems, employing a Lasso-based contingency filter is provided. All the above formulations have in common that the SCOPF model is formulated as a nonlinear optimization problem, which sharply contrast with the formulation presented in this doctoral thesis as it is based on linear programing.

The importance of SCOPF studies for utility-scale VSC-based AC/DC systems is unquestionable, as corroborated by the efforts placed by the power system research community, understanding that these calculations are even more demanding than those related to conventional AC transmission systems. For this, reduced execution times are often pursued using linear SCOPF models without ignoring the calculation errors that can appear in solutions of large AC/DC system models. So, the consideration of power losses becomes essential for more accurate SCOPF solutions. One effective way to deal with this situation is by applying the PWL technique to generators cost curves and transmission power losses due to its proven effectiveness in power system applications [52]. In this way, while most of the research efforts have been placed for AC systems only, Chapter 4 of this doctoral thesis bridges the existing gap in the existing open literature related to corrective SCOPF solutions for VSC-based AC/DC networks, particularly in considering the power rescheduling by power plants and VSC stations.

1.2.3. On unit commitment for AC/DC systems with BESS

Unit Commitment (UC) studies are also a fundamental part of the power systems analysis at the operation stage because their outcomes enable an optimum hourly schedule of generator units. Often, UC analysis implies the solution of a 24-hour operation day assuming a forecasted load trend and a predefined availability of generation units in what it is known as day-ahead market. Unsurprisingly, the UC attempts to meet the system load at a minimum cost which is conditioned by both generator unit operations (on and off) and network constraints [53, 54]. In this respect, a proper modeling of VSC-based AC/DC transmission systems and BESS is key to facilitate an efficient and reliable system operation over time. It is worth mentioning that BESS can make the system more flexible due to low charge and discharge costs, thus promoting more economical generation scheduling [55].

The research and application of UC to VSC-based AC/DC systems is still incipient and has a great deal of potential. Some research efforts have been carried out for purely AC systems [56, 57], AC grids with point-to-point HVDC links [58 - 60], or multi-terminal VSC-based transmission systems [61]. As in the case of SCED and SCOPF formulations, the UC modeling technique defines its applicability to a lesser or greater extent due to the execution times involved and the model complexity. In this sense, most UC formulations rely on Mixed-Integer Linear Programming (MILP) optimization when applied to AC networks [62 - 64]. Here, classical formulations have been widely used when the transmission system is represented through nodal angles, i.e., the generation-load balance is formulated as nodal power balances [64, 65]. But to reduce the computational burden even further, improved UC formulations based on linear sensitivity factors have been developed [56, 57]; one that leaves out the inclusion of power losses. Frequently, this is a common practice in control centers that allows to reduce the computational times at the system operation stage.

The research on UC for AC systems with HVDC links is a growing area but still very much limited [66], particularly when dealing with multi-terminal AC/DC grids [61]. Lossless UC formulations based on shift factors have been proposed [61, 67]. Yet, nonlinear methods predominate due to the improvement in computational capacities in recent times. There are in the open literature some remarkable examples of nonlinear UC models applied to AC

grids with HVDC links. For instance, those using semidefinite programming [58], mixed-integer quadratic programming [68, 69], and robust optimization [59, 60]. It should be also said that these models mainly concentrate on wind power integration [69], contingency analysis [68], and demand/generation uncertainties [58 - 60]. Another interesting topic related to UC studies is the so-called Security-constrained Unit Commitment (SCUC) problem, which addresses the UC considering contingencies in the model. The SCUC model has been also addressed using MILP formulations for AC grids with ESS [70 - 72] or with HVDC links [73, 74]. However, the goals of SCUC are diverse; two cases in point are the inclusion of the probability of contingencies leading to suitable system operational solutions [70] and the short-term voltage stability involving the system loadability [73]. Also, SCUC studies and system dynamic assessments can be used in combination to determine the impact of wind power variability on system frequency deviations [75]. Indeed, the above-mentioned UC formulations rely on nonlinear models.

Returning to the inclusion of BESS (or ESS) in electrical systems operation, the incorporation of BESS in UC algorithms [56, 62, 65] has been largely devoted to increasing the system operational benefits in combination with FACTS devices [63] to improve the scheduling of conventional generation units and wind power [62, 70, 76], and to provide post-contingency support [64, 65]. Aside from the above publications, the application of BESS applied to UC studies in hybrid power networks has yet to be investigated satisfactorily. In this tenor, Chapter 5 of this doctoral thesis presents an improved linear programming-based UC model with the incorporation of BESS with energy time-shifting strategy into VSC-based AC/DC grids, one that departs from existing approaches already discussed from the open technical literature.

1.3. Hypothesis

Economic operation studies are quite important for transmission system operators with which they can guarantee its proper performance. Due to the integration of VSC-HVDC links, BESS and PV plants, the related optimization models need to be updated to address these new technologies satisfactorily. Hence, the following hypothesis can be stated for this doctoral thesis:

i. Economic operation studies must be efficiently carried out, in time and precision, particularly for the real-time operation. In this sense, the development of linear optimization models can fulfill this requirement. Also, acceptable precision on the results can be obtained if nonlinear generation cost curves and transmission power losses are adequately considered by using the piecewise linearization technique.

ii. The inclusion of BESS with a load-following strategy reduces the output level of conventional generators during the SCED, thus helping relax their ramp up/down limitations while decreasing the system operating costs.

iii. In the context of SCOPF studies for AC/DC grids, the consideration of the discrete voltage/power droop controls of power plants and VSC stations permits to improve the network response for contingency conditions.

iv. The inclusion of BESS featured by an energy time-shifting strategy improves the UC performance by displacing the operation of the most expensive generation units of the AC/DC network, particularly during high demand periods.

1.4. Objectives and contributions

The main objective of this doctoral thesis is to contribute to the development of power system optimization models useful for the economic operation of VSC-based AC/DC networks including PV plants and BESS with different operational strategies. To accomplish this general objective, the following specific objectives are proposed:

- Develop a mathematical linear model for accurately representing hybrid VSC-based AC/DC transmission grids based on linear sensitivity factors, one that is general in nature and able to accommodate several power resources.
- Implement the optimization frameworks that enable the study of SCED, SCOPF and UC, all this conforming to standard practices at system control centers. These optimization models ought to be able to support the assessment of hybrid AC/DC networks, including the most fundamental security constraints.
- Improve these optimization models by considering quadratic generation cost curves and transmission power losses through the PWL technique.

- Develop two linear BESS models to be included into AC/DC system models with operating strategies related to energy-time shift and load-following.
- Develop a PV plant model whose power injection is modeled by the PWL.

In connection with the previous points, the main scientific contributions of this thesis can be summarized as follows:

- In this work, a novel modeling framework for the assessment of the economic operation of AC/DC power systems was developed, which is mainly characterized by the transmission network representation with shift factors and by the inclusion of generation cost curves and power losses using PWL, for efficient and accurate solutions. In this tenor, the following three models have been developed during this research:
    - A linear SCED model for AC grids including BESS and PV plants.
    - A linear SCOPF model for multi-terminal VSC-based AC/DC power grids considering power rescheduling of generation units and VSC stations.
    - A linear UC model for multi-terminal VSC-based AC/DC power systems including BESS facilities.
- Additional contributions of this research work are the development of linear BESS models with load-following and energy time-shifting strategies. Similarly, a novel linear PV plant model considering the MPPT strategy was presented. Both power source models seamlessly combine with the developed economic operation optimization models.

1.5. List of publications

[1] **Guzmán-Feria, J. S.**, Castro, L. M., Tovar-Hernández, J. H., González-Cabrera, N., & Gutiérrez-Alcaraz, G. (2022). Unit commitment for multi-terminal VSC-connected AC systems including BESS facilities with energy time-shifting strategy. *International Journal of Electrical Power & Energy Systems*, *134*, 107367.

[2] **Guzmán-Feria, J. S.**, Castro, L. M., González-Cabrera, N., & Tovar-Hernández, J. H. (2021). Security constrained OPF for AC/DC systems with power rescheduling by power plants and VSC stations. *Sustainable Energy, Grids and Networks*, *27*, 100517.

1.6. Thesis outline

The remainder of this thesis is organized as follows:

Chapter 2 describes the linear models of the transmission system and components adopted in this work. First, the linear modeling of conventional AC systems is presented, followed by the linear modeling of VSC devices and DC networks. Next, the two models of BESS units are presented, placing emphasis on load-following and energy time-shifting strategies. The PWL technique is also reviewed here aiming to model the quadratic generation cost curves and transmission power losses. Finally, the linear PV generation model considering the MPPT strategy is provided.

Chapter 3 presents the security-constrained economic dispatch model for conventional AC networks. BESS devices pursuing a load-following strategy supporting system operation are discussed. Also, PV systems are contemplated where PV injection is modeled in terms of solar irradiance through the PWL technique, i.e., considering the MPPT strategy of DC/DC converters.

Chapter 4 describes the security-constrained optimal power flow model for VSC-based AC/DC networks considering a corrective approach. The proposed formulation considers power rescheduling by generation units and VSC stations through voltage/power droop controls in view of contingencies.

Chapter 5 presents the unit commitment model for VSC-based AC/DC networks. The developed approach considers BESS devices describing an energy time-shifting strategy, where charge and discharge operation is defined in the 24-hours operational planning horizon, aiming to promote a high competition level of energy trading in the power system.

Chapter 6 shows the applicability of the newly developed models to carry out economic operation studies in AC and DC power systems with BESS devices and PV plants. The multi-period SCED model provided in Chapter 3 is initially assessed using two test AC systems. While the SCOPF model introduced in Chapter 4 and UC model developed in Chapter 5 are each studied using two compelling AC/DC test power system models.

Chapter 7 presents the concluding remarks of the thesis and points out possible future research work.

Chapter 2

2. AC/DC Transmission Systems and Power Sources

Power systems are paramount infrastructures whose operation directly influences the economic development of societies. These systems comprise several components acting in a coordinated fashion looking to always satisfy the energy demand. To this end, the development of suitable mathematical models is mandatory as these are used by TSO to operate the system in a preventive manner to guarantee its reliability and stability. Just like in other power system fields, power flow formulations are indispensable to feed the optimization models that allow establishing the best practices to achieve an economic power system operation. In this vein, linear power grid models are often necessary due to the high computational burden and related execution times that nonlinear models impose; rapid computational times are required at energy control centers, particularly for its real-time operation.

This chapter presents the linear models of power systems and components adopted in this thesis. It starts with a brief description on the nonlinear modeling of conventional AC transmission systems in steady state, accompanied by the corresponding assumptions that lead to its linear modeling. Following a similar reasoning, the linear modeling of VSC stations and DC grids is described to complete the AC/DC network modeling, all this considering state-of-the-art VSC control strategies. In combination with the linear models of VSC-based AC/DC transmission systems, this chapter also presents a brief review of the PWL technique that allows to linearly model the quadratic generation cost functions and transmission losses. In a similar way, a linearized PV plant model based on the representation of the MPPT curve through PWL is given, followed by the BESS models with load-following and energy time-shifting strategies. The models presented in this chapter serves as input for the power system optimization models formulated in the following chapters.

2.1. Fundamentals on the steady-state modeling of AC transmission systems

The steady-state modeling of AC transmission systems is intrinsically linked to power flow studies. The conventional modeling approach is nonlinear, and its initial objective is to estimate both nodal voltage magnitudes and nodal phase angles based on a given load/generation pattern with which it is possible to calculate the transmission system active and reactive power flows. This analysis is the foundation of other equally important power system analysis such as economic dispatch, optimal power flows, dynamic studies, etc. A power flow formulation departs from the concept of power balances in all system buses. That is, for any system node the sum of generated power minus demand and injected power to the network through transmission elements must be zero for both active and reactive powers, as schematically shown in Figure 2.1.

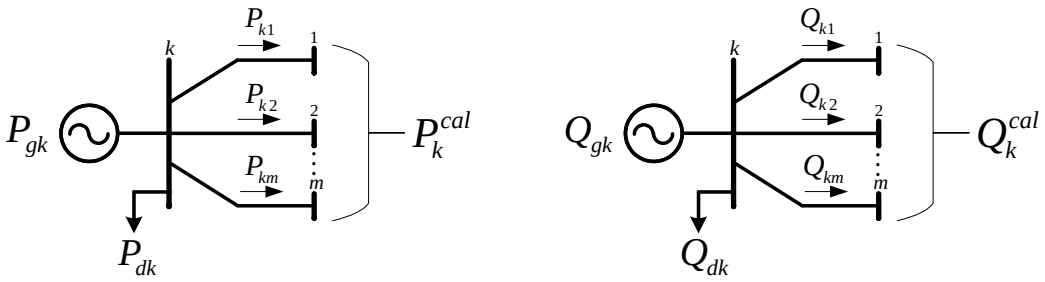

Figure 2.1 Nodal power balances for bus *k* of the system

The resulting expressions from the power balances are known as active and reactive power mismatch equations, which are shown in (2.1)-(2.2), respectively [1, 77, 78].

$$\Delta P_k = P_{gk} - P_{dk} - P_k^{cal} \tag{2.1}$$

$$\Delta Q_k = Q_{gk} - Q_{dk} - Q_k^{cal} \tag{2.2}$$

where P_{gk}, Q_{gk} represent the generated active and reactive power at bus *k*, respectively. The active and reactive power demands are P_{dk}, Q_{dk}, respectively, whereas P_k^{cal}, Q_k^{cal} stand for the calculated active and reactive powers, which are explicitly given by (2.3)-(2.4) assuming that bus voltage phasors are expressed in polar notation, i.e., $\mathbf{V}_k = V_k \angle \theta_k$ and $\mathbf{V}_m = V_m \angle \theta_m$.

$$P_k^{cal} = V_k^2 G_{kk} + V_k \sum_{m=1, m\neq k}^{\rho} V_m \left[G_{km} \cos\left(\theta_k - \theta_m\right) + B_{km} \sin\left(\theta_k - \theta_m\right) \right] \quad \forall m \in \mathbb{Z}_k \tag{2.3}$$

$$Q_k^{cal} = -V_k^2 B_{kk} + V_k \sum_{m=1, m\neq k}^{\rho} V_m \left[G_{km} \sin\left(\theta_k - \theta_m\right) - B_{km} \cos\left(\theta_k - \theta_m\right) \right] \quad \forall m \in \mathbb{Z}_k \tag{2.4}$$

where the system nodal conductances G_{kk}, G_{km} and susceptances B_{kk}, B_{km} are taken from the nodal admittance matrix $\mathbf{Y}_{\text{bus}}$ of the power system. ρ is the total number of buses and $\mathbb{Z}_k$ is the set of buses connecting with bus k.

The load flow problem solution implies solving the nonlinear equations (2.1) - (2.2) for each node of the system. For this, the Newton-Raphson algorithm is widely used in power systems analysis to solve this problem. For this purpose, it is necessary to define three types of buses before applying the method:

i. The slack bus (or swing bus) which provides the system reference angle; the bus with the largest generation unit is often selected.
ii. PV buses which are related to generation units exerting voltage magnitude control.
iii. PQ buses related to nodes having only active and reactive power demands.

In this sense, Table 2.1 presents the known and unknown variables related to bus types for the load flow solution procedure [77 - 80].

Table 2.1 Known and unknown variables for different bus types

Type	Known	Unknown
Slack	V_k, θ_k, P_{dk}, Q_{dk}	P_{gk}, Q_{gk}
PV	P_{gk}, V_k, P_{dk}, Q_{dk}	Q_{gk}, θ_k
PQ	P_{gk}, Q_{gk}, P_{dk}, Q_{dk}	V_k, θ_k

Once the bus types are defined, the Newton-Raphson algorithm can be straightforwardly applied to solve (2.1)-(2.2) by iteration until the mismatch equations of all nodes ΔP_k, ΔQ_k are both smaller than a specified error, for instance, ε = 10e-6. Once nodal phase angles θ and voltage magnitudes V are obtained, the network active and reactive power flows, P_{km} and Q_{km}, can be straightforwardly calculated as in (2.5).

$$\mathbf{S}_{km} = P_{km} + jQ_{km} = \mathbf{V}_k \cdot \mathbf{I}_{km}^{*} = \mathbf{V}_k \left(\frac{\mathbf{V}_k - \mathbf{V}_m}{\mathbf{z}_{km}} + \frac{\mathbf{y}_{sh}}{2}\mathbf{V}_k \right)^{*} \tag{2.5}$$

where $\mathbf{z}_{km}=r_{km}+jx_{km}$ is the impedance and $\boldsymbol{y}_{\text{sh}}$ is the shunt admittance of the transmission line.

2.2. Linear modeling of AC transmission systems using shift factors

When dealing with high-voltage AC transmission systems, it is feasible to obtain a linear model suitable for active power flow calculations aiming to reduce both the mathematical model complexity and computational burden [80]. This is possible assuming that:

i. The series reactance is much greater than the resistance, i.e., $x_{km}>>r_{km}$, which is characteristic of highly inductive networks.

ii. The nodal voltage magnitudes are close to nominal values, i.e., $V_k \approx V_m \approx 1$ p.u.

iii. The voltage angle differences between adjacent buses are small, i.e., $cos(\theta_k - \theta_m) \approx 1$ and $sin(\theta_k - \theta_m) \approx \theta_k - \theta_m$.

With these assumptions, the nonlinear equation for the calculated active power flows P_k^{calc}, given in (2.3), can be simplified as shown in (2.6) [79 - 81].

$$P_k^{cal} = \sum_{m=1, m\neq k}^{\rho} B_{km}\left(\theta_k - \theta_m\right) \quad \forall m \in \mathbb{Z}_k \tag{2.6}$$

Using (2.6) and formulating anew the nodal power balances, equation (2.7) is obtained.

$$\begin{bmatrix} \Delta P_1 \\ \vdots \\ \Delta P_k \\ \vdots \\ \Delta P_\rho \end{bmatrix} = \begin{bmatrix} B_{11} & \cdots & B_{1k} & \cdots & B_{1\rho} \\ \vdots & \ddots & \vdots & \ddots & \vdots \\ B_{k1} & \cdots & B_{kk} & \cdots & B_{k\rho} \\ \vdots & \ddots & \vdots & \ddots & \vdots \\ B_{\rho 1} & \cdots & B_{\rho k} & \cdots & B_{\rho\rho} \end{bmatrix} \begin{bmatrix} \theta_1 \\ \vdots \\ \theta_k \\ \vdots \\ \theta_\rho \end{bmatrix} \quad \Rightarrow \quad \Delta\mathbf{P} = \mathbf{B}\,\boldsymbol{\theta} \tag{2.7}$$

where $B_{kk} = \sum_{m\in k} x_{km}^{-1}$, and $B_{km} = -x_{km}^{-1}$. This linear system model can be expressed in compact form as $\mathbf{\Delta P = B\,\theta}$, where $\mathbf{\Delta P}$ is the vector of specified net power $\Delta\mathbf{P} = \mathbf{P}_g - \mathbf{P}_d$, with $\mathbf{P}_g$, $\mathbf{P}_d$ being vectors of generation and demand, respectively. $\mathbf{B}$ is the susceptance matrix of the

network considering the series branches only, and **θ** is the vector of nodal voltage phase angles. If node 1 is selected as the slack bus of the power network $\theta_1 = 0$, the system state variables are readily calculated, as shown in (2.8).

$$\begin{bmatrix} \theta_2 \\ \vdots \\ \theta_k \\ \vdots \\ \theta_\rho \end{bmatrix} = \begin{bmatrix} B_{22} & \cdots & B_{2k} & \cdots & B_{2\rho} \\ \vdots & \ddots & \vdots & \ddots & \vdots \\ B_{k2} & \cdots & B_{kk} & \cdots & B_{k\rho} \\ \vdots & \ddots & \vdots & \ddots & \vdots \\ B_{\rho 2} & \cdots & B_{\rho k} & \cdots & B_{\rho\rho} \end{bmatrix}^{-1} \begin{bmatrix} \Delta P_2 \\ \vdots \\ \Delta P_k \\ \vdots \\ \Delta P_\rho \end{bmatrix} = \begin{bmatrix} F_{22} & \cdots & F_{2k} & \cdots & F_{2\rho} \\ \vdots & \ddots & \vdots & \ddots & \vdots \\ F_{k2} & \cdots & F_{kk} & \cdots & F_{k\rho} \\ \vdots & \ddots & \vdots & \ddots & \vdots \\ F_{\rho 2} & \cdots & F_{\rho k} & \cdots & F_{\rho\rho} \end{bmatrix} \begin{bmatrix} \Delta P_2 \\ \vdots \\ \Delta P_k \\ \vdots \\ \Delta P_\rho \end{bmatrix} \tag{2.8}$$

Once the linear system model (2.8) is resolved, the calculation of active power flows of the transmission network branches can be carried out effortlessly as follows,

$$P_{km} = \frac{\theta_k - \theta_m}{x_{km}} \tag{2.9}$$

- *Transmission system modeling by shift factors*

Alternatively, the transmission line power flows can be calculated using linear sensitivity factors. Perhaps, one of the most employed to this end are the injection shift factors Γ. These permit to estimate the power flow change in a transmission element due to nodal power injection variations (2.10), according to [78],

$$\Gamma_{k-m,i} = \frac{\Delta P_{k-m}}{\Delta P_i} \tag{2.10}$$

where $\Delta P_{k\text{-}m}$ represents the active power flow variation in branch *k*-*m*, ΔP_i represents the power injection variation at bus *i*. Combining (2.9)-(2.10), the shift factors (2.11) are calculated as follows:

$$\Gamma_{k-m,i} = \frac{\Delta P_{k-m}}{\Delta P_i} = \frac{dP_{k-m}}{dP_i} = \frac{d}{dP_i}\left[\frac{\theta_k - \theta_m}{x_{km}}\right] = \frac{1}{x_{km}}\left[\frac{d\theta_k}{dP_i} - \frac{d\theta_m}{dP_i}\right] \tag{2.11}$$

If (2.8) is expressed as $\boldsymbol{\theta} = \mathbf{F}\,\boldsymbol{\Delta P}$ in compact form, where $\mathbf{F} = \mathbf{B}^{-1}$, it is noted that matrix **F** represents the change in phase angles with respect to power injections, i.e., $F = d\theta/dP$. Therefore, shift factors (2.11) transform into (2.12), that is,

$$\Gamma_{k-m,i} = x_{km}^{-1}\left(F_{ki} - F_{mi}\right) \tag{2.12}$$

If P_{k-m}^{0} is the power flow of the *km*-th transmission branch before the power injection variation at bus *i*, the power flow $P_{k\text{-}m}$ is obtained using shift factors in the following way,

$$P_{k-m} = P_{k-m}^{0} + \left(\Gamma_{k-m,i}\right)\Delta P_i \tag{2.13}$$

For later calculations, all shift factors (2.12) are accommodated in matrix $\mathbf{\Gamma}$ of order l x ρ, where l is the number of series branches, i.e., transmission lines and transformers and ρ is the number of nodes. Hence, the power system active power flows can be efficiently calculated, all at once, using (2.14).

$$\mathbf{P}_{km} = \mathbf{\Gamma}\ \Delta\mathbf{P} \tag{2.14}$$

recalling that $\Delta\mathbf{P}$ is the vector of specified nodal powers of order ρ x 1, while $\mathbf{P}_{km}$ of order l x 1 contains the transmission power flows. Note that the shift factors method avoids the use of busbar angles $\boldsymbol{\theta}$ in the power flow calculation process. This reduces both decision variables and computational burden of the associated optimization problems.

2.3. Steady-state modeling of VSC stations

A Voltage Source Converter (VSC) is a power electronics device able to transform AC power into DC power, and vice versa. This equipment is fundamental for building up High Voltage Direct Current links (VSC-HVDC links) either for point-to-point connections or multi-terminal arrangements. Some of the advantages of VSC-HVDC links over the classic AC lines are the transmission loss reduction, facilitation of electrical energy transportation over longer distances with higher power efficiency, and the interconnection of AC systems operating with different electrical frequencies, just to mention the most relevant ones. All these characteristics permit to anticipate future requirements of power grids [1]. With this idea in mind, the comprehension of the VSC-based transmission technology is a must for TSO.

2.3.1. Basic operating principles of VSC units

Several topologies can be employed at the VSC design stage, for instance, single-phase full-bridge converter, two-level three-phase converter, among others [82]. The common objective of these topologies consists of minimizing the operation frequency of the semiconductors to enlarge their life cycle and reduce power losses, while simultaneously obtain a high-quality sinusoidal wave with low filtering requirements. Figure 2.2 shows the schematic representation of a two-level, three-phase VSC unit composed of IGBTs devices [1, 82]. This configuration has six IGBTs devices (S_1 – S_6), two per branch, usually known as six-pulse converter. When the number of IGBTs per branch increases, it allows an increase in the converter voltage level. Moreover, it is worth noting that IGBTs have a diode in antiparallel connection to avoid damage due to inverse voltages. The VSC carries two capacitors on the DC side to stabilize its voltage while reducing its ripple.

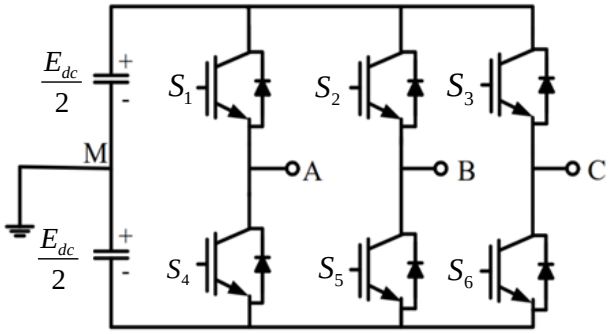

Figure 2.2 Two-level, three-phase VSC

The VSC performance is based on the on/off frequency of the semiconductors through its corresponding control module, which allows to obtain a voltage wave close to a sinusoidal shape. The VSC on/off strategy can be implemented in two different forms:

- Fundamental frequency: This technique consists of on/off processes where only one turn-on and turn-off is carried out at each cycle. This operation mode is disadvantageous because of the high harmonics content, requiring the installation of filters which increases the overall equipment cost.
- Pulse Width Modulation (PWM): this method increases the frequency of the turn-on and turn-off operation, much higher than the fundamental frequency. So, the output wave is clipped, and the width of the pulses is moduled. This permits to reduce the low order harmonic content and independently control the active and reactive powers.

It is worth mentioning that the PWM technique allows reproducing a sinusoidal voltage signal at a desired frequency, 50 or 60 Hz, with simplicity and effectiveness, this being the reason why it is the most widely used in VSC units for power system applications [1, 82].

2.3.2. Nonlinear modeling of VSC units for steady-state studies

Figure 2.3 a) shows the schematic representation of a VSC station including the capacitor bank C_{dc} employed to stabilize the DC voltage, where the injection/absorption of reactive power is carried out by the converter PWM control. On the other hand, Figure 2.3 b) depicts the equivalent circuit model of the VSC station for steady-state analysis. The reactive power exchange with the network is carried out through the electronic processing of the voltage and current waves in the VSC, which is suitably represented by the variable susceptance B_{eq}. It should be said that this VSC model is only useful for positive-sequence power system analysis [1], i.e., operating at the fundamental frequency, just as required for all the economic operation optimization models employed in this doctoral thesis.

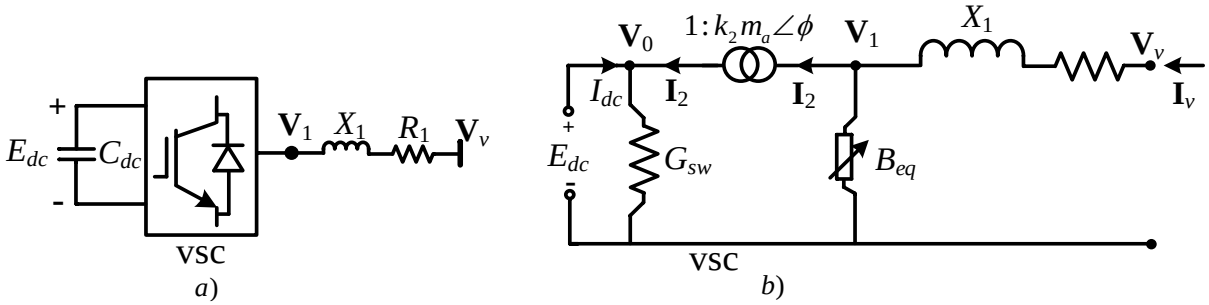

Figure 2.3 a) Schematic representation of the VSC **b)** Equivalent circuit of a VSC in steady state

The ideal phase shifting transformer with a complex transformation ratio, $1:k_2m_a\angle\phi$, of Figure 2.3 b) is the core component of the VSC circuit model due to this function as bridge between the AC and DC sides of the converter. Equation (2.15) describes the AC voltage, $\mathbf{V}_1$, as a function of the DC voltage E_{dc} [1].

$$\mathbf{V}_1 = k_2 m_a E_{dc} e^{j\phi} \qquad (2.15)$$

$$G_{sw} = G_0 \left(\frac{I_v}{I_{nom}} \right)^2 \qquad (2.16)$$

where $\mathbf{V}_1$ is the complex voltage relative to the system reference phase, the transformer tap magnitude, m_a, corresponds to the VSC modulation index ranging from 0 to 1. The constant $k_2 = \sqrt{3}/8$ for the case of two-level, three-phase VSC stations. The phase angle of $\mathbf{V}_1$, ϕ, is the phase-shifting angle of the VSC and the voltage at the DC port is E_{dc}. On the other

hand, the reactance X_1 represents the magnetic interface of the converter with the grid, whereas the resistance R_1 represents the ohmic losses. The variable susceptance B_{eq} provides the reactive power requirements and is shunt-connected to the AC side of the circuit. On the DC side, the constant conductance G_{sw} is connected to account for the switching losses of the converter, which is calculated as in (2.16), where G_0 is a constant conductance representing the switching losses under nominal operation conditions, I_{nom} is the nominal current and I_v is the VSC current output.

Returning to the VSC circuit model, the voltage and current relations of the phase-shifting transformer are given by (2.17)-(2.18).

$$\frac{\mathbf{V}_1}{E_{dc}} = \frac{k_2 m_a e^{j\phi}}{1} \qquad (2.17) \qquad \frac{\mathbf{I}_2}{\mathbf{I}_1} = \frac{k_2 m_a e^{-j\phi}}{1} \qquad (2.18)$$

Combining the previous equations, the AC-side current, $\mathbf{I}_v$, an DC-side current, $\mathbf{I}_{0v}$, can be obtained as expressed in (2.19)-(2.20), respectively.

$$\mathbf{I}_v = \mathbf{Y}_1\left(\mathbf{V}_v - \mathbf{V}_1\right) = \mathbf{Y}_1 V_v - k_2 m_a \angle\phi \cdot \mathbf{Y}_1 E_{dc} \qquad (2.19)$$

$$\mathbf{I}_{0v} = -\mathbf{I}_2 + G_{sw} E_{dc} = -k_2 m_a \angle -\phi \cdot \mathbf{Y}_1 \mathbf{V}_v - k_2^2 m_a^2 \mathbf{Y}_1 E_{dc} + jB_{eq} k_2^2 m_a^2 E_{dc} + G_{sw} E_{dc} \qquad (2.20)$$

where $\mathbf{Y}_1 = (R_1 + \mathrm{j}X_1)^{-1} = G + \mathrm{j}B$. Arranging (2.19)-(2.20) in matrix form, we have:

$$\begin{bmatrix} \mathbf{I}_v \\ \mathbf{I}_{0v} \end{bmatrix} = \begin{bmatrix} \mathbf{Y}_1 & -k_2 m_a \angle\phi \cdot \mathbf{Y}_1 \\ -k_2 m_a \angle\phi \cdot \mathbf{Y}_1 & k_2^2 m_a^2 \left(\mathbf{Y}_1 + jB_{eq}\right) + G_{sw} \end{bmatrix} = \begin{bmatrix} \mathbf{V}_v \\ E_{dc} \end{bmatrix} \qquad (2.21)$$

With the nodal current injection equation (2.21) and recalling that $\mathbf{S} = \mathbf{V}\,\mathbf{I}^*$, it is a straightforward matter to obtain the power flow injections shown in (2.22).

$$\begin{bmatrix} \mathbf{S}_v \\ \mathbf{S}_{0v} \end{bmatrix} = \begin{bmatrix} \mathbf{V}_v & 0 \\ 0 & E_{dc} \end{bmatrix} \left[\begin{pmatrix} \mathbf{Y}_1 & -k_2 m_a \angle\phi \cdot \mathbf{Y}_1 \\ -k_2 m_a \angle\phi \cdot \mathbf{Y}_1 & k_2^2 m_a^2 \left(\mathbf{Y}_1 + jB_{eq}\right) + G_{sw} \end{pmatrix} \begin{pmatrix} \mathbf{V}_v \\ E_{dc} \end{pmatrix} \right]^* \qquad (2.22)$$

Defining $\mathbf{V}_v = V_v \angle\theta_v$ and carrying out some complex algebra for (2.22), the nodal active and reactive powers at the AC and DC nodes of the VSC can be obtained. These powers are explicitly shown in (2.23)-(2.24), respectively [1, 83].

$$\begin{aligned}(a)\,P_v &= V_v^2 G - k_2 m_a V_v E_{dc}\left[G\cos(\theta_v-\phi)+B\sin(\theta_v-\phi)\right]\\ (b)\,Q_v &= -V_v^2 B - k_2 m_a V_v E_{dc}\left[G\sin(\theta_v-\phi)-B\cos(\theta_v-\phi)\right]\end{aligned} \tag{2.23}$$

$$\begin{aligned}(a)\,P_{0v} &= k_2^2 m_a^2 E_{dc}^2 G - k_2 m_a V_v E_{dc}\left[G\cos(\theta_v-\phi)-B\sin(\theta_v-\phi)\right]+E_{dc}^2 G_0\left(\frac{I_v}{I_{nom}}\right)^2\\ (b)\,Q_{0v} &= -k_2^2 m_a^2 E_{dc}^2 B - k_2 m_a V_v E_{dc}\left[-G\sin(\theta_v-\phi)-B\cos(\theta_v-\phi)\right]-k_2^2 m_a^2 E_{dc}^2 B_{eq}\end{aligned} \tag{2.24}$$

2.4. Linear modeling of VSC stations and control strategies

The power flow expressions obtained previously correspond only to the VSC unit. But these can be easily extended when considering the auxiliary equipment making up the VSC station, as illustrated in Figure 2.4. In this case, it is considered the series connection of the AC filter ($\mathbf{z}_{ph}=r_{ph}+jx_{ph}$; $\mathbf{y}_f=\mathrm{j}b_f$) and the step-up transformer ($\mathbf{z}_{tr}=r_{tr}+jx_{tr}$) to interface the VSC unit with the AC system at bus *k*. On the DC side, the VSC is assumed to be connected at bus *j* of the DC grid. Note that to simplify matters, the subscript 'dc' has been dropped when representing DC voltages *E*.

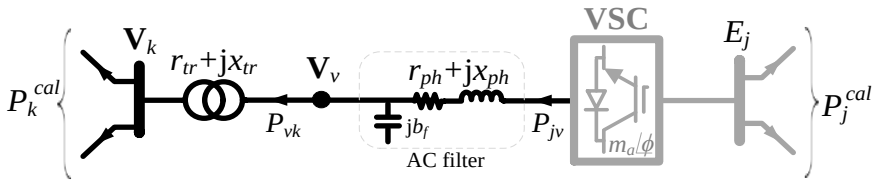

Figure 2.4 VSC station with ancillary equipment

Making use of (2.3) and (2.23a), the active power flow equations P_{vk} and P_{jv} can be stated as (2.25a) and (2.25b). It should be recalled that these results from applying Kirchhoff's laws to both AC and DC terminals of the converter, buses *k* and *j* in this case [80 – 83].

$$\begin{aligned}(a)\,P_{vk} &= V_v^2 g_{tr} - V_v V_k\left[g_{tr}\cos(\theta_v-\theta_k)+b_{tr}\sin(\theta_v-\theta_k)\right]\\ (b)\,P_{jv} &= k_2^2 m_a^2 E_j^2\, g_{ph} - k_2^2 m_a E_j V_v\left[g_{ph}\cos(\phi-\theta_v)+b_{ph}\sin(\phi-\theta_v)\right]\end{aligned} \tag{2.25}$$

where the transformer impedance is $\mathbf{z}_{tr} = r_{tr}+\mathrm{j}x_{tr}$ and $\mathbf{z}_{ph} = r_{ph}+\mathrm{j}x_{ph}$ is the VSC phase reactor impedance, and so $g_{tr}+\mathrm{j}b_{tr} = (\mathbf{z}_{tr})^{-1}$ and $g_{ph}+\mathrm{j}b_{ph} = (\mathbf{z}_{ph})^{-1}$. The powers P_{vk} and P_{jv} flow in directions indicated in Figure 2.4; *E* is the converter DC voltage and the phasor modulating variable is $\mathbf{m}_a = m_a\, e^{\mathrm{j}\phi}$; the AC voltages are defined as $\mathbf{V}_k = V_k\, e^{\mathrm{j}\theta k}$ and $\mathbf{V}_v = V_v\, e^{\mathrm{j}\theta v}$.

To obtain linear power flow equations of the VSC station, similar assumptions to those adopted for the linear power flows in AC transmission lines are made, see Section 2.2. Therefore, the converter and transformer power losses are neglected, while the converter AC voltage is assumed to operate at its nominal value, that is, $V_v = |k_2\ m_a\ E_j| \approx 1$. With these considerations, the linear VSC power flow expressions are given by (2.26).

$$(a)\ P_{vk} = \frac{(\theta_v - \theta_k)}{x_{tr}}, \qquad (b)\ P_{jv} = \frac{(\phi - \theta_v)}{x_{ph}} \tag{2.26}$$

- *VSC control strategies*

To complete the VSC modeling that will enable comprehensive representations of VSC-based AC/DC power grids, it is necessary to discuss the converter's control strategies. With these, the converter's power flow behaviors will be described properly. The state-of-the-art VSC control strategies are listed below [1, 81, 83, 84]:

i. ***Voltage control***, also known as "slack mode" or "E_{ctrl} mode." In this operation mode, the VSC exerts voltage regulation in the associated DC bus, $E_j = E^{ref}$, being this the *reference nodal voltage* for the DC grid.

ii. ***Fixed power control***, also known as "scheduled mode" or "P_{set} mode." With this strategy, the VSC sets the power flow between the converter's AC and DC sides, $P_{jv} = P^{ref}$, thus enabling control of the active power exchange through the VSC link.

iii. ***Passive control***, also known as "passive mode." In this operation strategy, the VSC feeds a passive grid without generation of its own. Here, the converter phase angle ϕ serves as the angular reference for the passive network, where usually $\phi = \phi^{ref} = 0$.

iv. ***Voltage/power droop control***. This operation strategy is a mix of the slack and scheduled modes, where the power flow P_{jv} varies according to changes in the DC port voltage, that is, according to $P_{jv} = P^{ref} - K_c\ (E^{ref} - E_j)$, with K_c being the droop gain.

In connection with the previous descriptions, Table 2.2 summarizes the four VSC operation strategies. Departing from (2.26b), this table also shows the resulting linear VSC power flow equations useful for the subsequent modeling of VSC-based AC/DC systems.

Table 2.2 VSC control strategies and associated variables

Type	Controlled variable	Reference value	VSC equation
Slack	E_j	E^{ref}	$P_{jv} = (\phi - \theta_v)/x_{ph}$
Schedule	P_{jv}	$P_{jv} = P^{ref}$	$P^{ref} = (\phi - \theta_v)/x_{ph}$
Passive	P_{jv}	• $\phi = \phi^{ref}$	$P_{jv} = (\phi^{ref} - \theta_v)/x_{ph}$
Droop control	E_j , P_{jv}	E^{ref} , P^{ref}	$P_{jv} = P^{ref} - K_c\,(E^{ref} - E_j)$

2.5. Modeling of DC systems

Subsections 2.3 and 2.4 described the VSC models, which permit to link, mathematically wise, the AC systems with the DC power grid. In this sense, the present subsection introduces the power flow modeling of the DC system aiming to describe generic VSC-based AC/DC power systems in steady state. Returning to Figure 2.4, it is inferred from this schematic that the DC bus of the VSC unit may connect to a large, complex DC power grid. Just like in the case of AC power systems, it is necessary to count on the calculated DC power injection at bus *j* to enable the formulation of nodal power balances.

Following similar principles of AC power flow modeling, equation (2.27) can be used as the calculated power flow at DC bus *j*, which is obtained from the AC active power flow expression (2.3) by simply exchanging the subscripts *k* for *j*, the variables V_k for E_j and V_m for E_m, and making $\theta_k = \theta_m = 0$ since it is about a DC system [85, 86].

$$P_j^{cal} = E_j^2 G_{jj} + E_j \sum_{m=1, m\neq j}^{\sigma} E_m G_{jm} \qquad \forall m \in \mathbb{Z}_j \tag{2.27}$$

where P_j^{cal} is the calculated DC power at node *j*; σ is the number of DC nodes; $\mathbb{Z}_j$ is the set of nodes connecting with node *j*; r_{jm} is the series resistance of the DC transmission line connecting nodes *j*-*m*; $G_{jm} = -r_{jm}^{-1}$ and $G_{jj} = \sum_{m=1, m\neq j}^{\sigma} G_{jm}$. And formulating the *j*-th nodal power balance of the DC system, the following mismatch equation is obtained,

$$\Delta P_j = P_{gj} - P_{dj} - P_j^{cal} \tag{2.28}$$

where P_{gj} in this case represents the power injection by the VSC at bus *j* and P_{dj} is the load consumed at the same bus. As it turns out, the resulting DC system power flow model is

nonlinear and its solution must be found by iteration, all this in a similar way as carried out for the power flow problem formulated for AC transmission systems, see Section 2.1.

2.5.1. Linear modeling of DC systems

As in the case of AC systems, it is possible to obtain the DC network's power flows linearly, avoiding resolving nonlinear equations thus reducing the associated computational times. Adopting similar assumptions to those discussed in Section 2.2, if neighboring DC bus voltage magnitudes are near each other and close to their nominal values, $E_j \approx E_m$, the nonlinear power injection (2.27) reduces to (2.29), which corresponds to a lossless DC grid power flow model [87].

$$P_j^{cal} = \sum_{m=1, m\neq j}^{\sigma} \left(E_j - E_m\right) r_{jm}^{-1} \qquad \forall m \in \mathbb{Z}_j \tag{2.29}$$

Using (2.29) and formulating the nodal power balances (2.28) for a generic DC system containing σ nodes, the ensuing steady-state power flow model is obtained (2.30).

$$\begin{bmatrix} \Delta P_1 \\ \vdots \\ \Delta P_k \\ \vdots \\ \Delta P_\sigma \end{bmatrix} = \begin{bmatrix} G_{11} & \cdots & G_{1k} & \cdots & G_{1\sigma} \\ \vdots & \ddots & \vdots & \ddots & \vdots \\ G_{k1} & \cdots & G_{kk} & \cdots & G_{k\sigma} \\ \vdots & \ddots & \vdots & \ddots & \vdots \\ G_{\sigma 1} & \cdots & G_{\sigma k} & \cdots & G_{\sigma\sigma} \end{bmatrix} \begin{bmatrix} E_1 \\ \vdots \\ E_k \\ \vdots \\ E_\sigma \end{bmatrix} \quad \Rightarrow \quad \Delta \mathbf{P}_{dc} = \mathbf{G}\, \mathbf{E}_{dc} \tag{2.30}$$

2.6. Linear modeling of AC/DC systems using shift factors

Having introduced the linear power flow models of AC systems (2.6), VSC stations (2.26), and DC systems (2.29), comprehensive VSC-based AC/DC power system models can be straightforwardly determined. All this by resorting anew to fundamental principles of power flow theory that implies the formulation of nodal power balances in the AC grids and DC system, both interfaced by VSC stations. But for the sake of completeness, a summary of these models is given next,

Table 2.3 Summary of the linear modeling of VSC-based AC/DC systems

	AC transmission systems	**DC transmission grid**	**VSC unit***
Power flow	$P_{km} = \dfrac{\theta_k - \theta_m}{x_{km}}$	$P_{jm} = \dfrac{E_j - E_m}{r_{jm}}$	$P_{jv} = \dfrac{(\phi - \theta_v)}{x_{ph}}$
Nodal power injection	$P_k^{cal} = \sum_{m=1, m\neq k}^{\rho} (\theta_k - \theta_m) x_{km}^{-1}$	$P_j^{cal} = \sum_{m=1, m\neq j}^{\sigma} (E_j - E_m) r_{jm}^{-1}$	---
Nodal power balance	$\Delta P_k = P_{gk} - P_{dk} - P_k^{cal}$	$\Delta P_j = P_{gj} - P_{dj} - P_j^{cal}$	---

*Note: this equation changes according to the control strategy, see Table 2.2.

It is worth emphasizing that the consideration of the VSC control strategies is key for obtaining adequate calculations related to the steady-state performance of this kind of hybrid power networks. In this sense, equation (2.31) represents the relationship between net power injections and state variables of the VSC-based AC/DC transmission system. In other words, this formulation is expressed in terms of busbar angles of AC nodes, voltage magnitudes of DC nodes, and the VSC phase-shifting angles. From here, it can be inferred that this generic formulation can accommodate several VSC stations carrying different control strategies; additional details can be found in [85, 86].

$$\begin{pmatrix} \Delta\mathbf{P}_{Ectrl} \\ \Delta\mathbf{P}_{Pset} \\ \Delta\mathbf{P}_{Pass} \\ \Delta\mathbf{P}_{dc} \end{pmatrix} = \begin{pmatrix} \mathbf{B}'_{Ectrl} & \mathbf{0} & \mathbf{0} & \mathbf{0} \\ \mathbf{0} & \mathbf{B}'_{Pset} & \mathbf{0} & \mathbf{0} \\ \mathbf{0} & \mathbf{0} & \mathbf{B}'_{Pass} & \mathbf{0} \\ \mathbf{B}''_{\phi-E} & \mathbf{B}''_{\phi-Ps} & \mathbf{B}''_{\phi-Pa} & \mathbf{G}_{dc} \end{pmatrix} \begin{pmatrix} \mathbf{\Phi}_{Ectrl} \\ \mathbf{\Phi}_{Pset} \\ \mathbf{\Phi}_{Pass} \\ \mathbf{E}_{dc} \end{pmatrix} \quad \Rightarrow \quad \mathbf{P}_{ACDC} = \mathbf{\Psi}_{ACDC}\, \mathbf{\Omega}_{ACDC} \tag{2.31}$$

where the nodal net power injections ($\Delta P = P_g - P_d$) are represented in [$\Delta\mathbf{P}_{Ectrl}$, $\Delta\mathbf{P}_{Pset}$, $\Delta\mathbf{P}_{Pass}$] = [$\Delta P_1, \ldots, \Delta P_\rho$] for VSC-connected AC systems related to converters with DC voltage control, fixed power flow, and passive grids, respectively. While $\Delta\mathbf{P}_{dc}$ = [$\Delta P_1, \ldots, \Delta P_\sigma$] accounts for the net power injections in the DC grid. Vectors $\mathbf{\Phi}_{Ectrl}$, $\mathbf{\Phi}_{Pset}$, $\mathbf{\Phi}_{Pass}$ contain the state variables of the AC networks related to VSC units with the different control strategies, i.e., phase angles of AC nodes and VSC units: [$\theta_1, \ldots, \theta_\rho, \phi$]. Likewise, the DC system state variables are accommodated in $\mathbf{E}_{dc}$ = [$E_1, \ldots, E_\sigma$]. The entries **0** are zero-padded matrices of suitable order. Submatrices **B** in (2.31) are like the susceptance matrix of AC power systems, with little modifications:

- $\mathbf{B}'_{Ectrl}$, $\mathbf{B}'_{Pset}$, $\mathbf{B}'_{Pass}$ are the susceptance matrices of the VSC-connected AC grids whose converters operate in slack, scheduled and passive modes, respectively. These matrices also contain the susceptances of their corresponding VSC's coupling phase reactors.
- $\mathbf{B}''_{\phi-E}$, $\mathbf{B}''_{\phi-Ps}$, $\mathbf{B}''_{\phi-Pa}$ contain the susceptance associated with the VSC power flow model that links it with the nodal balance at the converter's DC node, all this for the three VSC models, i.e., slack, scheduled and passive, respectively.
- $\mathbf{G}_{dc}$ represents the conductance matrix of the DC grid.

- *VSC-based AC/DC system modeling by shift factors*

The linear power flow model for VSC-based AC/DC networks (2.31) can be solved for the associated state variables, AC phase angles and DC voltages, as $\mathbf{\Omega}_{ACDC} = (\mathbf{\Psi}_{ACDC})^{-1}\,\mathbf{P}_{ACDC}$. With this solution, the AC/DC power flows can be determined using the models reported in Table 2.3. But power flows can be calculated more efficiently if using the shift factors theory already discussed in detail in Section 2.2. In this sense, the terms *F* of (2.32) can be properly used to obtain the shift factors for both AC systems and DC system [85, 86], as shown in (2.33a) and (2.33b), respectively.

$$\mathbf{F} = \left(\mathbf{\Psi}_{ACDC}\right)^{-1} = \begin{bmatrix} F_{22} & \cdots & F_{2k} & \cdots & F_{2n} \\ \vdots & \ddots & \vdots & \ddots & \vdots \\ F_{k2} & \cdots & F_{kk} & \cdots & F_{kn} \\ \vdots & \ddots & \vdots & \ddots & \vdots \\ F_{n2} & \cdots & F_{nk} & \cdots & F_{nn} \end{bmatrix} \quad (2.32)$$

$$\begin{aligned} &(a) \quad \Gamma_{k-m,i} = x_{km}^{-1}\left(F_{ki} - F_{mi}\right) \\ &(b) \quad \Gamma_{j-m,i} = r_{jm}^{-1}\left(F_{ji} - F_{mi}\right) \end{aligned} \quad (2.33)$$

where (2.33a) calculates the shift factors for AC branches connecting nodes *k–m*, whereas (2.33b) does it for DC branches connecting nodes *j–m*. All these factors can be suitably accommodated in matrix form $\mathbf{\Gamma}$ (2.34), recalling that ρ and σ are the number of AC buses and DC nodes, respectively. And with expression (2.35), the power flow calculation is carried out for all *k-m* AC branches and *j-m* DC lines using the net power injections of both AC and DC nodes.

$$\mathbf{\Gamma} = \begin{pmatrix} \mathbf{\Gamma}_{km,1} & \cdots & \mathbf{\Gamma}_{km,\rho} \\ \mathbf{\Gamma}_{jm,1} & \cdots & \mathbf{\Gamma}_{jm,\sigma} \end{pmatrix} \quad (2.34)$$

$$\begin{pmatrix} \mathbf{P}_{km} \\ \mathbf{P}_{jm} \end{pmatrix} = \mathbf{\Gamma} \begin{pmatrix} \Delta\mathbf{P}_{ac} \\ \Delta\mathbf{P}_{dc} \end{pmatrix} \tag{2.35}$$

where $\Delta\mathbf{P}_{ac} = [\Delta\mathbf{P}_{Ectrl}, \Delta\mathbf{P}_{Pset}, \Delta\mathbf{P}_{Pass}]^T$ and $\Delta\mathbf{P}_{dc} = [\Delta P_1, \ldots, \Delta P_\sigma]^T$.

It is worth emphasizing that shift factors avoid the use of AC busbar angles θ and DC voltages E in power flow calculations for VSC-based AC/DC networks, something that is also advantageous, computationally wise, for the power system optimization analysis of interest to this doctoral thesis.

2.7. Linear modeling of AC/DC power losses using piecewise linearization

It is worth recalling that the research developed in this doctoral thesis relies on linear programming models of SCED, SCOPF and UC. But to improve the accuracy of results, the nonlinear features of AC/DC transmission power losses are segmented using Piecewise Linearization (PWL). This is a mathematical procedure enabling the linearization, by segments, of nonlinear functions. Figure 2.5 illustratively shows the PWL method, where a quadratic function, $y = a\ x^2$, is approximated through several linear segments so that the summation of these segments represents the original function [88]. Next, it is presented the application of PWL for AC/DC transmission power losses.

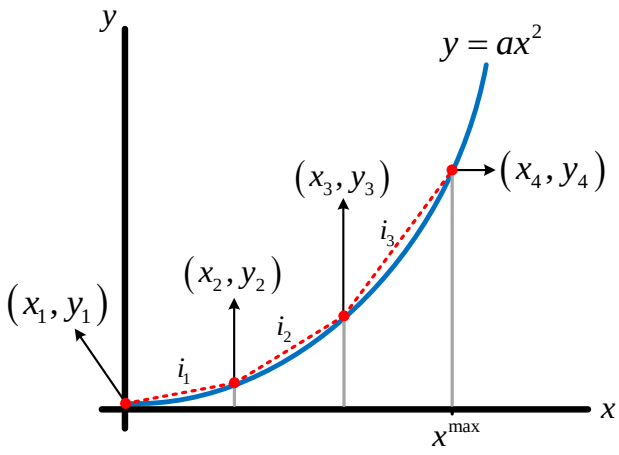

Figure 2.5 Illustration of the PWL technique

By way of example, it is first explained the application of the PWL technique to the quadratic function depicted in Figure 2.5, which is expressed in (2.36), where this function is defined for the closed interval [0, $x^{\max}$].

$$y = a\,x^2 \;\; ; \;\; \forall x \in \left[0, x^{\max}\right] \tag{2.36}$$

As can be appreciated, the function y is formed by four points and divided into three pieces i_1, i_2 and i_3, respectively, which can be linearly approximated through the sum of i_1, i_2 and i_3. To this end, it is necessary to calculate the slope of each segment, as shown in (2.37).

$$m_i = \frac{a\left(x_{i+1}\right)^2 - a\left(x_i\right)^2}{x_{i+1} - x_i} \tag{2.37}$$

Once having calculated the slopes, it is possible to express the quadratic function linearly by summing up all the linear segments, as in (2.38)

$$\overline{y} = \sum_{i=1}^{ns} m_i \overline{x}_i \tag{2.38}$$

$$0 \le \overline{x} \le \frac{x^{\max}}{ns} \tag{2.39}$$

where ns is the number of lineal segments dividing the quadratic function; $\overline{y}$ represents the linearized function; $\overline{x}$ is the *i-th* linear segment of x; m_i is the *i-th* slope of the linearized function. Likewise, it is worth highlighting that each linear segment is bounded between zero and $x^{\max}/ns$, as expressed in (2.39).

- *AC transmission line power losses*

The power losses of an AC branch connecting nodes *k-m* can be calculated using the transmitted power flow in the following way $P_{km}^{loss} = P_{km} + P_{mk}$, as explicitly shown in (2.40a). And applying the same assumptions discussed in Section 2.2 and recalling that the power flow is $P_{km} = (\theta_k - \theta_m)/x_{km}$, this expression can be simplified as (2.40b) [85] .

$$\begin{aligned} &(a)\, P_{km}^{loss} = g_{km}\left(V_k^2 - V_m^2\right) - 2g_{km}V_kV_m\cos\left(\theta_k - \theta_m\right) \\ &(b)\, P_{km}^{loss} = 2g_{km}\left[1 - \cos\left(\theta_k - \theta_m\right)\right] = \left(\frac{g_{km}}{b_{km}^2}\right)P_{km}^2 \end{aligned} \tag{2.40}$$

- *DC transmission line power losses*

The power losses in DC transmission lines connecting nodes *j-m* can be estimated using the well-known expression (2.41a). Recalling that the linear DC power flow expression holds true $P_{jm} = (E_j - E_m)/r_{jm}$, and by making the approximation $P_{jm} \approx I_{jm}$, hence the DC transmission power losses can be estimated with (2.41b).

$$\begin{aligned} &(a)\, P_{jm}^{loss} = r_{jm} I_{jm}^2 \\ &(b)\, P_{jm}^{loss} = r_{jm} P_{jm}^2 \end{aligned} \tag{2.41}$$

As seen from (2.40b) and (2.41b), both AC and DC transmission losses are quadratic functions of their corresponding power flows. Such nonlinearities can be addressed with PWL as expressed in (2.42), in the same sense as it was described in (2.36) - (2.39) [85].

$$\begin{aligned} &(a)\, \bar{P}_{km}^{loss} = \sum_{i=1}^{ns} m_{km,i} \bar{P}_{km,i};\ 0 \le \bar{P}_{km,i} \le \frac{P_{km}^{\max}}{ns} \\ &(b)\, P_{km} = P_{km}^{+} - P_{km}^{-} \\ &(c)\, \left|P_{km}\right| = \sum_{i=1}^{ns} \bar{P}_{km,i} = P_{km}^{+} + P_{km}^{-} \\ &(d)\, P_{km}^{+},\ P_{km}^{-} \ge 0 \end{aligned} \tag{2.42}$$

where *ns* is the number of linear segments dividing the loss function; $\bar{P}_{km}^{loss}$ is the linearized loss function; $m_{km,i}$ is i-*th* slope of the linearized loss function; $\bar{P}_{km,i}$ is *i-th* segment of the power flow; $P_{km}^{\max}$ is the upper power flow limit of the *k-m* branch. P_{km}^{+} and P_{km}^{-} are two non-negative auxiliary variables used to obtain the absolute values of the segments of power flow $\left|P_{km}\right|$. The previous set of equations (2.42) permit to linearize by segments the AC transmission power losses, but a similar set of equations can be obtained for the PWL of DC power losses simply by exchanging the subscripts *km* by *jm*.

Just as important, when the number of linear segments increases for representing the functions of power losses, generation costs curves, and PV generation, the results of the PWL model improve, i.e., the more segments used for the piecewise linearization, the more it resembles the nonlinear function.

2.8. Modelling of thermal generation units

For most power system economic operation analysis, generation cost curves are represented by quadratic functions (2.43) [78, 80]. But, another way to improve the outcomes of the SCED, OPF and UC formulations developed in this thesis, besides including power losses, is by considering the nonlinear features of the thermal units' generation cost functions by PWL [85, 86], in the same sense as it was described in (2.36)-(2.39).

$$C\left(P_g\right) = c + b\,P_g + a\,P_g^2 \tag{2.43}$$

Based on the backgrounds presented in Section 2.7, in applying PWL to (2.43) we obtain the linearized cost function shown in (2.44), where the total generation power output is given by (2.45), i.e., this power is the sum of segments by which the cost curve was initially divided.

$$\bar{C} = c + \sum_{i=1}^{ns} m_{g,i}\,\bar{P}_{g,i}, \qquad 0 \le \bar{P}_{g,i} \le \frac{P_g^{\max}}{ns} \tag{2.44}$$

$$P_g = \sum_{i=1}^{ns} \bar{P}_{g,i} \tag{2.45}$$

where *ns* is the number of linear segments dividing the generation cost curve and $\bar{C}$ is the linearized generation cost function; $m_{g,i}$ is the *i-th* slope of the generation cost curve; $\bar{P}_{g,i}$ corresponds to the *i-th* linear segment, and $P_g^{\max}$ is the upper generation limit.

2.9. Modeling of PV plants

Photovoltaic (PV) plants are among the soundest renewable generation technologies [89], easily scalable and integrated to power grids through power converters, as shown in Figure 2.6(a) for a three-stage PV system. The PV array model itself can be represented by *ns* series and *np* parallel PV modules, as shown in Figure 2.6(b). Regardless of the PV plant configuration, the Maximum Power Point Tracking (MPPT) guarantees that the maximum available power is always extracted according to the solar irradiance conditions S_i [90].

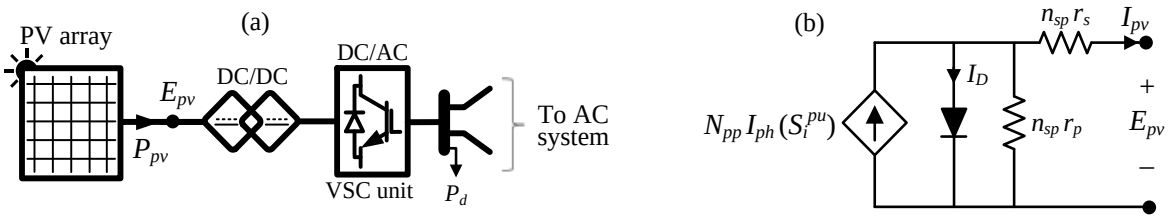

Figure 2.6 (a) PV plant representation; (b) PV array equivalent model $S_i^{pu} = S_i/S_i^{nom}$, $n_{sp} = n_s/n_p$

In this topology, the MPPT curve is established by the DC/DC converter as it looks for the optimum voltage E_{pv} continuously. Figure 2.7(a) shows a typical set of PV power curves together with the MPPT curve. It can be observed that the MPPT curve, from $S_i = 0$ to $S_i = 1$ [kW/m^2], is not strictly linear, particularly in low irradiance conditions. The nominal irradiance $S_i^{nom} = 1$ [kW/m^2] does not necessarily imply that the PV plant reaches the rated power, $P_{pv} = 1$ [pu], because of the internal losses of the PV modules, i.e., due to r_s and r_p. This aspect can be verified by looking at Figure 2.7(b) which illustrates the optimum PV power, P_{mmp}, versus the whole range of irradiances. So, it can be stated that the PV plant power is not entirely proportional to the irradiance conditions, this being an aspect that should not be overlooked when carrying out power system calculations.

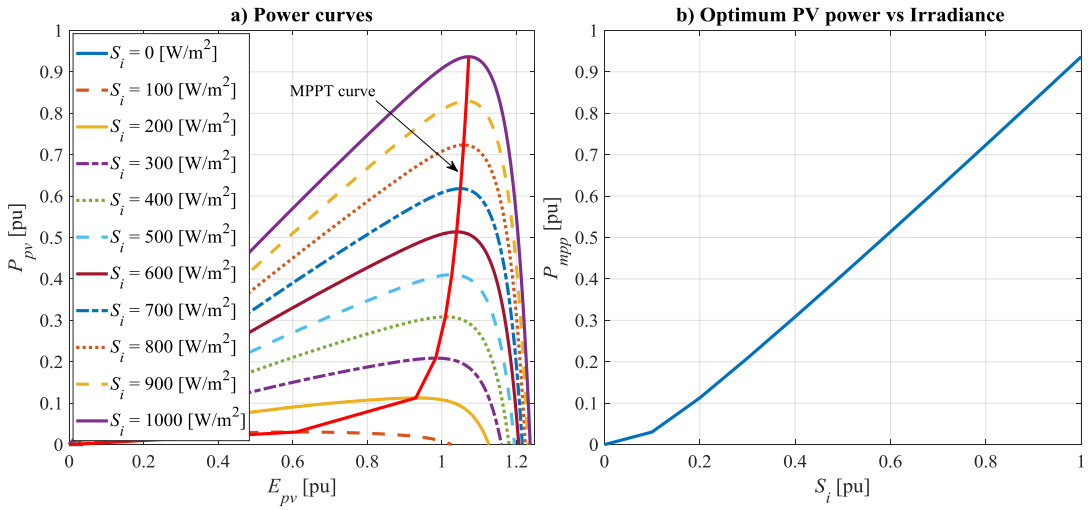

Figure 2.7 PV power curves, MPPT curve, and normalized curve P_{mpp} vs S_i

Based on these backgrounds, in this doctoral thesis it is taken advantage of the linear programming approach to correctly estimate the PV plant output power as function of forecasted irradiances, $P_{pv} = f(S_i)$, during the hours associated with the power system

economic operation. To this end, the PWL technique can be also employed to properly characterize the curve P_{mpp} vs S_i depicted in Figure 2.7(b), which is expressed by (2.46).

$$P_{pv} = \sum_{\eta=1}^{ns_{pv}} m_{pv,\eta} \bar{S}_{i,\eta} \ , \qquad 0 \le \bar{S}_{i,\eta} \le \frac{S_i^{nom}}{ns_{pv}} ; \tag{2.46}$$

where ns_{pv} is the number of segments dividing the curve P_{mpp} vs S_i; P_{pv} is the piecewise linearized power of the PV plant; $m_{pv,\eta}$ is the η-*th* slope of the MPPT curve; $\bar{S}_{i,\eta}$ corresponds to the η-*th* segment of solar irradiance, and S_i^{nom} is the nominal solar irradiance.

2.10. BESS Modelling

Energy storage systems (ESS) are cutting-edge technologies experiencing a solid push by industrial and commercial parties in the last few years. ESS bring a wide range of applications in power system planning and operation because they can cope with some of the current and future challenges of electrical networks associated with power controllability. For instance, to accommodate great amounts of renewable energy in power grids, to support the operation of conventional generators units, or to reduce the overall system operation costs. In this sense, Battery Energy Storage Systems (BESS) are leading the race of energy storage technologies. These power devices are receiving vast attention in power network applications with a promising future to their continuous development [4, 91]. This doctoral thesis addresses the BESS technology in the power system economic operation context, placing emphasis on load-following and energy time-shifting strategies. Both operating strategies are explained in detail next.

BESS facilities can be conceptually seen as generation or load when integrated to power systems, depending on their discharging/charging operation mode. When the BESS is charging, it takes energy from the power system thus acting as load. While it acts as generation in the opposed situation when the BESS discharges, thus providing its stored energy to the power grid. These operating actions are schematically illustrated in Figure 2.8 [9, 86].

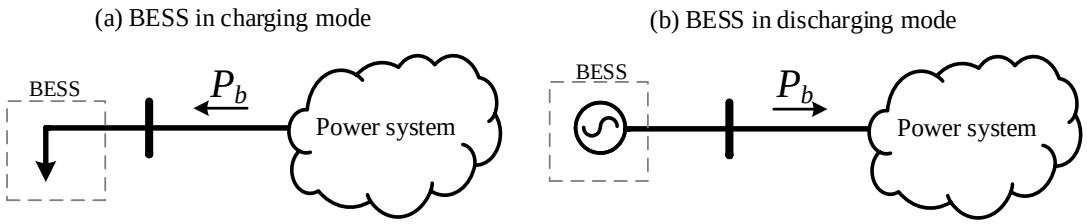

Figure 2.8 BESS in discharging mode $P_b>0$ and charging mode $P_b<0$

The BESS charging/discharging operations over time, can be well established by relating its output power and stored energy, as detailed by (2.47). It is well-known, however, that BESS can inject/absorb power to/from the power grid faster than conventional generation units. Additionally, to avoid impairing the ramp-up and ramp-down operations by grid-connected conventional power plants, it is desirable for TSO to have the possibility to limit the associated charging and discharging operations, as considered in (2.48). Furthermore, BESS must keep their State of Charge (SoC) between minimum and maximum energy storage limits as shown in (2.49). And for similar reasons, with (2.50) the minimum and maximum power delivered by the BESS are observed.

$$W_{(t)} = W_{(t-1)} - \Delta t \eta_B P_{b(t)} \tag{2.47}$$

$$-CR \le P_{b(t)} - P_{b(t-1)} \le DR \tag{2.48}$$

$$W^{\min} \le W_{(t)} \le W^{\max} \tag{2.49}$$

$$P_b^{\min} \le P_{b(t)} \le P_b^{\max} \tag{2.50}$$

where $W_{(t)}$ is the stored energy at time t and η_B is the round-trip efficiency of the BESS; $P_{b(t)}$ is the injected or absorbed power by the BESS at time t, and Δt is the time step. CR and DR represent the BESS charging and discharging rates, respectively. P_b^{min}, P_b^{max} are the minimum and maximum BESS power limits, whereas W^{min}, W^{max} are the minimum and maximum energy storage limits, where $\text{SoC}_{(t)} = W_{(t)}/W^{max}$.

With the idea of incorporating BESS facilities within a power system economic operation environment, it is important to estimate their associated cost per use. These costs can be well estimated with (2.51) which mainly depend upon the investment cost. As it turns out, the operating costs can be calculated by (2.52) [86].

$$\xi = \frac{IC}{2n_c W^{\max}} \qquad (2.51)$$

$$OC = \xi \left| P_{b(t)} \right| \qquad (2.52)$$

where ξ [$/MWhr] is the cost per use, IC [$] includes the investment, operation, and maintenance costs, expressed approximately in terms of present value, considering the time of the BESS life cycle and a certain discount rate, and n_c [cycles] is the BESS life cycle. In (2.51) it is assumed that a full cycle corresponds to a complete charge and discharge operation, so the total energy in a cycle is equivalent to $2W^{max}$, with the total amount of energy of the BESS in its entire life cycle being $2\eta_c W^{max}$. It is also worth noting that BESS can operate in charging or discharging modes ($P_{b(t)} < 0$ or $P_{b(t)} > 0$), hence this fact is correctly considered by $|P_{b(t)}|$ in (2.52).

2.10.1. Load-following strategy

BESS are flexible devices that can offer several services to the power system, where different control strategies can be implemented depending upon the technical impact expected on the power grid, e.g., loss reduction, reliability improvement, economic operation, among others. In this doctoral thesis, the load-following strategy is developed in such a way that BESS support the system economic operation by injecting energy concurrently with system load changes. Specifically, the BESS discharges power according to the load pattern variation, in proportion to the system demand level and by certain periods of interest, as schematically shown in Figure 2.9.

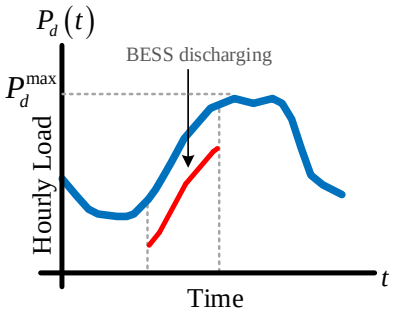

Figure 2.9 Load-following strategy

Based on the previously described operation strategy, the power delivered by the BESS must follow the demand variation for a predefined period, say 2 hours. Hence, in addition to (2.47)-(2.50), constraint (2.53) should be considered in the BESS modeling aiming at establishing the maximum power P_b to be discharged by the BESS unit at each time t,

noticing that this is calculated in proportion to the maximum demand of the system hourly load curve.

$$(a)\ 0 \le P_{b(t)} \le \lambda_{(t)} P_b^{\max}$$
$$(b)\ \lambda_{(t)} = \frac{P_{d(t)}}{P_d^{\max}} \tag{2.53}$$

where $\lambda_{(t)}$ in (2.53b) denotes a time-varying relationship between the current system demand $P_{d(t)}$ and the peak demand P_d^{max}.

2.10.2. Energy time-shifting strategy

Figure 2.9 illustrates the energy time-shifting strategy of BESS [86]. This emerges from the idea that an independent system operator (ISO) calls for one BESS installation of convenient size and location, in such a way that its energy time-shifting strategy assists the power network in reducing the daily peak load and/or transmission congestion during selected time periods within the real-time or day-ahead markets, e.g., SCED or UC. A reduction of system marginal prices is expected thus promoting a high competition level of energy trading in the power grid, a fact that will be later discussed in this thesis accompanied by case studies. The BESS operating strategy simply consists in charging energy in periods of low demand and discharging energy during peak demand hours, thus taking advantage of low prices in low demand hours and high prices during high demand hours, i.e., charging during cheap hours and discharging in the expensive periods.

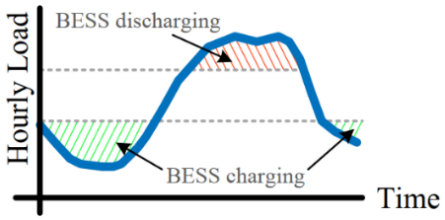

Figure 2.10 Energy time-shifting strategy

Based on these backgrounds, it should be realized that the BESS model (2.47)-(2.50) would not necessarily facilitate its operation in charging mode (consuming power), because power system economic operation problems (SCED, SCOPF or UC) always look for minimization of costs. Therefore, all BESS would be always forced to discharge (produce power) throughout the planning horizon, say Z_T = {1 - 24} hr, since their associated operating costs

ξ are much smaller than those of thermal generation units. For this reason, the BESS model must be accompanied by (2.54) to consider the charging periods ($P_b < 0$) subject to the corresponding charging rate *CR*.

$$\begin{aligned} &P_{b(t)} \le P_{b(t-1)} - P^{CR}_{b(t)} \\ &P^{CR}_{b(t)} = \min\left\{ CR\,\Delta t, P_{b(t-1)} - P^{min}_{b(t)} \right\} \end{aligned} \qquad \forall t \in \mathbb{Z}'_T \tag{2.54}$$

where $\mathbb{Z}'_T \neq \mathbb{Z}_T$ which means that charging hours form a subset of the operation horizon. Knowing from typical hourly demand curves that inferior load levels appear during the first and last hours, it makes sense for instance that $\mathbb{Z}'_T$ = {1-10, 23-24} hr. Therefore, during the rest of periods (peak power demand), the BESS would operate in discharging mode thus enabling the energy time-shifting strategy [86].

Chapter 3

3. Security-constrained Economic Dispatch Including PV Plants and BESS with Load-following Strategy

The economic operation of power systems deals with satisfying the demand in the most economic manner while fulfilling all network constraints [11, 78, 80]. The most fundamental tool employed at control centers is the Security-constrained Economic Dispatch (SCED) running every specific time intervals, e.g., every 5 or 10 minutes. This aims at determining the output power of all generators that reduces the overall operating costs, while observing their physical limitations including those of transmission lines [11]. The SCED solution depends on the energy matrix which is mainly characterized by conventional plants such as thermal and hydro. But in recent times the renewable resources of considerable capacities are gaining prominence in power systems. Perhaps, photovoltaic (PV) plants are one of the most deployed generation technologies nowadays due to positive environmental impacts and decreasing PV module prices [89, 90]. With intermittent renewable sources in play, BESS devices arise as one of the leading technologies that can enable a massive incorporation of renewable generation due to their flexible features that can help support the network operation [4-6]. Hence, the proper modeling of PV plants and BESS devices within SCED studies is more important than ever.

This chapter addresses the SCED problem including BESS facilities driven by a load-following strategy, while providing spinning reserve to the system. PV plants are also considered by modeling the Maximum Power Point Tracking (MPPT) strategy using the PWL technique, as discussed in Subsection 2.9. The SCED model features a transmission network modeling based on shift factors, as described in Section 2.2. The proposed approach relies entirely on linear programming, where nonlinear transmission losses and generation costs are both considered through PWL, as discussed in Sections 2.7 and 2.8, respectively.

3.1. Classic SCED model

The SCED tool is an optimization model useful for finding the most economic power dispatch of generation units. The model often considers operating constraints such as the generation/demand balance, transmission limits, power reserve requirements, generator's minimum and maximum outputs, ramp rates, among others [11, 78, 80]. In practice, SCED runs in look-ahead time intervals, usually ranging from 5 to 30 minutes (a 10-minute interval is selected in this doctoral thesis). Next, the basic modeling framework of the SCED problem is stated, which is commonly used for real-time operation analysis at control centers, and must be solved for T periods, $t \in \mathbb{Z}_T$, considering all the ng generation units available to be dispatched, $k \in \mathbb{Z}_{ng}$, as follows:

$$\min\left(\sum_{t=1}^{T}\sum_{k=1}^{ng} b_k P_{gk(t)}\right) \tag{3.1}$$

$$P_{gk(t)} - P_{dk(t)} = \sum_{m=1, m\neq k}^{\rho}\left[\left(\theta_{k(t)} - \theta_{m(t)}\right)x_{km}^{-1}\right], \qquad \forall k \in \mathbb{Z}_n,\ \forall t \in \mathbb{Z}_T \tag{3.2}$$

$$-P_{km}^{\max} \leq \left[\left(\theta_{k(t)} - \theta_{m(t)}\right)x_{km}^{-1}\right] \leq P_{km}^{\max};\ \forall km \in \mathbb{Z}_{la},\ \forall t \in \mathbb{Z}_T \tag{3.3}$$

$$P_{gk}^{\min} \leq P_{gk(t)} \leq P_{gk}^{\max}; \qquad \forall k \in \mathbb{Z}_{ng},\ \forall t \in \mathbb{Z}_T \tag{3.4}$$

$$P_{gk(t)} - P_{gk(t-1)} \leq RU_k; \qquad \forall k \in \mathbb{Z}_{ng},\ \forall t \in \mathbb{Z}_T \tag{3.5}$$

$$P_{gk(t-1)} - P_{gk(t)} \leq RD_k; \qquad \forall k \in \mathbb{Z}_{ng},\ \forall t \in \mathbb{Z}_T \tag{3.6}$$

$$\sum_{k=1}^{ng} P_{gk}^{\max} - P_{gk(t)} \geq SR_t; \qquad \forall k \in \mathbb{Z}_{ng},\ \forall t \in \mathbb{Z}_T \tag{3.7}$$

where $\mathbb{Z}_n$ in (3.2) is the set of n system buses, $\mathbb{Z}_{la}$ in (3.3) is the set of la transmission branches, i.e., lines and transformers; RU_k, RD_k stand for the ramp-up and ramp-down constraints of the *k-th* generation unit, respectively, while SR_t represents the power system spinning reserve requirement at period *t*. In this model, (3.1) is the objective function which minimizes the system operating costs, noting that in this basic SCED model only the linear term, b, of the generation cost curve is employed (see Subsection2.8). Equation (3.2)

represents the power balance constraint for each system node, through its corresponding demand, P_d, and generation, P_g. The transmission limits of the network are guaranteed with (3.3), subject to the transmission branch physical limits P^{max}. The minimum generation output, P_g^{min}, and maximum generation output, P_g^{max}, are observed with (3.4). Expressions (3.5) - (3.6) represent the generation units' ramp-up, *RU*, and ramp-down, *RD*, constraints, respectively. The required spinning reserve or the power system, *SR*, is ensured through (3.7), which is an operating margin between the dispatched power and maximum output power of each generation unit, with this anticipating to possible generation outages. Note that this traditional SCED model does not include transmission losses, nor does it consider quadratic generation curves, as opposed to the proposed SCED model detailed in Subsection 3.2.

3.2. Proposed SCED formulation

The multi-period SCED model developed in this thesis is presented herein. BESS devices pursuing a load-following strategy and PV plants with the MPPT strategy explicitly represented are also considered in the optimization model. In sharp contrast with the basic model previously discussed, the proposed SCED approach uses the complete quadratic cost function, albeit linearized through the PWL method. Furthermore, the modeling of the transmission network is based on shift factors **Γ**, with the generation-demand balance being attained by only one global balance equation, something that clearly differ from the network model by busbar angles where it is needed as many equations as power system nodes. Each expression of the new SCED model is explained in detail next, recalling that this must be solved for all T periods, $t \in \mathbb{Z}_T$, considering the ng dispatchable units, $k \in \mathbb{Z}_{ng}$, the nb BESS units, $j \in \mathbb{Z}_{nb}$, and the np PV plants, $k \in \mathbb{Z}_{np}$, as follows:

- **Objective function**

Expression (3.8) is the minimization of the objective function whose costs are minimized, i.e., the generation production cost plus the BESS operating cost. It is worth noting that quadratic generation costs are linearly represented by PWL, as detailed in Subsection 2.8. Likewise, the BESS operating cost is included in this formulation, as addressed in Subsection 2.10.

$$\min \sum_{t\in\mathbb{Z}_T}\left[\sum_{k\in\mathbb{Z}_{ng}}\left(c_k+\sum_{i=1}^{ns} m_{gk,i}\bar{P}_{gk,i(t)}\right)+\sum_{j\in\mathbb{Z}_{nb}}\xi_j\left|P_{bj(t)}\right|\right] \tag{3.8}$$

- **Power balance constraint**

The generation-consumption active power balance is carried out by a single equation due to advantages of the network modeling based on the shift factors method described in Subsection 2.2. And this is shown in (3.9) where the balance equation considers the BESS operation in discharging mode when pursuing a load-following strategy. In addition, this global equation accounts for the PV plant power injections. Further details on the power injection modeling of conventional generation units P_g, PV plants P_{pv}, BESS units P_b, and transmission losses modeling P_{km}^{loss} can be found in Subsections2.8, 2.9 and 2.10.

$$\sum_{k\in\mathbb{Z}_{ng}} P_{gk(t)}+\sum_{k\in\mathbb{Z}_{np}} P_{pvk(t)}+\sum_{j\in\mathbb{Z}_{nb}} P_{bj(t)}=\sum_{k\in\mathbb{Z}_{n}} P_{dk(t)}+\sum_{km\in\mathbb{Z}_{la}} P_{km(t)}^{loss}, \qquad \forall t\in\mathbb{Z}_T \tag{3.9}$$

- **Generation operating limits**

The generation units physical limits are considered with (3.10), which are enforced by using the PWL technique, as detailed in Subsection2.8, recalling that *ns* is the number of pieces dividing the nonlinear generation cost function. Indeed, all generator units must fulfill the minimum and maximum powers, so that, $P_g^{min}\le P_{g(t)}\le P_g^{max}$.

$$0\le \bar{P}_{gk,i(t)}\le \frac{P_{gk}^{\max}}{ns}, \qquad \forall k\in\mathbb{Z}_{ng},\ \forall t\in\mathbb{Z}_T \tag{3.10}$$

- **Transmission limits**

The transmission power flow limits are enforced by (3.11) using shift factors $\mathbf{\Gamma}$,

$$-\mathbf{P}_{im}^{\max}\le \mathbf{\Gamma}\left(\mathbf{P}_{g(t)}+\mathbf{P}_{pv(t)}+\mathbf{P}_{b(t)}-\mathbf{P}_{d(t)}\right)+\mathbf{P}_{(t)}^{loss}\le \mathbf{P}_{im}^{\max}, \qquad \forall t\in\mathbb{Z}_T \tag{3.11}$$

where vectors $\mathbf{P}_{g(t)}$, $\mathbf{P}_{pv(t)}$, $\mathbf{P}_{b(t)}$, $\mathbf{P}_{d(t)}$, and $\mathbf{P}_{(t)}^{loss}$ represents the generated power by thermal units, output power by PV plants, generated power by BESS, power consumed by the loads, and transmission losses, respectively; $\mathbf{P}_{im}^{max}$ is a vector with the maximum power capacities of all series branches comprising the transmission network. Further details on power flow calculation by shift factors can be found in Subsection 2.2.

- **Ramp-up, ramp-down limits and spinning reserve of conventional units**

The generation units' ramp-up, *RU*, and ramp-down, *RD*, characteristics are given by (3.12) - (3.13), respectively, this being an important physical limitation of power generators. The individual spinning reserve, *SR*, provided by each generation unit is achieved with (3.14), which is a key operating security requirement in power grids; therefore, it must be included in any practical SCED formulation like the ne developed in this thesis project.

$$P_{gk(t)} - P_{gk(t-1)} \leq RU_k, \quad \forall k \in \mathbb{Z}_{ng}, \ \forall t \in \mathbb{Z}_T \tag{3.12}$$

$$P_{gk(t-1)} - P_{gk(t)} \leq RD_k, \quad \forall k \in \mathbb{Z}_{ng}, \ \forall t \in \mathbb{Z}_T \tag{3.13}$$

$$P_{gk}^{\max} - P_{gk(t)} \geq SR_k, \quad \forall k \in \mathbb{Z}_{ng}, \ \forall t \in \mathbb{Z}_T \tag{3.14}$$

- **BESS modeling with load-following strategy**

In the developed SCED model, equations (3.15) - (3.20) model the BESS units considering the load-following strategy. In (3.15) the BESS power limits related to charge/discharge operations are enforced, whereas (3.16) represents the physical limits of the stored energy of the battery packs, i.e., this is associated with the minimum and maximum allowed State of Charge (SoC) of the BESS. The relationship between power and energy in the BESS is modeled by (3.17), which allows to calculate the stored energy level $W_{(t)}$ at any time *t*. In a similar way to ramp-up/ramp-down characteristics of conventional units, BESS devices also feature charge/discharge rates, *CR* / *DR*, indicating how quickly these devices take/release load which is suitably considered by (3.18). In this work, it is assumed that BESS can provide spinning reserve to support the system operation in the same way that conventional generation units do. In this sense, (3.19) permits to attain a spinning reserve at each BESS through a power margin between the BESS injection P_b and maximum discharge P_b^{max}. Expression (3.20), on the other hand, describes the proposed load-following strategy, where the power injection of each BESS follows the system demand variation. Additional details on the BESS modeling with load-following strategy are provided in Subsection 2.10 of this document.

$$P_{bj}^{\min} \le P_{bj(t)} \le P_{bj}^{\max}; \quad \forall j \in \mathbb{Z}_{nb},\ \forall t \in \mathbb{Z}_T \tag{3.15}$$

$$W_j^{\min} \le W_{j(t)} \le W_j^{\max}; \quad \forall j \in \mathbb{Z}_{nb},\ \forall t \in \mathbb{Z}_T \tag{3.16}$$

$$W_{j(t)} = W_{j(t-1)} - \Delta t \eta_B P_{bj(t)}; \quad \forall j \in \mathbb{Z}_{nb},\ \forall t \in \mathbb{Z}_T \tag{3.17}$$

$$-CR_j \le P_{bj(t)} - P_{bj(t-1)} \le DR_j; \quad \forall j \in \mathbb{Z}_{nb},\ \forall t \in \mathbb{Z}_T \tag{3.18}$$

$$P_{bj}^{\max} - P_{bj(t)} \ge SR_j; \quad \forall j \in \mathbb{Z}_{nb},\ \forall t \in \mathbb{Z}_T \tag{3.19}$$

$$0 \le P_{bj(t)} \le \lambda_{j(t)} P_{bj}^{\max}; \quad \forall j \in \mathbb{Z}_{nb},\ \forall t \in \mathbb{Z}_T \tag{3.20}$$

It is noteworthy that this BESS model is applied for a subset of the operation horizon, where BESS performs discharge operations according to the load-following strategy.

- **PV plant power injection**

Expressions (3.21) - (3.22) describe the new PV generation model developed in this SCED formulation, which is based on the PWL of the MPPT strategy. So, the PV injection is accounted for with (3.21), where the total generated power is the sum of the linear segments, which are bounded with (3.22).

$$P_{pvk(t)} = \sum_{\eta \in ns_{pv}} m_{k,\eta} \bar{S}_{i,\eta(t)}; \ \forall k \in \mathbb{Z}_{np},\ \forall t \in \mathbb{Z}_T \tag{3.21}$$

$$0 \le P_{pvk(t)} \le P_{pvk}^{\max}; \quad \forall k \in \mathbb{Z}_{np},\ \forall t \in \mathbb{Z}_T \tag{3.22}$$

Further details on the PV modeling are provided in Subsection 2.9 of this manuscript.

- **Concluding remarks on the proposed SCED formulation**

Various aspects of the SCED problem were explained in detail until to this point, starting with the fundamentals of the classical SCED formulation (3.1) - (3.7), as background for understanding the basic optimization model and its application to power systems economic operation. Subsequently, the proposed multi-period SCED model (3.8) - (3.22) of this thesis, which is solved via a linear programming was explained step by step. Models of the objective function along with the power sources – thermal units, BESS, PV plants – and

network constraints were described in detail. In this sense, the optimization problem related to the new SCED formulation is summarized as follows:

Eqn. (3.8)

subject to **Eqns. (3.9) - (3.22)**

3.2.1. Summary of the proposed SCED formulation

The proposed algorithm deals with the multi-period SCED problem, considering BESS featured by a load-following strategy, and PV plants modeling directly the MPPT strategy as function of the solar irradiance conditions. In this regard, Figure 3.1 shows a flowchart illustrating the proposed methodology, whose main steps are summarized as follows:

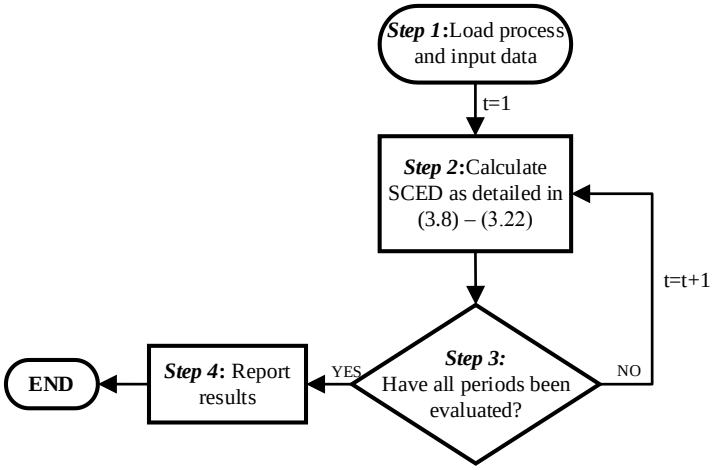

Figure 3.1 Flowchart for the proposed multi-period SCED algorithm

- **Step 1:** The required input parameters for the SCED algorithm are loaded, that is: generation costs functions, transmission system parameters, BESS parameters, and forecasted system demand and solar irradiance.
- **Step 2:** The SCED obtained by solving the model described in (3.9) - (3.22).
- **Step 3:** It is checked if all periods related to the SCED operating horizon have been evaluated.
- **Step 4:** The results report is carried out in this last step.

Chapter 4

4. Security-constrained OPF for AC/DC Systems with Power Rescheduling by Power Plants and VSC Stations

One of the main challenges of power system economic operation analysis is the complexity and size of the optimization models, which increase further for AC/DC power networks. In this sense, VSC-based transmission links are at the forefront of the hybrid AC/DC electrical networks due to well-identified benefits that the VSC-HVDC technology brings to the power system operation [1, 83-87]. Furthermore, the adequate consideration of HVDC lines in the Optimal Power Flow (OPF) problem is a must for modern power system economic analysis. It should be said that the OPF tool is the backbone of many optimization models for power grids, which enables an operation cost minimization with simultaneous power loss reduction, while taking care of operating limits related to generators and transmission line capacities [34, 78].

Based on these backgrounds, this chapter addresses the Security-constrained Optimal Power Flow (SCOPF) problem in multi-terminal VSC-based AC/DC systems using a corrective approach. That is, generation units and VSC devices are featured with power rescheduling through voltage/power droop controls in view of contingencies. Indeed, the power sharing provided during transmission line or generation outages is an expected, realistic behavior in power systems operation. And the foundation of the SCOPF modeling is the one developed for the SCED model, which is also characterized by linear programming modeling framework. Here, not only quadratic generation cost curves are modeled by PWL, but also AC/DC power losses are calculated by piecewise linear functions, as detailed in Subsections 2.8 and 2.7, respectively. In this case, however, the VSC-based AC/DC transmission system is linearly represented by busbar angles for the AC grids and voltages magnitudes for the DC grid, as presented in Subsections 2.20, respectively. The SCOPF model is general in nature as it can accommodate any network topology with multiple VSC-connected AC grids.

4.1. Fundamentals of the SCOPF problem

The OPF formulation can be simply stated as in (4.1) - (4.5), where (4.1) is the minimization of the objective function F usually minimizing the system operating costs, subject to (4.2) which stands for equality constraints g, usually generation-demand balance equations. This is also subject to inequality constraints h (4.3), commonly representing series branch power flow limits. The optimal solution is bounded around lower and upper limits on state (4.4) and control (4.5) variables, respectively [78].

$$min\ F(x,u) \tag{4.1}$$

Subject to:

$$g(x,u) = 0 \tag{4.2}$$
$$h(x,u) \leq 0 \tag{4.3}$$
$$x^{min} \leq x \leq x^{max} \tag{4.4}$$
$$u^{min} \leq u \leq u^{max} \tag{4.5}$$

where u represents control variables and x are state variables. In the context of a linear OPF model, u usually contains power generations and x are busbar angles of the power grid.

An OPF can be characterized by an operating security analysis considering the related network constraints while assessing the well-known N-1 criterion, i.e., executing the N-1 contingency analysis. In this sense, the security constrained OPF (SCOPF) aims at minimizing the generation dispatch costs considering different transmission and generation outages, one at a time. In this sense, there are two main SCOPF models widely used in the literature, i.e., (*i*) preventive and (*ii*) corrective formulations [34]:

i. The preventive formulation considers N-1 contingencies in the model constraints, i.e., the generation dispatches account for the possible contingencies that can occur in the power system. Therefore, an increase on the system operating costs is expected.

ii. The corrective approach permits changes over control variables when solving the optimization problem, i.e., a corrective action takes place to achieve safe operating points in post-contingency conditions, e.g., power rescheduling action by generators. It is worth mentioning that this is the approach adopted in this thesis work.

4.2. AC systems and generators with power rescheduling

The post-disturbance, steady-state turbine-governor response of conventional generation units is suitably represented by (4.6a), which enables power rescheduling driven by the droop control response following a contingency [85, 92]. If the internal losses of generators are to be ignored and assuming that the power plant is connected at bus *k*, (4.6b) holds true.

$$(a)\ P_m = P_m^{ref} - \left(D + \frac{1}{R}\right)\Delta f \qquad \Rightarrow \qquad (b)\ P_{gk} \approx P_{gk}^{ref} - \left(D + \frac{1}{R}\right)\Delta f \tag{4.6}$$

where P_m represents the post-contingency generator mechanical power and P_m^{ref} is the pre-contingency operating point of the generator's turbine. P_{gk} is the post-contingency active power output of the generator, P_{gk}^{ref} stands for the pre-contingency reference power; D is the damping and R is the droop constant, also known as statism; $\Delta f = f - f_0$ is the system frequency deviation, being f the actual frequency and f_0 the nominal frequency, respectively.

In this sense, the load dependency on the system frequency deviations can be considered as shown in (4.7). Equation (4.7a) is the frequency/voltage dependence load model for active power demand, which is widely used in power systems contingencies assessment [85, 93]. For high-voltage networks and on the assumption *ii*) discussed in Subsection 2.2, (4.7a) can be linearly represented by (4.7b). This means the load model is only a function of the frequency variation Δf, which is used in the SCOPF model developed in this thesis.

$$(a)\ P_{dk} = P_{dk}^0\left(1 + k_p\Delta f\right)\left[p_p + p_c\left(\frac{V_k}{V_k^0}\right) + p_z\left(\frac{V_k}{V_k^0}\right)^2\right] \ \Rightarrow\ (b)\ P_{dk} \approx P_{dk}^0\left(1 + k_p\Delta f\right) \tag{4.7}$$

where P^0_{dk} represents the pre-contingency active power demand at bus k; p_p, p_c, and p_z, are the coefficients of the voltage-dependency characteristic; V_k^0 stands for the pre-contingency voltage at bus k and k_p is the coefficient of the frequency dependency.

Based on these backgrounds, it is possible to obtain a linear power flow model considering both power rescheduling by generators and frequency-dependency of loads, all this departing from the linear power flow model given in Subsection 2.2. Therefore, by suitably combining (4.6b), (4.7b) and (2.6), (4.8) is derived which permits to estimate the post-

contingency power flows and frequency after load/generation outages, all this for ρ-bus AC systems.

$$\begin{bmatrix} P_{g1}^{ref} - P_{d1}^{0} \\ \vdots \\ P_{gi}^{ref} - P_{di}^{0} \\ \vdots \\ P_{g\rho}^{ref} - P_{d\rho}^{0} \end{bmatrix} = \begin{bmatrix} D_1 + R_1^{-1} + k_{p1} P_{d1}^{0} & B_{11} & \cdots & B_{1i} & \cdots & B_{1\rho} \\ \vdots & \vdots & \ddots & \vdots & \ddots & \vdots \\ D_i + R_i^{-1} + k_{pi} P_{di}^{0} & B_{k1} & \cdots & B_{ii} & \cdots & B_{i\rho} \\ \vdots & \vdots & \ddots & \vdots & \ddots & \vdots \\ D_\rho + R_\rho^{-1} + k_{p\rho} P_{d\rho}^{0} & B_{n1} & \cdots & B_{\rho i} & \cdots & B_{\rho\rho} \end{bmatrix} \begin{bmatrix} \Delta f \\ \theta_1 \\ \theta_i \\ \vdots \\ \theta_\rho \end{bmatrix} \tag{4.8}$$

where susceptances are $B_{kk} = \sum_{m \in k} x_{km}^{-1}$ and $B_{km} = -x_{km}^{-1}$, as explained in detail in Subsection 2.2.

Expression (4.8) can be consequently expressed in compact form as in (4.9a). Furthermore, for multi-terminal VSC-HVDC grids with α AC sub-systems, there will be as many sets of linear equations (4.9a) as the number of AC sub-systems, each one with its own frequency, as expressed in (4.9b).

$$(a)\ \ \mathbf{P}_{ac} = \mathbf{B}_{ac}^{droop} \boldsymbol{\Psi}, \qquad \Rightarrow \qquad (b)\ \ \mathbf{P}_{aci} = \mathbf{B}_{aci}^{droop} \boldsymbol{\Psi}_i, \quad \forall i \in \mathbb{Z}_\alpha \tag{4.9}$$

where $\mathbb{Z}_\alpha$ is the set of AC subsystems comprising the AC/DC system. In line with the previous derivations, it can be stated that for each AC sub-system there are ρ power balance equations and ρ+1 state variables. In the same way that conventional power flow methods, one reference angle must be defined for each AC sub-network, say $\theta_1 = 0$. Nevertheless, this does not imply that this angle is related to a slack generation necessarily. Equally important is the fact that the output power by the power plants is rescheduled according to their corresponding droop control characteristic, as determined by (4.6b).

4.3. DC system and VSC stations with power rescheduling

The VSC and DC network models introduced in Subsections 2.4 and 2.5 are used in this subsection to formulate their linear power flow equations in matrix form, aiming at their preparation for the SCOPF optimization model described later in Subsection 4.4. In this regard, the power balance equations at ports *v* and *j* of the VSC units, shown in Figure 2.4, can be represented as in (4.10) by expressing the mismatch equations at the converter's internal AC node *v* and DC node *j*, using the VSC power flows (2.26) and (2.29).

$$\begin{bmatrix} \mathbf{P}_v \\ \mathbf{P}_{dc} \end{bmatrix} = \begin{bmatrix} \mathbf{B}_{vv} & -\mathbf{B}_{v\phi} & \mathbf{0} \\ -\mathbf{B}_{v\phi} & \mathbf{B}_{v\phi} & \mathbf{G}_{dc} \end{bmatrix} \begin{bmatrix} \boldsymbol{\theta}_v \\ \boldsymbol{\Phi} \\ \mathbf{E}_{dc} \end{bmatrix} \tag{4.10}$$

where submatrices in (4.10) are given in detail in equations (4.11), (4.12) and (4.13), that is,

$$\mathbf{P}_v = \begin{bmatrix} -P_{d1}^0 & \cdots & -P_{d\alpha}^0 \end{bmatrix}^T, \ \mathbf{P}_{dc} = \begin{bmatrix} -P_{dc1}^0 & \cdots & -P_{dc\alpha}^0 \end{bmatrix}^T \tag{4.11}$$

$$\mathbf{B}_{vv} = \begin{bmatrix} x_{ph1}^{-1} + x_{tr1}^{-1} & & 0 \\ & \ddots & \\ 0 & & x_{ph\alpha}^{-1} + x_{tr\alpha}^{-1} \end{bmatrix}, \ \mathbf{B}_{v\phi} = \begin{bmatrix} x_{ph1}^{-1} & & 0 \\ & \ddots & \\ 0 & & x_{ph\alpha}^{-1} \end{bmatrix}, \ \mathbf{G}_{dc} = \begin{bmatrix} G_{11} & \cdots & G_{1\sigma} \\ \vdots & \ddots & \vdots \\ G_{\sigma 1} & \cdots & G_{\sigma\sigma} \end{bmatrix} \tag{4.12}$$

$$\boldsymbol{\theta}_v = \begin{bmatrix} \theta_{v1} & \cdots & \theta_{v\alpha} \end{bmatrix}^T, \ \boldsymbol{\Phi} = \begin{bmatrix} \phi_1 & \cdots & \phi_{v\alpha} \end{bmatrix}^T, \ \mathbf{E}_{dc} = \begin{bmatrix} E_1 & \cdots & E_\sigma \end{bmatrix}^T \tag{4.13}$$

where σ is the number of DC nodes and α is the number of VSC stations, i.e., it is the same number of AC sub-systems. Vectors $\mathbf{P}_v$, $\mathbf{P}_{dc}$ contain the power injections at busbars v and DC busbars, respectively. Matrix $\mathbf{G}_{dc}$ is the conductance matrix whose terms are calculated based on the DC grids linear modeling explained in Subsection 2.5.1, following the same procedure for AC systems modeling, see Subsection 2.2. Submatrix $\mathbf{B}_{vv}$ is a diagonal matrix containing the sum of the inverses of the filter and step-up transformer reactances. Submatrix $\mathbf{B}_{v\phi}$ is a diagonal matrix containing the inverse of the filter reactance. Likewise, vectors $\boldsymbol{\theta}_v$, $\boldsymbol{\Phi}$, and $\mathbf{E}_{dc}$ accommodate the state variable of the AC/DC system, i.e., the AC nodal voltage angles, the VSC phase angles and the DC voltage magnitudes, respectively.

- *On the consideration of VSC control strategies including power rescheduling*

It should be emphasized that one of the features of the proposed SCOPF model is the power rescheduling by VSC stations in the AC/DC grid. And this must be carried out through the voltage/power droop control characteristic of the converters, just like it was made for the generator units in the previous section. However, for a comprehensive formulation, all the state-of-the-art VSC control strategies should be considered. It should be then recalled that there are four VSC control strategies which were addressed in Subsection 0, particularly in Table 2.2: voltage control, scheduled power control, passive control and voltage/power droop control, with the latter being the one enabling power rescheduling according to

voltage drops in the DC bus ports E_j. For clarity, that table is replicated below showing the control strategies and associated power flow equations,

Table 4.1 VSC control strategies and associated variables

Type	Acronym	Controlled variable	Reference value	VSC equation
Slack	VSC - E_{ctrl}	E_j	E^{ref}	$P_{jv} = (\phi - \theta_v)/x_{ph}$
Schedule	VSC - P_{ctrl}	P_{jv}	$P_{jv} = P^{ref}$	$P^{ref} = (\phi - \theta_v)/x_{ph}$
Passive	VSC - P_{ass}	P_{jv}	$\phi = \phi^{ref}$	$P_{jv} = (\phi^{ref} - \theta_v)/x_{ph}$
Droop control	VSC - E/P_{ctrl}	E_j , P_{jv}	E^{ref} , P^{ref}	$P_{jv} = P^{ref} - K_c\,(E^{ref} - E_j)$

Using the previous VSC power flow definitions of Table 4.1 and formulating the nodal power balances in the classic way as it is made for AC or DC networks, equation (4.14) is obtained to represent the linear power flow model for the γ VSC-connected AC systems with scheduled power control, VSC - P_{ctrl}. Similarly, (4.15) is the linear power flow model for δ VSC-connected AC systems with voltage/power droop control, VSC - E/P_{ctrl}.

$$\mathbf{P}_P^{ref} = \begin{bmatrix} \mathbf{B}_{p1} & -\mathbf{B}_{p1} & 0 \\ \vdots & \vdots & \vdots \\ \mathbf{B}_{p\gamma} & -\mathbf{B}_{p\gamma} & 0 \end{bmatrix} \begin{bmatrix} \boldsymbol{\theta}_v \\ \boldsymbol{\Phi} \\ \mathbf{E}_{cd} \end{bmatrix} \tag{4.14}$$

$$\mathbf{P}_{E/P}^{ref} = \begin{bmatrix} \mathbf{B}_{p1} & -\mathbf{B}_{p1} & \mathbf{K}_1 \\ \vdots & \vdots & \vdots \\ \mathbf{B}_{p\delta} & -\mathbf{B}_{p\delta} & \mathbf{K}_\delta \end{bmatrix} \begin{bmatrix} \boldsymbol{\theta}_v \\ \boldsymbol{\Phi} \\ \mathbf{E}_{cd} \end{bmatrix} - \mathbf{E}^{ref}\mathbf{K}_c \tag{4.15}$$

$$\begin{aligned} &\mathbf{P}_P^{ref} = \begin{bmatrix} P_1^{ref} & \cdots & P_\gamma^{ref} \end{bmatrix}^T,\ \mathbf{P}_{E/P}^{ref} = \begin{bmatrix} P_1^{ref} & \cdots & P_\delta^{ref} \end{bmatrix}^T,\ \mathbf{B}_{pi} = \begin{bmatrix} 0 & \cdots & x_{phi}^{-1} & 0 & \cdots \end{bmatrix}^T \\ &\mathbf{K}_i = \begin{bmatrix} 0 & \cdots & K_{ci} & 0 & \cdots \end{bmatrix}^T,\ \mathbf{E}^{ref} = \mathbf{I}\begin{bmatrix} E_1^{ref} & \cdots & E_\delta^{ref} \end{bmatrix}^T,\ \mathbf{K}_c = \begin{bmatrix} K_{c1} & \cdots & K_{c\delta} \end{bmatrix}^T \end{aligned} \tag{4.16}$$

where submatrices in (4.14) and (4.15) are given in (4.16). Vectors $\mathbf{P}_p^{ref}$, $\mathbf{P}_{E/P}^{ref}$ contain the reference powers of the γ and δ converters with fixed power and voltage/power droop controls, respectively. Matrices $\mathbf{B}_p$ include the inverse of reactor reactances, x_{ph}. Vector $\mathbf{K}_i$ contains the droop control gain of the *i-th* VSC - E/P_{ctrl}. $\mathbf{E}^{ref}$ is a diagonal matrix containing δ reference DC voltages relating to converters VSC - E/P_{ctrl}, and $\mathbf{I}$ is an identity matrix of suitable order. Vector $\mathbf{K}_c$ accommodates the droop gains for stations VSC - E/P_{ctrl}.

4.4. Proposed SCOPF for VSC-based AC/DC grids with power rescheduling

The proposed SCOPF model for multi-terminal VSC-based AC/DC networks developed in this thesis is presented herein. This is a formulation where, as discussed in previous sections, generator units and VSC stations are set to provide power rescheduling according to their own voltage/power droop control characteristics. Each set of equality and inequality constraints of the optimization model is presented in detail. As observed next, the proposed SCOPF model is formulated for β converters VSC - E_{ctrl}, γ converters VSC - P_{ctrl}, δ converters VSC -E/P_{ctrl}, and η converters of the type VSC - P_{ass}.

- **Objective function**

Equation (4.17) represents the minimization of the objective function of the proposed SCOPF model, where the total operation cost is minimized, considering *ng* dispatchable generators.

$$\min \sum_{k=1}^{ng}\left(c_k + \sum_{i=1}^{ns} m_{gk,i}\bar{P}_{gk,i} \right) \tag{4.17}$$

It is worth emphasizing that generation unit costs functions are linearly described according to the PWL technique, as it was detailed in Subsection 2.8.

- **Nodal power balances of the AC/DC system**

In judiciously combining (4.9) - (4.10), expression (4.18) is obtained to represent the linear power flow model, through nodal power balances, of the entire AC/DC system, which involves all α VSC-connected AC sub-systems, $i \in \mathbb{Z}_\alpha$.

$$\begin{bmatrix} \mathbf{P}_{aci} \\ \mathbf{P}_{v} \\ \mathbf{P}_{dc} \end{bmatrix} = \begin{bmatrix} \mathbf{B}_{aci}^{droop} & \mathbf{0} & \cdots & \mathbf{0} \\ \mathbf{0} & \mathbf{B}_{vv} & -\mathbf{B}_{v\phi} & \vdots \\ \mathbf{0} & -\mathbf{B}_{v\phi} & \mathbf{B}_{v\phi} & \mathbf{G}_{dc} \end{bmatrix} \begin{bmatrix} \boldsymbol{\Psi}_{i} \\ \boldsymbol{\theta}_{v} \\ \boldsymbol{\Phi} \\ \mathbf{E}_{dc} \end{bmatrix} + \mathbf{C}_{m}^{T} \begin{bmatrix} \bar{\mathbf{P}}_{ac}^{loss} \\ \vdots \\ \bar{\mathbf{P}}_{dc}^{loss} \end{bmatrix}, \qquad \forall i \in \mathbb{Z}_{\alpha} \tag{4.18}$$

where $\mathbf{C}_m$ denotes the incidence matrix of order [*LT x NB*], being $LT = la + ld$, the number of transmission branches, and $NB = \alpha{\cdot}\rho + \sigma$ is the number of buses of the entire AC/DC system. In this model it is considered that the AC/DC grid contains *la* AC branches, *ld* DC branches, α AC subsystems with ρ nodes each one, and with the DC grid containing σ

nodes. Note that this SCOPF formulation includes the AC losses, $\bar{\mathbf{P}}_{ac}^{loss}$, and DC losses, $\bar{\mathbf{P}}_{dc}^{loss}$, by PWL technique, just in the same way as it was described in Subsection 2.7.

- **Power flows through AC/DC branches**

Expression (4.19) allows the calculation of AC/DC transmission power flows, noticing that both AC losses, $\bar{\mathbf{P}}_{ac}^{loss}$, and DC losses, $\bar{\mathbf{P}}_{dc}^{loss}$, also appear here, as expected, for improved accuracy of the SCOPF results.

$$\begin{bmatrix} \mathbf{P}_{ac,km} \\ \vdots \\ \mathbf{P}_{dc,jm} \end{bmatrix} = \begin{bmatrix} \mathbf{b}_{bri} & & \mathbf{0} \\ & \mathbf{b}_{vbr} & \\ \mathbf{0} & & \mathbf{g}_{br} \end{bmatrix} \mathbf{C}_m \begin{bmatrix} \boldsymbol{\Psi}_i \\ \boldsymbol{\theta}_v \\ \boldsymbol{\Phi} \\ \mathbf{E}_{cd} \end{bmatrix} + \begin{bmatrix} \bar{\mathbf{P}}_{ac}^{loss} \\ \vdots \\ \bar{\mathbf{P}}_{dc}^{loss} \end{bmatrix}, \qquad \forall i \in \mathbb{Z}_{\alpha} \tag{4.19}$$

where submatrices $\mathbf{b}_{bri}$ and $\mathbf{b}_{vbr}$ are diagonal matrices containing the inverse of the AC branches reactances, $(x_{km})^{-1}$, and VSC phase reactors $(x_{ph})^{-1}$, respectively. Besides, submatrix $\mathbf{g}_{br}$ is a diagonal matrix containing the inverse of DC line resistances, $(r_{jm})^{-1}$.

- **Constraints related to converters VSC - P_{ctrl} and VSC - E/P_{ctrl}**

The operating constraints associated with converters with fixed power flow control VSC - P_{ctrl} and voltage/power droop control VSC - E/P_{ctrl} are given in (4.20a) - (4.20b), respectively. The detailed mathematical model (4.20) can be found in Subsection 4.3.

$$\begin{aligned} (a)\ \ \mathbf{P}_P^{ref} &= \begin{bmatrix} \mathbf{B}_{p1} & -\mathbf{B}_{p1} & \mathbf{0} \\ \vdots & \vdots & \vdots \\ \mathbf{B}_{p\gamma} & -\mathbf{B}_{p\gamma} & \mathbf{0} \end{bmatrix} \begin{bmatrix} \boldsymbol{\theta}_v \\ \boldsymbol{\Phi} \\ \mathbf{E}_{dc} \end{bmatrix} \\ (b)\ \ \mathbf{P}_{E/P}^{ref} &= \begin{bmatrix} \mathbf{B}_{p1} & -\mathbf{B}_{p1} & \mathbf{K}_1 \\ \vdots & \vdots & \vdots \\ \mathbf{B}_{p\delta} & -\mathbf{B}_{p\delta} & \mathbf{K}_{\delta} \end{bmatrix} \begin{bmatrix} \boldsymbol{\theta}_v \\ \boldsymbol{\Phi} \\ \mathbf{E}_{dc} \end{bmatrix} - \mathbf{E}^{ref}\mathbf{K}_c \end{aligned} \tag{4.20}$$

- **Generation operating limits**

Expression (4.21) permits to enforce the generators operating limits through the PWL technique, noticing that each linear segment of the generator power is bounded, where *ns* is the total number of segments dividing the nonlinear cost function, see Subsection 2.8. Indeed, all generator units must fulfill the minimum power limit, P_g^{min}, and the maximum power output, P_g^{max}, i.e., $P_g^{min} \leq P_g \leq P_g^{max}$.

$$0 \le \bar{P}_{gk,i} \le \frac{P_{gk}^{\max}}{ns}, \qquad \forall k \in \mathbb{Z}_{ng},\ \forall i \in \mathbb{Z}_{ns} \tag{4.21}$$

- **Frequency deviation limits**

In this proposed corrective SCOPF method, the response of generators and loads are both dictated by the frequency deviation of each AC sub-system, Δf, as consequence of the selected contingencies to be evaluated. With expression (4.22), the minimum, Δf_i^{min}, and maximum, Δf_i^{max}, frequency deviation limits are enforced for all AC sub-systems, $i \in \mathbb{Z}_\alpha$, forming the multi-terminal AC/DC arrangement. That is,

$$\Delta f_i^{\min} \le \Delta f_i \le \Delta f_i^{\max}, \qquad \forall i \in \mathbb{Z}_\alpha \tag{4.22}$$

- **AC/DC power losses**

The AC/DC power losses obtained by PWL are given by (4.23), according to Subsection 2.7. Equation (4.23a) permits to estimate the AC branch power losses, whereas (4.23b) enables the power loss calculation for the transmission lines forming the DC grid.

$$\begin{aligned}
&\bar{P}_{ac}^{loss} = \sum_{i=1}^{ns} m_{km,i}\bar{P}_{km,i},\ \ 0 \le \bar{P}_{km,i} \le \frac{P_{km}^{\max}}{ns}, \qquad \forall km \in \mathbb{Z}_{la},\ \forall i \in \mathbb{Z}_{ns} \\
(a)\quad &\bar{P}_{km} = \bar{P}_{ac}^{(+)} + \bar{P}_{ac}^{(+)},\ \ \bar{P}_{ac}^{(+)},\ \bar{P}_{ac}^{(+)} \ge 0 \\
&\bar{\mathbf{P}}_{ac}^{loss} = \left[\, \bar{P}_{ac,1}^{loss} \quad \cdots \quad \bar{P}_{ac,km}^{loss} \,\right]^T, \qquad \forall km \in \mathbb{Z}_{la}
\end{aligned} \tag{4.23}$$

$$\begin{aligned}
&\bar{P}_{dc}^{loss} = \sum_{i=1}^{ns} m_{jm,i}\bar{P}_{jm,i},\ \ 0 \le \bar{P}_{jm,i} \le \frac{P_{jm}^{\max}}{ns}, \qquad \forall jm \in \mathbb{Z}_{la},\ \forall i \in \mathbb{Z}_{ns} \\
(b)\quad &\bar{P}_{jm} = \bar{P}_{dc}^{(+)} + \bar{P}_{dc}^{(+)},\ \ \bar{P}_{dc}^{(+)},\ \bar{P}_{dc}^{(+)} \ge 0 \\
&\bar{\mathbf{P}}_{dc}^{loss} = \left[\, \bar{P}_{dc,1}^{loss} \quad \cdots \quad \bar{P}_{dc,jm}^{loss} \,\right]^T, \qquad \forall jm \in \mathbb{Z}_{ld}
\end{aligned}$$

where this is carried out for the AC sub-systems, $km \in \mathbb{Z}_{la}$, and with the same being true for the DC grid branches, $jm \in \mathbb{Z}_{ld}$. Note that these power losses are used in (4.18) - (4.19).

- **AC/DC transmission limits**

Aiming to preserve the operation security of the VSC-based AC/DC system, it is necessary to consider the transmission limits for both AC systems and DC grid. In this sense, with (4.24a) the maximum power limits of the AC transmission branches are observed, whereas (4.24b) allows observing the maximum power limits of DC lines.

$$\begin{aligned} &(a)\quad \mathbf{P}_{ac,km} \le P_{km}^{\max} && \forall km \in \mathbb{Z}_{la} \\ &(b)\quad \mathbf{P}_{dc,jm} \le P_{jm}^{\max} && \forall jm \in \mathbb{Z}_{ld} \end{aligned} \tag{4.24}$$

where vector $\mathbf{P}_{ac,km}$ contains the AC power flows including AC power losses, with the same being true for $\mathbf{P}_{dc,jm}$ which contains the DC power flows plus losses, as seen in (4.19).

- **Concluding remarks on the proposed SCOPF formulation**

Key information related to the SCOPF problem was addressed in previous sections, starting with the general philosophy of OPF studies, as summarized by (4.1) - (4.5). Indeed, this is the basis for the comprehension of OPF models within the power system economic operation context. Hence, the SCOPF model proposed in this doctoral thesis was given in (4.17) - (4.24), where the objective function and model constraints were explained with enough detail. The formulation related to the new corrective SCOPF problem for VSC-based AC/DC systems is summarized as follows:

Eqn. (4.17)

subject to **Eqns. (4.18) - (4.24)**

4.4.1. Pre-contingency OPF calculations

The first step consists in initializing the method. For this purpose, it is necessary to know the AC/DC system pre-contingency condition, this being the reference point for subsequent calculations in the post-contingency stage. At the outset, it is necessary to define the reference power for all γ and δ converters, with power control, $\mathbf{P}_{P}^{ref}$, and voltage/power droop control, $\mathbf{P}_{E/P}^{ref}$, respectively, as well as the power network load pattern. With it, the pre-contingency operating point is calculated by solving the SCOPF model (4.17) - (4.24), but without considering the droop control responses of generator units and VSC stations. This implies the following considerations:

i. For all the α AC sub-systems, the generators' droop control response is overlooked by deleting the rows and columns related to the droop control modeling in (4.8), thus obtaining the power flow model given by (2.7).

ii. For all the δ converters featuring power rescheduling by voltage/power droop control response, VSC - E/P_{ctrl}, this characteristic is omitted by setting $\{\mathbf{K}_1,\ldots,\mathbf{K}_\delta\} = \mathbf{0}$ and $\mathbf{K}_c = \mathbf{0}$ in (4.20b).

Upon successful calculation of the AC/DC system pre-contingency condition by solving (4.17) - (4.24) using the previous considerations, the reference powers of the *ng* generators, P_{gk}^{ref}, and the DC voltage reference of the δ converters with power rescheduling, E^{ref}, can be determined to enable the droop control response of these two power equipment in post contingency conditions.

4.4.2. Post-contingency SCOPF calculations

The second step of the proposed method involves the calculation of the AC/DC system post-contingency conditions, using (4.17) - (4.24). In this case, the droop control response by generators and converters is considered as described in Subsections 4.2 and 4.3, respectively. It is worth mentioning that the proposed method permits the evaluation of any element disconnection through the *N*-1 criterion.

4.4.3. Summary of the proposed SCOPF formulation

Figure 4.1 shows a flowchart illustrating how the proposed SCOPF model is applied to solving VSC-based AC/DC systems with power rescheduling by generators and converters. In this methodology, the assessment of the system response of all AC sub-networks and DC grid is carried out simultaneously when considering the *N*-1 contingency criterion. The main steps involved in this algorithm are explained next:

- **Step 1:** All the data required for the pre-contingency OPF calculation are charged and processed, that is, system demand, generation cost curves, AC/DC transmission grid parameters, and VSC parameters and controls.
- **Step 2:** The pre-contingency OPF calculation is carried out to set up reference values of the generation dispatch and VSC power flows. All assumptions described in Subsection 4.4.1 are considered in this step.
- **Step 3:** Each contingency is evaluated using the proposed SCOPF model (4.17) - (4.24). All parameters required for power rescheduling generators and VSC units are considered in this step. Likewise, the set of contingencies, *nc*, is to be assessed.

- **Step 4:** This step seeks to check if the selected set of contingencies, *nc*, has been evaluated, aimed to obtain the optimal solution for the multi-terminal VSC-based AC/DC grid within the proposed corrective SCOPF method.
- **Step 5:** The results report is carried out in this last step.

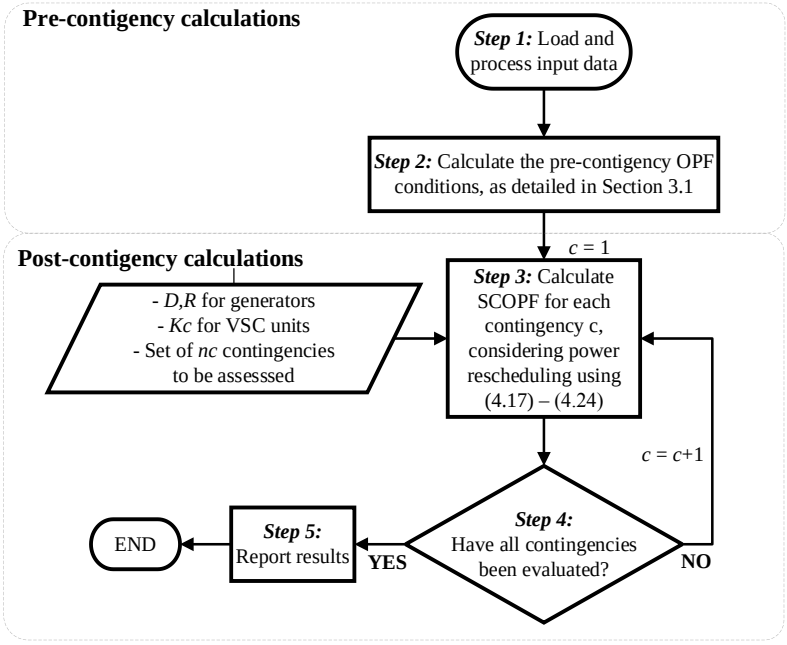

Figure 4.1 Flowchart for the proposed SCOPF formulation

Chapter 5

5. Unit Commitment for AC/DC Systems Including BESS with Energy Time-shifting Strategy

The transmission system operators (TSO) in control centers are responsible for establishing the scheduling (on/off) of generating units to be committed and dispatched, usually one day in advance in an hourly basis. This procedure is known as unit commitment (UC), whose resulting committed generation units are key supplies for the SCED and SCOPF models [53, 78, 93]. These power system calculations are quite demanding because not only there is an obligation for TSO to yield useful results, but also these must be available in time to take the most pertinent decision on the system operation. This problem aggravates further when power system models increase in complexity, as is the case of UC models applied to VSC-based AC/DC networks. Indeed, the study of hybrid networks is unavoidable because they are being deployed worldwide to upgrade the existing transmission systems with proven technical benefits [1, 83-87]. Furthermore, TSO must deal with other kinds of controllable power sources, such as BESS, to make the power grid more flexible due to its relatively low-cost charge/discharge actions [4-6].

This chapter addresses the UC problem in multi-terminal VSC-based AC/DC grids considering BESS with energy time-shifting strategy. The BESS charge/discharge operations are defined within the 24-hour planning horizon for the day ahead, thus promoting a high competition level of energy trading in the power grid. The AC/DC transmission network is formulated via shift factors, where power losses and nonlinear generation cost functions are suitably considered by the PWL technique. Considering all these aspects, the UC model developed in this thesis is featured by a Mixed-integer Linear Programming (MILP) formulation.

5.1. Fundamentals of the UC problem

The UC problem in power systems aims to find the optimal start-up and shut-down schedule of all generation units possible to be committed, looking to always satisfying the system demand for predefined planning horizon periods, e.g., 24 hours a day. This optimization problem considers the security and operating constraints in combination with binary variables that permit to determine the on/off statuses of the generator units over the planning horizon. UC analyses are often addressed by a MILP formulation through the linearization of both objective function and set of constraints [53, 54, 93]. A classic formulation of the UC problem is presented next, observing that the intrinsic nature of the optimization model is characterized by a multiperiod problem. Hence, the UC model must be solved for T periods, $t \in \mathbb{Z}_T$, considering ng generation units, $k \in \mathbb{Z}_{ng}$, as follows:

$$\min \sum_{t=1}^{T}\sum_{k=1}^{ng}\left(b_k P_{gk(t)} + c_k v_{k(t)} + s_k^{su}\tau_{k(t)}^{on} + s_k^{sd}\tau_{k(t)}^{off}\right) \tag{5.1}$$

Subject to:

$$\mathbf{\Delta P}_{(t)} = \mathbf{B}\boldsymbol{\theta}_{(t)} + \mathbf{P}_{(t)}^{loss}, \qquad \forall t \in \mathbb{Z}_T \tag{5.2}$$

$$-P_{km}^{\max} \le \left(\frac{\theta_{k(t)} - \theta_{m(t)}}{x_{km}}\right) + P_{km(t)}^{loss} \le P_{km}^{\max}, \qquad \forall km \in \mathbb{Z}_{la},\ \forall t \in \mathbb{Z}_T \tag{5.3}$$

$$\sum_{k=1}^{ng} P_{gk}^{\max} v_{k(t)} - \sum P_{d(t)} \ge SR_{(t)}, \qquad \forall t \in \mathbb{Z}_T \tag{5.4}$$

$$P_{gk}^{\min} v_{k(t)} \le P_{gk(t)} \le P_{gk}^{\max} v_{k(t)}, \qquad \forall k \in \mathbb{Z}_{ng}, \forall t \in \mathbb{Z}_T \tag{5.5}$$

$$P_{gk(t)} - P_{gk(t-1)} \le RU_k, \qquad \forall k \in \mathbb{Z}_{ng}, \forall t \in \mathbb{Z}_T \tag{5.6}$$

$$P_{gk(t-1)} - P_{gk(t)} \le RD_k, \qquad \forall k \in \mathbb{Z}_{ng}, \forall t \in \mathbb{Z}_T \tag{5.7}$$

$$v_{k(t)} - v_{k(t-1)} = \tau_{k(t)}^{on} - \tau_{k(t)}^{off}, \qquad \forall k \in \mathbb{Z}_{ng}, \forall t \in \mathbb{Z}_T \tag{5.8}$$

$$\sum_{i=t-UT_k+1}^{t} \tau_{k(i)}^{on} \le v_{k(t)}, \qquad \forall k \in \mathbb{Z}_{ng}, \forall t \in \left[UT, \mathbb{Z}_T\right] \tag{5.9}$$

$$\sum_{i=t-DT_k+1}^{t} \tau_{k(i)}^{off} \le 1 - v_{k(t)}, \qquad \forall k \in \mathbb{Z}_{ng}, \forall t \in \left[DT, \mathbb{Z}_T\right] \tag{5.10}$$

where (5.1) is the minimization of the objective function related to the power system operation costs while committing the most economic generation units. Note that as opposed to the classical SCED model of Chapter 3 which only considers the linear variable costs *b*, the objective function of the UC model also includes the generation fix costs *c*, together with the generation start-up costs s^{su} and shut-down costs s^{sd}. Also, it is worth highlighting that (5.1) incorporates three binary variables: $v_{k(t)}$ which indicates the on/off status of the *k-th* generation unit at time *t*, $\tau^{on}_{k(t)}$ which indicates if the *k-th* generator turns on at time *t*, and $\tau^{off}_{k(t)}$ indicating if the *k-th* generator turns off at time *t*.

The power system nodal power balances are established by (5.2) which uses the well-known matrix **B** defined in (2.7) of Subsection 2.2. Generation powers P_g and nodal demands P_d are accommodated in the nodal power injection vector $\Delta\mathbf{P} = [P_{g1}\text{-}P_{d1},\ldots, P_{gn}\text{-}P_{dn}]$, while the phase angle vector is $\boldsymbol{\theta} = [\theta_1,\ldots, \theta_\rho]$ and power losses are included in $\mathbf{P}^{loss}$. With respect to transmission limits, these are enforced with (5.3) and bounded by the physical limit P^{max}, while considering the transmission losses, P^{loss}_{km}. Equation (5.4) refers to the power reserve constraint that must be satisfied very time interval *t*. This considers that the available power by all generation units must be higher than the total system demand at time *t* by a certain quantity established by the value of *SR*. The generation lower bound, $P_g{}^{min}$, and upper bound $P_g{}^{max}$, are considered by (5.5). Note that unlike SCED and SCOPF models where generators are always turned on, in the UC model both possibilities are considered, i.e., on/off states of the generation units $v_{k(t)}$, recalling that the UC problem aims to find the on/off statuses of generating units upon solution of the optimization model.

From one period to the next, generators cannot increase its power production beyond physical limitations; therefore, the ramp-up limit *RU* is considered by constraint (5.6), while the ramp-down limit *RD* is enforced with (5.7). On the other hand, if a generating unit is on at time *t*, $v_{k(t)} = 1$, then it can be turned off, $\tau^{off} = 1$, but not turned on. Similarly, when a generator is off, $v_{k(t)} = 0$, then it can be turned on, $\tau^{on} = 1$, but not turned off. Following this reasoning, equation (5.8) can be stated to control the on/off operations of generation units, which is known as the logical status equation. When a generating unit is turned on, it must be kept running for a minimum set of time periods before it can be turned off again, which has to do with the thermal processes of the steam turbines. Similarly, when

a generator is turned off, it must be kept off for some periods before it can be turned on again. These aspects are modeled through minimum up-time *UT* and down-time *DT* of generation units, as expressed by (5.9) and (5.10), respectively.

It should be stated that this classic UC model (5.1) – (5.10) is intended for AC transmission system models only. This model must be suitably adapted for VSC-based AC/DC power grids incorporating BESS facilities, this being the hallmark of the proposed UC model introduced in the present work. To this end, both the AC/DC transmission network by shift factors and AC/DC power losses are considered in this novel formulation. One where the operating costs and constraints associated with BESS featured by the energy time-shifting strategy are also included. These improvements of the UC model are duly addressed in the next subsections.

5.2. Generation-demand balances in VSC-based AC/DC systems

For efficient UC calculations, the proposed formulation for VSC-based AC/DC power systems should introduce the hybrid power network through shift factors $\boldsymbol{\Gamma}$, as described in Subsection 2.6. However, it is worth noting that the use of shift factors reflects the relationship between transmission power flows and net power injections $\Delta\mathbf{P}$, as inferred from (2.10). But, as we are dealing with VSC-based HVDC transmission systems, it is quite important to pay attention to the effects of VSC stations on the AC/DC transmission power flows, especially when the hybrid grid contains converters VSC - P_{ctrl}, whose main characteristic is to fix (schedule) the power flow between their corresponding AC and DC ports. For this reason, the variations on nodal power injections applied to an AC sub-system coupled to a converter VSC - P_{ctrl} do not alter the power flows in any other part of the hybrid AC/DC system. Another way to see it is that AC grids connected to the DC network through a converter VSC - P_{ctrl} are electrically decoupled from the rest of the hybrid network.

To illustrate the above discussion, Figure 5.1 depicts a four-terminal VSC-based AC/DC network, where VSC 1 operates in slack mode with voltage control, VSC 2 and VSC 3 are in scheduled power mode, and VSC 4 is a passive type converter feeding into a system with no conventional generation of its own. Based on these definitions, both AC 2 and AC 3

each form one separated area. In contrast, the rest of AC grids, coupled to VSC operating in slack and passive modes, and the DC grid, form one unique area denoted as Π in the figure. In this sense, for the network depicted in Figure 5.1, it is necessary to use three different power balance equations to faithfully describe the interactions in any AC/DC system.

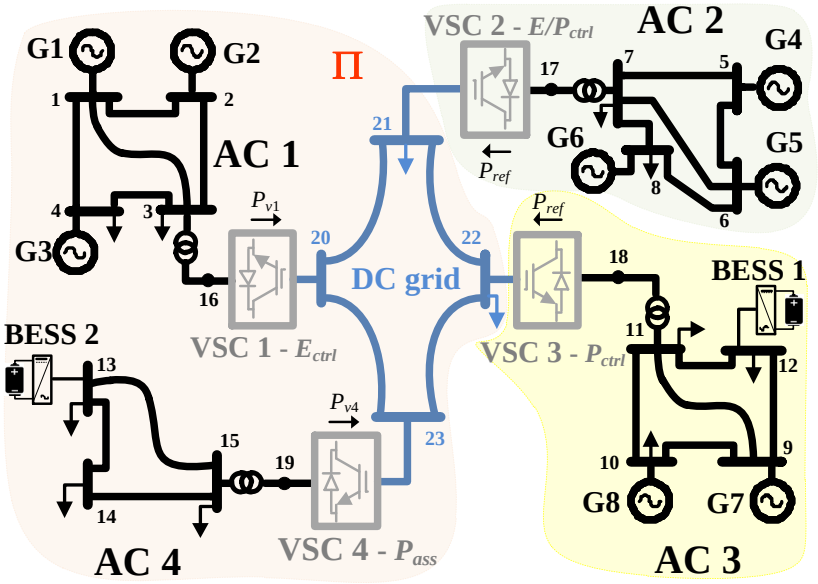

Figure 5.1 Four-terminal VSC-based AC/DC grid with two BESS units

Based on the previous discussion, more than one balance equation is necessary to correctly carry out the power-demand balance in UC calculations when the VSC-based AC/DC network representation is addressed through shift factors. Returning to the power system of Figure 5.1, there must be three balance constraints: (a) the first considering generation, demand, and losses associated with area Π = {AC 1, AC4, DC grid}, (b) the second related to AC 2, and (c) the third related to AC 3, as explicitly formulated by (5.11).

$$
\begin{aligned}
&(a)\ \ \sum P_{gk} = \sum P_{dk} + \sum P_{km}^{loss} + \sum P_{jm}^{loss}; && \forall \{k, km, jm\} \in \Pi \\
&(b)\ \ \sum P_{gk} = \sum P_{dk} + \sum P_{km}^{loss}; && \forall \{k, km\} \in \text{VSC}\,2 - E/P_{ctrl} \\
&(c)\ \ \sum P_{gk} = \sum P_{dk} + \sum P_{km}^{loss}; && \forall \{k, km\} \in \text{VSC}\,3 - P_{ctrl}
\end{aligned}
\tag{5.11}
$$

From this modeling philosophy, it can be generalized that DC grid and AC grids related to converters VSC - E_{ctrl}, VSC – *Pass* require one power balance equation together, whereas one balance equation for each AC grid coupled to converters VSC- P_{ctrl} is needed.

5.3. Proposed UC model for VSC-based AC/DC grids with BESS facilities

The proposed UC model for VSC-based AC/DC power grids incorporating BESS operating with an energy time-shifting strategy is presented next. Each model expression is explained in detail, recalling that the UC model must be solved for *T* periods, $t \in \mathbb{Z}_T$, and considering *ng* committable generation units, $k \in \mathbb{Z}_{ng}$, together with *nb* BESS stations, $j \in \mathbb{Z}_{nb}$.

- **Objective function**

The minimization of the objective function of the proposed UC model is given in (5.12), where the total operation costs are minimized. Here, generation production costs plus BESS operating costs when performing an energy time-shifting strategy are simultaneously minimized. Note that the generator cost function, $\bar{C}_{k(t)}$, shown in (5.12), includes the complete nonlinear cost function linearized by the PWL technique, see Subsection 2.8. Furthermore, (5.12) also includes the operating costs of BESS facilities, as discussed in Subsection 2.10.

$$\min \quad \sum_{t=1}^{T}\left(\sum_{k=1}^{ng}\left[\left(c_k+\sum_{i=1}^{ns} m_{gk,i}\bar{P}_{gk,i(t)}\right)+c_k v_{k(t)}+s_k^{su}\tau_{k(t)}^{on}+s_k^{sd}\tau_{k(t)}^{off}\right]+\sum_{j=1}^{nb}\xi_k\left|P_{bk(t)}\right|\right) \tag{5.12}$$

- **Power balance constraints**

The generation-demand power balances in VSC-based AC/DC systems are given in (5.13). Equation (5.13a) represents the global balance equation for the AC systems coupled to slack and passive converters including the DC grid, all of them belonging to area Π, $\forall \alpha \in \Pi$. Expression (5.13b) denotes the power balance equation for each one of the AC systems coupled to a VSC operating in scheduled power mode, $\forall \beta \in VSC_{Pctrl}$. Note that in both cases, transmission power losses are being considered. Further details on this modeling philosophy of power balance constraints are given in Subsection 5.2.

$$\left.\begin{array}{ll}(a) & \sum P_{g\alpha(t)} = \sum P_{d\alpha(t)} + \sum P_{\alpha(t)}^{loss} \\ (b) & \sum P_{g\beta(t)} = \sum P_{d\beta(t)} + \sum P_{\beta(t)}^{loss}\end{array}\right\} \quad \forall \alpha \in \Pi,\ \forall \beta \in \mathrm{VSC}_{Pctrl},\ \forall t \in \mathbb{Z}_T \tag{5.13}$$

- **Spinning power reserve constraints**

Expression (5.14) represents the spinning power reserve *SR* requirements of the AC/DC grid, aiming at preserving the system operating security. It is worth noting that, as in the case of the power balance constraints, the power reserve margin provided by the generating units will be summed up according to the control strategy of the VSC-connected AC system. In this regard, (5.14a) represents the spinning reserve requirement for generators contained in the Π area, $\forall\alpha\in\Pi$, as explained in Subsection 5.2. Similarly, (5.14b) accounts for the spinning power reserves of generators located at each of the AC systems coupled to VSC units operating in fixed power control mode, $\forall\beta\in VSC_{Pctrl}$.

$$\left.\begin{array}{ll}(a) & \sum P_{g\alpha}^{\max} v_{\alpha(t)} - \sum P_{d\alpha(t)} \geq SR_{\alpha(t)} \\ (b) & \sum P_{g\beta}^{\max} v_{\beta(t)} - \sum P_{d\beta(t)} \geq SR_{\beta(t)}\end{array}\right\} \quad \forall \alpha \in \Pi,\ \forall \beta \in \mathrm{VSC}_{P_{ctrl}},\ \forall t \in \mathbb{Z}_T \tag{5.14}$$

- **Generator related constraints**

As for the UC model for VSC-based AC/DC systems proposed in this thesis, it is necessary to model the generator constraints that also appear in the classic UC model. In this sense, equations (5.5) - (5.10) are incorporated to the developed UC modeling framework as expressed in (5.15). With it, the physical limitations of the generating units are guaranteed.

$$\text{Equations}(5.5)-(5.10), \qquad \forall k \in \mathbb{Z}_{ng}, \forall t \in \mathbb{Z}_T \tag{5.15}$$

- **Power flows through AC/DC branches**

The transmission power flow calculations of the AC/DC branches (5.16) are carried out through shift factors **Γ**, see Subsection 2.6 for more details, recalling that vector $\mathbf{P}_{ac,km}$ accommodates the AC power flows, and $\mathbf{P}_{dc,jm}$ is the vector containing those of DC lines.

$$\begin{pmatrix}\mathbf{P}_{ac,km(t)}\\ \mathbf{P}_{dc,jm(t)}\end{pmatrix} = \boldsymbol{\Gamma}\cdot\Delta\mathbf{P}_{(t)} + \begin{pmatrix}\bar{\mathbf{P}}^{loss}_{ac(t)}\\ \bar{\mathbf{P}}^{loss}_{dc(t)}\end{pmatrix}, \qquad \Delta\mathbf{P}_{(t)} = \begin{pmatrix}\Delta\mathbf{P}_{ac(t)}\\ \Delta\mathbf{P}_{dc(t)}\end{pmatrix} + \begin{pmatrix}\mathbf{P}^{ac}_{b(t)}\\ \mathbf{P}^{dc}_{b(t)}\end{pmatrix}; \qquad \forall t \in \mathbb{Z}_T \tag{5.16}$$

Note that this UC model includes both AC power losses, $\bar{\mathbf{P}}^{loss}_{ac(t)}$, and DC power losses, $\bar{\mathbf{P}}^{loss}_{dc(t)}$. It is worth remembering that the use of shift factors **Γ** avoids the use of AC nodal phase angles and DC voltage magnitudes. In these calculations, the net AC power injections are

placed in vector $\Delta\mathbf{P}_{ac(t)}$, and those of DC power injections are contained in $\Delta\mathbf{P}_{dc(t)}$. Likewise, the BESS power (generation or consumption) injected to AC systems or DC grid are considered in vectors $\mathbf{P}^{ac}_{b(t)}$, $\mathbf{P}^{dc}_{b(t)}$ in suitable locations, respectively.

- **Operating constraints of converters VSC - P_{ctrl}**

The power flows through converters VSC - P_{ctrl} are enforced to a fixed power P_{ctrl} using expression (5.17). Note that these equality constraints of stations VSC - P_{ctrl} are expressed in terms of shift factors. In this sense, (5.17a) permits to control the power at the AC side of the VSC to a value of P_{ctrl}. Similarly, (5.17b) permits to control the power at the DC side of the VSC at the same value but in the opposed sense, i.e., to a power of -P_{ctrl}.

$$\begin{aligned}
&(a)\quad \sum_{k\in m}\left[\Gamma_{km}\cdot\Delta\mathbf{P}_{(t)}+P^{loss}_{km(t)}\right]=P_{ctrl}, \qquad \forall km\in \mathrm{VSC}_{P_{ctrl}},\ \ \forall t\in\mathbb{Z}_T\\
&(b)\quad \sum_{j\in m}\left[\Gamma_{jm}\cdot\Delta\mathbf{P}_{(t)}+P^{los}_{jm(t)}\right]=-P_{ctrl}, \qquad \forall jm\in \mathrm{VSC}_{P_{ctrl}},\ \ \forall t\in\mathbb{Z}_T
\end{aligned} \tag{5.17}$$

- **AC/DC power losses**

Expression (5.18) enables the power loss calculations of the AC/DC transmission network in a linearized way, i.e., by using the PWL technique. Here, (5.18a) represents the AC branch power losses and (5.18b) enables the DC line power loss calculations. This is carried out for all AC branches, $km\in\mathbb{Z}_{la}$, and all DC lines, $jm\in\mathbb{Z}_{ld}$, comprising the entire AC/DC transmission grid. Further details on these power loss calculations can be consulted at Subsection 2.7.

$$\begin{aligned}
&\bar{P}^{loss}_{ac}=\sum_{i=1}^{ns} m_{km,i}\bar{P}_{km,i},\ \ 0\le\bar{P}_{km,i}\le\frac{P^{\max}_{km}}{ns}, \qquad \forall km\in\mathbb{Z}_{la},\ \forall i\in\mathbb{Z}_{ns}\\
&(a)\quad \bar{P}^{loss}_{km}=\bar{P}^{(+)}_{ac}-\bar{P}^{(-)}_{ac};\quad \bar{P}^{(+)}_{ac},\bar{P}^{(-)}_{ac}\ge 0,\\
&\quad \bar{\mathbf{P}}^{loss}_{ac(t)}=\left[\bar{P}^{loss}_{ac,1}\cdots\bar{P}^{loss}_{ac,la}\right]^T, \qquad \forall km\in\mathbb{Z}_{la}\\
&\bar{P}^{loss}_{dc}=\sum_{i=1}^{ns} m_{jm,i}\bar{P}_{jm,i},\ \ 0\le\bar{P}_{jn,i}\le\frac{P^{\max}_{jn}}{ns}, \qquad \forall jm\in\mathbb{Z}_{ld},\ \forall i\in\mathbb{Z}_{ns}\\
&(b)\quad \bar{P}^{loss}_{jm}=\bar{P}^{(+)}_{dc}-\bar{P}^{(-)}_{dc};\quad \bar{P}^{(+)}_{dc},\bar{P}^{(-)}_{dc}\ge 0,\\
&\quad \bar{\mathbf{P}}^{loss}_{dc(t)}=\left[\bar{P}^{loss}_{dc,1}\cdots\bar{P}^{loss}_{dc,ld}\right]^T, \qquad \forall jm\in\mathbb{Z}_{ld}
\end{aligned} \tag{5.18}$$

- **AC/DC transmission limits**

Expression (5.19) enforces the AC/DC transmission limits fulfillment, an aspect that is vital for ensuring a secure system operation. Particularly, (5.19a) ensures that AC branch power flows, $\mathbf{P}_{ac,km(t)}$, remain below the maximum allowed power limits $P_{km}^{\max}$. Analogously, (5.19b) guarantees that DC line power flows, $\mathbf{P}_{dc,jm(t)}$, are smaller than or equal to the upper transmission limit $P_{jm}^{\max}$. Note that both AC/DC power losses are useful for the power flow calculations carried out in (5.16).

$$\begin{aligned} &(a)\ \mathbf{P}_{ac,km(t)} \le P_{km}^{\max}; && \forall km \in \mathbb{Z}_{la},\ \forall t \in \mathbb{Z}_T \\ &(b)\ \mathbf{P}_{dc,jm(t)} \le P_{jm}^{\max}; && \forall jm \in \mathbb{Z}_{ld},\ \ \forall t \in \mathbb{Z}_T \end{aligned} \tag{5.19}$$

- **BESS modeling with energy time-shifting strategy**

The BESS model with energy time-shifting strategy developed in this thesis for the purpose of UC studies is given in (5.20). Particularly, with (5.20a) the basic operating principles of the BESS are captured, ones that have been explained in Subsection 2.10. Meanwhile, the BESS power absolute value linearization is shown in (5.20b), which is important to account for both charge and discharge operation modes of BESS, this being used in the objective function (5.12). Indeed, it should be kept in mind that the energy time-shifting strategy involves both charge and discharge BESS operations, see Subsection 2.10.2. This is a subtle difference with respect to the BESS operating with a load-following strategy, see Subsection 2.10.1, where the discharge feature of the BESS is only considered. Equally important is the fact that the absolute value linearization follows the same mathematical principles applied to generation cost functions and power losses, as discussed in Subsections 2.7 and 2.8.

$$
\begin{aligned}
&(a)\quad \left.\begin{array}{c} W_{j(t)} = W_{j(t-1)} - \Delta t \eta_B P_{bj(t)} \\ -CR_j \le P_{bj(t)} - P_{bj(t-1)} \le DR_j \\ W_j^{\min} \le W_{j(t)} \le W_j^{\max} \\ P_{bj}^{\min} \le P_{bj(t)} \le P_{bj}^{\max} \end{array}\right\} \begin{array}{l} \forall j \in \mathbb{Z}_{nb} \\ \forall t \in \mathbb{Z}_T \end{array} \\
&(b)\quad \left.\begin{array}{c} P_{bj(t)} = \bar{P}_{bj(t)}^{(+)} - \bar{P}_{bj(t)}^{(-)} \\ \left|P_{bj(t)}\right| = \bar{P}_{bj(t)}^{(+)} + \bar{P}_{bj(t)}^{(-)} \\ \bar{P}_{bj(t)}^{(+)},\ \bar{P}_{bj(t)}^{(-)} \ge 0 \end{array}\right\} \begin{array}{l} \forall j \in \mathbb{Z}_{nb} \\ \forall t \in \mathbb{Z}_T \end{array} \\
&(c)\quad \left.\begin{array}{c} P_{bj(t)} \le P_{bj(t-1)} - P_{j(t)}^{CR} \\ P_{j(t)}^{CR} = \min\left\{CR_k\, \Delta t,\ P_{bj(t-1)} - P_{bj(t)}^{\min}\right\} \end{array}\right\} \begin{array}{l} \forall k \in \mathbb{Z}_{nb} \\ \forall t \in \mathbb{Z}'_T \end{array}
\end{aligned}
\tag{5.20}
$$

Expression (5.20c) permits to account for the BESS charging periods of the energy time-shifting strategy, $\forall t \in \mathbb{Z}'_T$, which depends on the BESS charging rate, *CR*. It should be also recalled that the charging hours form a subset of the entire planning horizon $\mathbb{Z}_T$. In this regard, it makes sense to charge the BESS when the demand is low, i.e., during the first and last hours of the day. Therefore, during the rest of the periods, BESS units would operate in discharging mode, thus enabling the so-called energy time-shifting strategy.

- **Concluding remarks on the proposed UC formulation**

Several key aspects related to the UC problem have been addressed in previous sections. For one, to introduce the UC formulation philosophy, the general modeling framework of the UC was described in (5.1) – (5.10). Consequently, the UC model for multi-terminal VSC-based AC/DC grids developed in this doctoral thesis was reported in (5.12) – (5.20), addressing in detail, the objective function, equality, and inequality constraints. The problem formulation related to the new UC model based on MILP for VSC-based AC/DC systems including BESS units is summarized as follows:

Eqn. (5.12)

subject to **Eqns. (5.13) - (5.20)**

5.3.1. Summary of the proposed UC formulation

The proposed algorithm useful for UC studies incorporating BESS with an energy time-shifting strategy in AC/DC grids, is depicted in Figure 5.2. This shows a flowchart illustrating the proposed methodology, whose main steps are summarized next:

- **Step 1:** All the required parameters for the UC study are loaded: system demand curve, generation cost functions, generators start-up and shut-down costs, transmission system parameters, and BESS parameters.
- **Step 2:** The UC is executed according to the model described by (5.12) - (5.20).
- **Step 3:** It is checked if all periods of the UC planning horizon have been assessed.
- **Step 4:** The results report is obtained in this last step.

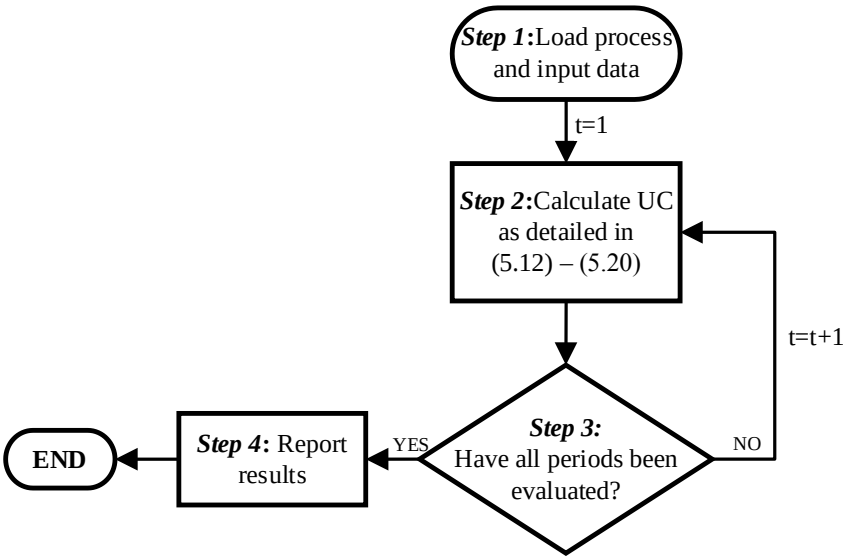

Figure 5.2 Flowchart for the proposed UC formulation

Chapter 6

6. Case studies

This chapter investigates the application of the power system optimization models developed in previous chapters, addressing the economic operation of AC/DC systems including PV plants and BESS. It must be emphasized that the set of power system tools – SCED, SCOPF, and UC – are characterized by a linear programming framework but, regardless of this aspect, it includes the nonlinear effects of transmission power losses and generation cost curves in the formulations by judiciously using the PWL technique.

In this sense, the applicability of the SCED model developed in Chapter 3 is shown first, using two AC test systems with 4-hour operation horizons and 10-minute look-ahead intervals. The first one is the 10-generator IEEE RTS 24-bus system incorporating two BESS with load-following strategy and one PV plant, and the second one is the 69-generator IEEE 300-bus system with five distributed BESS and three PV plants. Next, the SCOPF model for multi-terminal VSC-based AC/DC power systems developed in Chapter 4 [85] is studied using two test systems, one with four VSC-connected AC sub-systems, and the second with seven VSC-coupled AC grids and seventy dispatchable generators. In both cases, the corrective SCOPF method is shown to find the optimum operating points under the N-1 contingency analysis. Finally, the performance of UC model for VSC-based AC/DC grids described in Chapter 5 [86] is analyzed using two case studies. The first contains a four-terminal VSC-based AC/DC grid with eight committable generators and two BESS with energy time-shifting strategy, and to show its practicality, a hybrid power grid with seven VSC-coupled AC grids, five BESS units, and seventy committable generators is studied.

It is worth mentioning that the algorithms related to SCED, SCOPF, and UC, were implemented in Matlab© R2022a, using the optimization tool supported by *linprog* and *intlinprog* solvers.

6.1. Study cases with the SCED model

The optimization SCED model developed in Chapter 3 is studied in this subsection. To this end, a modified version of the IEEE RTS-24 bus test system is used to corroborate the proposed formulation. Then, a modified version of the IEEE 300-bus test system is studied to show the performance of the SCED model using fair-sized power networks.

6.1.1. IEEE 24-bus test system with 2 BESS and 1 PV plant

To conceptually analyze the SCED formulation, for a multi-period power system operation, the IEEE RTS-24 bus test system has been slightly modified to incorporate two BESS operating with a load-following strategy and one PV plant, as depicted in Figure 6.1. This is a power system formed by 24 buses and 10 dispatchable generation units, where the 100-MW PV plant is connected to bus 11, and the two BESS with capacities of P_b^{max} = {40, 50} [MW] are integrated at buses 6 and 8, respectively. The spinning power reserve considered for each generation unit and BESS facility is taken to be of $SR_k = SR_j = 5$ %.

The parameters related to the system load for a base power of S_b =100 MVA are shown in Table 6.1, while Table 6.2 shows the parameters of the BESS, Table 6.3 presents the parameters of PV plants together with the points of the normalized curve P_{mpp} vs S_i, shown in Figure 2.7,2.9, whereas

Table 6.4 provides the parameters of conventional generation units. It should be recalled that the PWL technique is applied to the nonlinear generation cost functions with ns = 12 segments, transmission power losses using ls =12 segments, and PV plant power injection with ns_{pv} = 4 linear segments. For the SCED study, the operation horizon consists of 24 periods, from 10:00 to 14:00 [hr], $\mathbb{Z}_T$ = {10-14} [hr], using time intervals of 10 minutes. The per-unit load pattern of the power system and the per-unit solar irradiance pattern that enables the calculation of the optimum PV power generation are both given in Figure 6.2.

With these input parameters and operating conditions, the multi-period SCED model is run; the results of the optimization tool are discussed next, concentrating on power generation dispatches by conventional generating units, BESS and PV plant, including the total system operating costs.

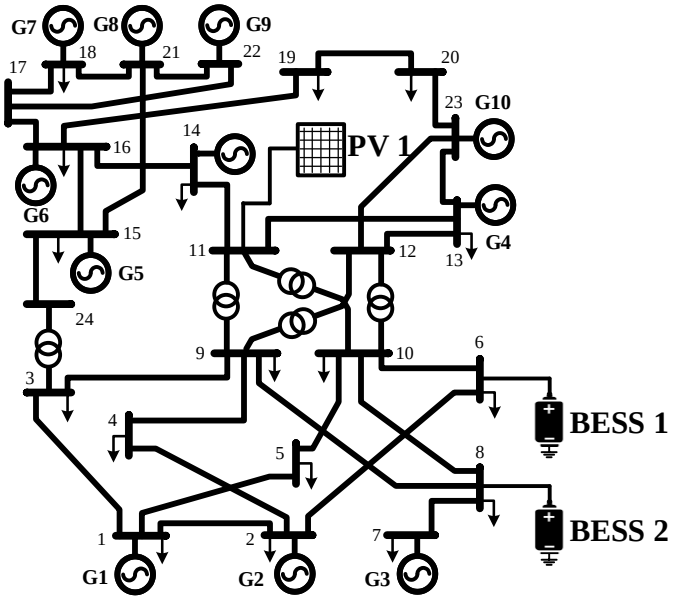

Figure 6.1 Modified IEEE 24-bus test system with two BESS and one PV plant

Table 6.1 System nodal demands

Bus	**Load** [MW]	**Bus**	**Load** [MW]
1	75.6	10	136.5
2	67.9	13	185.5
3	126	14	135.8
4	51.8	15	221.9
5	49.7	16	70.0
6	95.2	18	233.1
7	87.5	19	126.7
8	119.7	20	89.6
9	122.5		

Table 6.2 Parameters of BESS

BESS	*IC* [$]	W^{min}, W^{max} [MWhr]	P^{min}, P^{max} [MW]	*CR*, *DR* [MW/hr]	n_c, $\cdot\,\eta_B$ [cycles], [pu]
1	4.62E+07	192, 960	-40, 40	40, 40	10e3, 0.98
2	5.78E+07	240, 1200	-50, 50	50, 50	10e3, 0.98

Table 6.3 Parameters of PV plants

Plant	**Bus**	P^{max} [MW]	**Points of the MPPT curve, P_{mpp} vs S_i** (S_i[pu], P_{mpp} [pu]), see Figure 2.7b
PV 1	11	100	(0.1, 0.03); (0.2, 0.119); (0.3, 0.21); (0.4, 0.31); (0.5, 0.41) (0.6, 0.51); (0.7, 0.615); (0.8, 7.22); (0.9, 0.83); (1, 0.935)

Table 6.4 Parameters of conventional generating units

Unit	Gen	P^{min} [MW]	P^{max} [MW]	a_k [$/h]	b_k [$/MWh]	c_k [$/MW^{2}h]	RU [MW/h]	RD [MW/h]
U1	G1	62	192	400.6849	130	0.014545	120	120
U2	G2	62	192	212.3076	16.0811	0.014142	120	120
U3	G3	75	300	781.521	43.6615	0.052672	300	300
U4	G4	206.85	591	86.3852	48.5804	0.00717	240	240
U5	G5	66.25	215	382.2391	56.564	0.328412	215	215
U6	G6	66.25	215	382.2391	12.3883	0.008342	155	155
U7	G7	100	400	395.3749	4.4231	0.000213	280	280
U8	G8	100	400	395.3749	4.4231	0.000213	280	280
U9	G9	0	300	0.001	0.001	0.00321	300	300
U10	G10	248.5	660	665.1094	11.8945	0.004895	420	420

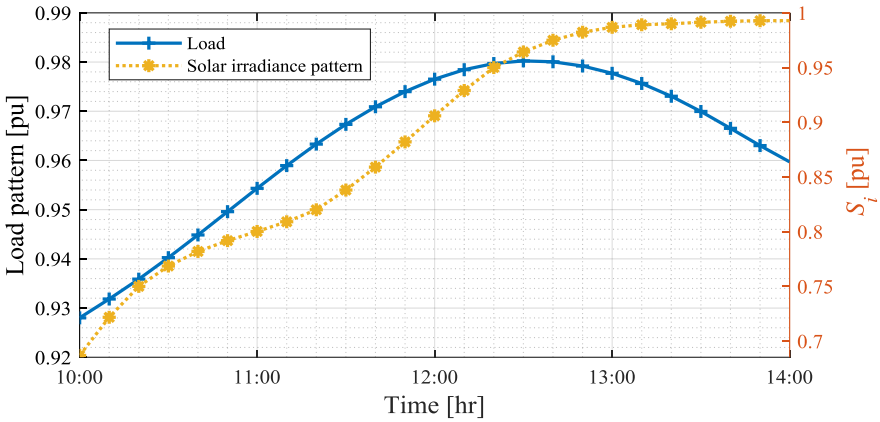

Figure 6.2 Forecasted load and solar irradiance S_i for 24-period operation horizon, 10-min intervals.

The multi-period generation dispatch of the 10 conventional generating units comprising the power system is shown in Figure 6.3, this without considering the inclusion of the two BESS, i.e., the multi-period SCED neglects the BESS contribution. While Figure 6.4 provides the generation dispatch for the same generation units, but this time in considering the effect of the BESS units on the system operation. From these results, it can be clearly appreciated how the inclusion of BESS supports the power system economic operation by displacing the most expensive thermal unit during peak demand periods. A case in point is G8, whose output power reaches its maximum level P_{g8} = 4.0 [pu] from 10:50 [hr] until the end of the operation horizon when the power grid has no BESS in operation. In sharp contrast, when the two BESS are delivering power to the power system, G8 decreases its generation over the entire operation horizon, reaching a power dispatch of only P_{g8} = 3.5

[pu] approximately, at 12:20 [hr]. A similar situation also occurs for generating unit G10. When there are no BESS operating in the power grid, its output power remains at P_{g10} = 2.5 [pu] from 10:00 [hr] until 11:00 [hr], which increases to about P_{g10} = 2.9 [pu] from 12:00 [hr] until 12:50 [hr]. Consequently, its output power reduces in the rest of periods, settling to P_{g10} = 2.5 [pu] at the end of operation horizon at 14:00 [hr]. Nonetheless, when the two BESS are considered, the output power of unit G10 remains constant at P_{g10} = 2.5 [pu]. In conclusion, it can be inferred from this behavior that the aggregation of BESS impacts positively the power system operation, economic wise, by displacing some of the most expensive generating units in certain periods of the operation horizon.

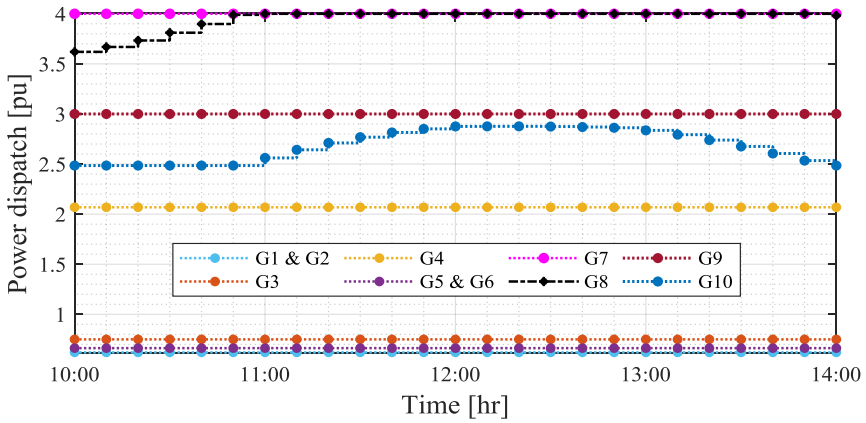

Figure 6.3 Generation dispatch without BESS

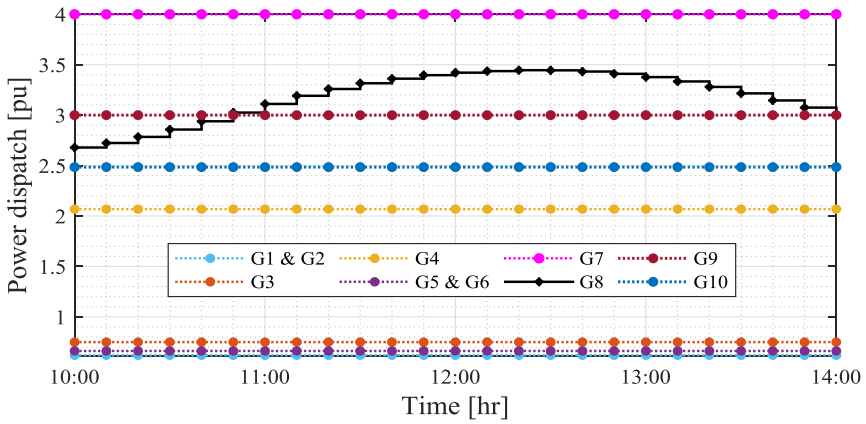

Figure 6.4 Generation dispatch with BESS

The BESS powers throughout the operation horizon and the PV plant generation are both given in Figure 6.5. This figure shows the power injections of the two BESS behaving similarly to the load pattern variation given in Figure 6.2. It is observed that both BESS are fittingly carrying out the load-following strategy, as defined in Subsection 2.10.1. More

precisely, this scheme enables an upward and downward load following when the load increases and decreases, respectively. As expected, both BESS reach maximum power injections of P_{b1} = 39.25 [MW] and P_{b2} = 49.06 [MW] at 12:30 [hr], which is precisely the time when the system load also experiences its maximum demand. While intrinsically, both BESS are supporting the system economic operation by reducing the conventional power generation while relaxing the ramp rate restrictions, as previously discussed. Also, Figure 6.2 shows that when the solar irradiation reaches the nominal value of S_i = 1 [pu] at 14:00 [hr], according to Figure 6.2, the PV plant does not inject its nominal power, but it reaches only P_{pv} = 0.93 [pu]. This fact corroborates that PV plant power is not entirely proportional to solar irradiances due to the internal power losses of the PV modules, which were captured by the MPPT strategy modeled by the PWL technique; these aspects were duly discussed in Subsection 2.9.

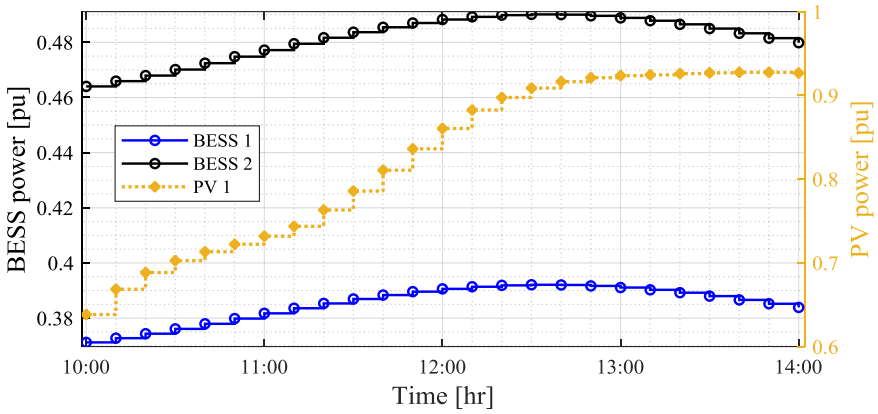

Figure 6.5 Power generation by BESS and PV plant

To further corroborate that the incorporation of BESS in the power network positively affects its economic operation, Figure 6.6 shows a comparison between the system operation costs with and without BESS. It can be seen that the maximum operating costs occur at 12:20 [hr], with 6766.81 [$/10min] when there are no BESS operating in the powr grid, but the operating costs reduce to 6623.51 [$/10min] when the BESS are delivering power to the system. The difference between both scenarios is evident throughout the operation horizon. A total cost saving of 2690.96 [$] is obtained during the 1 operation horizon, i.e., about 2.3 % of the operating costs are saved when both BESS in the power system perform the load-following strategy.

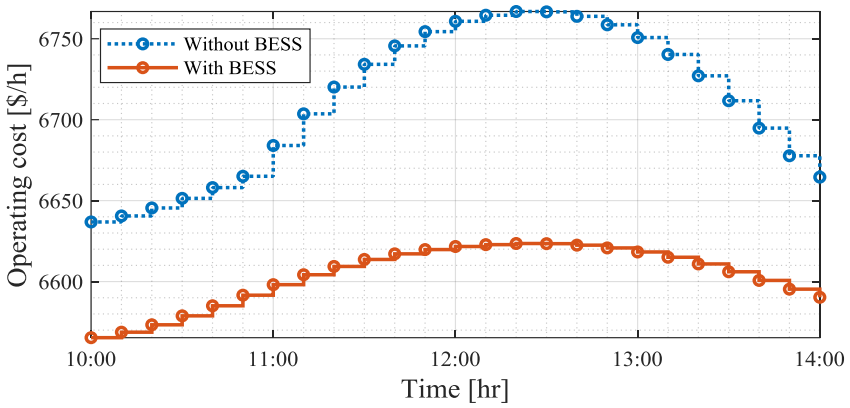

Figure 6.6 Operating costs with and without BESS

The computational burden related to this multi-period SCED study is worth discussing. The elapsed time taken to carry out the whole study was only 0.21 [s] on average for 100 runs of the algorithm. This fact clearly shows the computational efficiency of the proposed linear SCED model in solving power grids with BESS and PV plants.

6.1.2. IEEE 300-bus test system with 5 BESS and 3 PV plants

The SCED formulation is tested with a large-scale power system model to demonstrate its applicability. To this end, the IEEE 300-bus test system has been modified to incorporate five BESS operating with load-following strategy, BESS 1 – BESS 5, and three PV plants, PV 1 – PV 3, as depicted in Figure 6.7. This power system is formed by 300 buses and 69 dispatchable generation units, where three PV plants carrying the capacities of P_{pv}^{max} = {150, 50, 70} [MW] are connected to buses 141, 15 and 26, respectively. While the five BESS stations are of capacities P_b^{max} = {110, 110, 105, 100, 100} [MW], which are connected to buses 153, 75, 232, 124 and 187, respectively. The spinning reserve considered for each generation unit and BESS facility is taken to be $SR_k = SR_j$ = 5 %.

The parameters of nodal loads were directly taken from [95], using a base power of S_b = 100 MVA. Table 6.5 shows the parameters of BESS units, Table 6.6 provides the parameters of PV plants, and Table 6.7 presents parameters of conventional generation units. The PWL technique is applied to the nonlinear generation cost functions with ns = 12, transmission losses using ls =12, and MPPT curve of PV plants with ns_{pv} = 4 linear segments. For this SCED study, the operation horizon ranges from 14:00 [hr] to 18:00 [hr],

$\mathbb{Z}_T$ = {14-18} [hr], using intervals of 10 minutes. The per-unit load pattern together with the per-unit solar irradiance pattern for each PV plant are presented in Figure 6.8.

Considering the above parameters and operating conditions, the multi-period SCED is run. The obtained results are discussed next, focusing on conventional generation unit dispatches, BESS powers and PV power injections, including the power system operating costs.

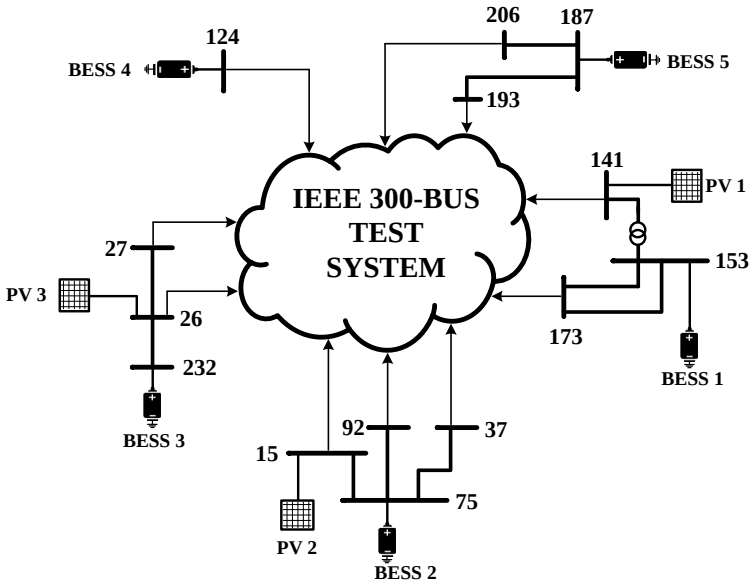

Figure 6.7 IEEE 300-bus test system with five BESS stations and three PV plants

Table 6.5 BESS Parameters

BESS	*IC* [$]	*nc* [cycles]	η_B [pu]	W^{min}, W^{max} [MWhr]	P^{min}, P^{max} [MW]	*CR*, *DR* [MW/hr]
1	57.75e6	10e3	0.98	480, 2400	-110, 110	-110, 110
2	57.75e6	10e3	0.98	480, 2400	-110, 110	-110, 110
3	69.30e6	10e3	0.98	432, 2160	-105, 105	-105, 105
4	69.30e6	10e3	0.98	432, 2160	-100, 100	-100, 100
5	69.30e6	10e3	0.98	432, 2160	-100, 100	-100, 100

Table 6.6 PV plants parameters

PV plant	**Bus**	P^{max} [MW]	**Points of the MPPT curve, P_{mpp} vs S_i**
PV1	141	150	(S_i[pu], P_{mpp} [pu]) See Table 6.2
PV2	15	50	
PV3	26	70	

Table 6.7 Parameters of conventional generating units

Generators	Unit See Table 6.4
G1, G11, G21, G31, G41, G51, G61	**U1**
G2, G12, G22, G32, G42, G52, G62	**U2**
G3, G13, G23, G33, G43, G53, G63	**U3**
G4, G14, G24, G34, G44, G54, G64	**U4**
G5, G15, G25, G35, G45, G55, G65	**U5**
G6, G16, G26, G36, G46, G56, G66	**U6**
G7, G17, G27, G37, G47, G57, G67	**U7**
G8, G18, G28, G38, G48, G58, G68	**U8**
G9, G19, G29, G39, G49, G59, G69	**U9**
G10, G20, G30, G40, G50, G60	**U10**

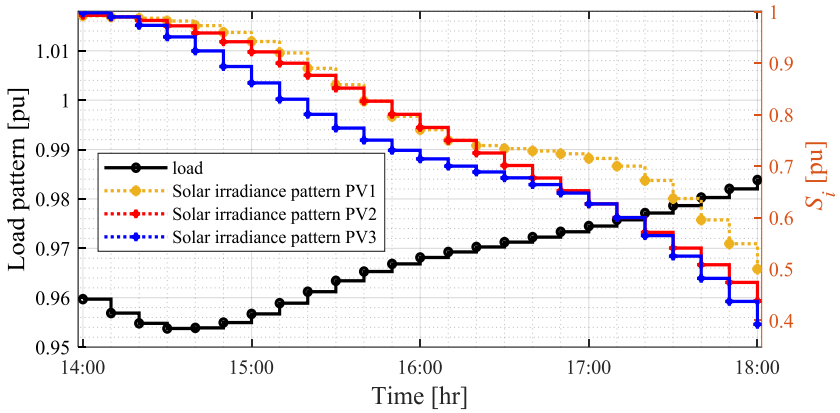

Figure 6.8 Forecasted load and solar irradiance patterns for 24 periods using 10-min intervals.

Figure 6.9 presents the generation dispatch for selected generation units when BESS are not operating in the power network, and Figure 6.10 shows those of the same generating units, but considering the operation of BESS featured by a load-following strategy. From these results, it can be appreciated anew how the incorporation of BESS supports the system operation by reducing the power generation of certain conventional units. For instance, G59 increases its output power from P_{g59} = 2.5 [pu] at 15:00 [hr] to P_{g59} = 3.6 [pu] at 18:00 [hr] when the BESS facilities are not operating, whereas with BESS included, G59 reaches a maximum power production of P_{g59} = 3.0 [pu] at 18:00 [hr]. Another interesting example is the generating unit G32, whose dispatch level settles to $P_{g32} \approx 2.1$ [pu] at 18:00 [hr] when the five BESS are not operating. In contrast, its power dispatch is always smaller than $P_{g32} \approx 0.8$ [pu] when the BESS are operating throughout the operation horizon. The same phenomenon occurs with G17, whose output level reaches $P_{g17} \approx 1.9$ [pu] from 17:00 [hr]

to 18:00 [hr] without BESS operation but it never exceeds $P_{g17} \approx 1.5$ [pu] when all five BESS are active. In conclusion, the BESS support the system operation in such a way that avoids conventional generation units from taking more load, thus making the power system operation less expensive.

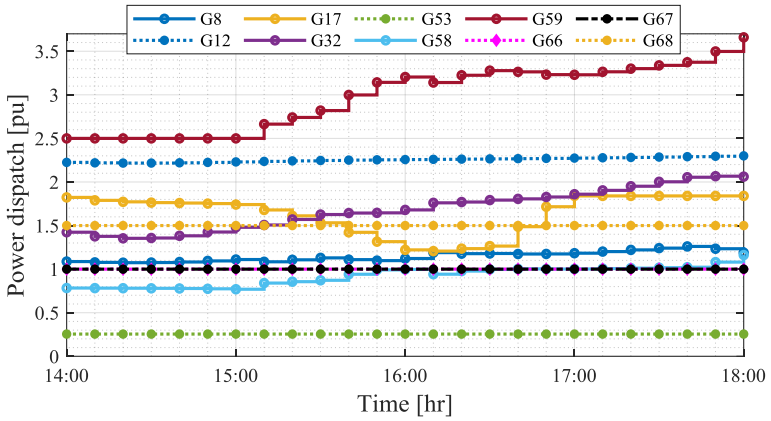

Figure 6.9 Generation dispatch for selected generation units – without BESS in the system

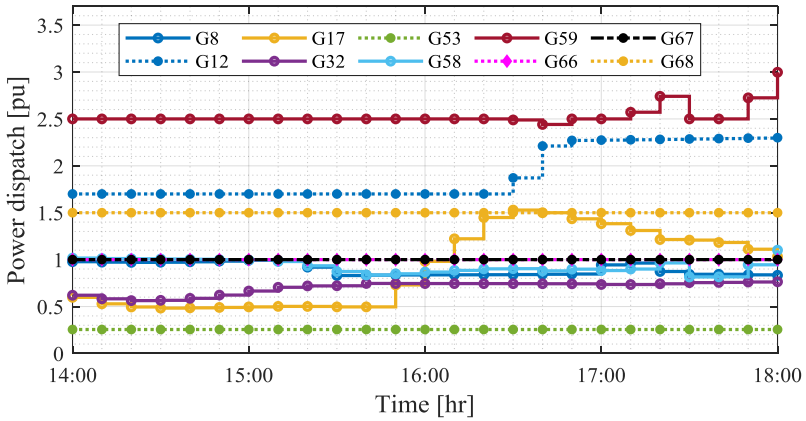

Figure 6.10 Generation dispatch for selected generation units – with BESS in the system

The power generated by BESS and PV plants are depicted in Figure 6.11. It can be appreciated that BESS operating in discharge mode clearly obeys to the proposed load-following strategy. It is also worth noting that, contrary to the first case study, in this scenario all PV plants are all reducing their energy production throughout the operation horizon, moving from P_{pv} = {140.2, 46.7, 65.4} [MW] at 14:00 [hr] to P_{pv} = {55.4, 16.6, 19.4} [MW] at 18:00 [hr], for the three power plants, i.e., PV 1, PV 2 and PV 3, respectively. In this sense, it is also observed that in this case, the five BESS start generating P_b = {105.2, 105.2, 100.4, 95.6, 95.6} [MW] at 14:00 [hr] and end injecting

P_b = {108.4, 108.4, 103.4, 98.5, 98.5} [MW] at 18:00 [hr]. Admittedly, the BESS can provide upward and downward following at the pace of load variation, which can be of paramount importance when there are limitations regarding up/down ramps for the conventional generating units.

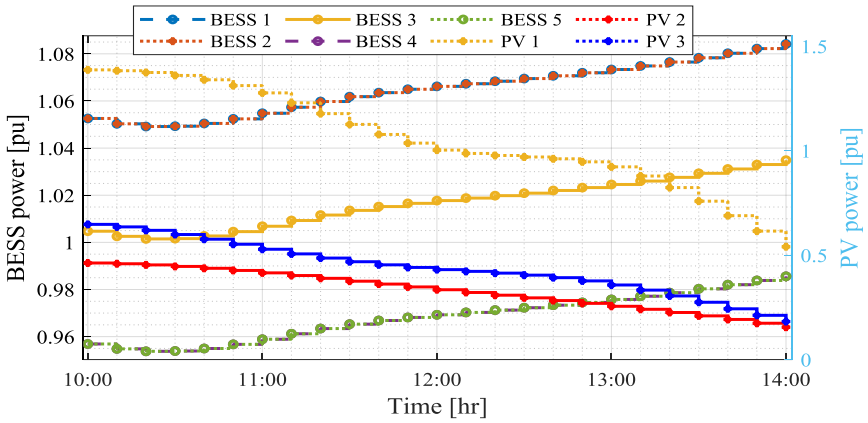

Figure 6.11 Power injected by BESS and PV plants

The system operating cost is also an important information for TSO in this kind of SCED studies. In this sense, Figure 6.12 compares the power system operating costs with and without BESS, where it is seen that both follow similar tendencies, as expected. From here, however, it is possible to observe that the incorporation of BESS favors the economic operation of the grid because there is a significant reduction in the operating costs, about 2624.64 [$], i.e., 2.9 % with respect to the case when there are no BESS in the system. This is so because the BESS operate in discharge mode in pursuing the load-following strategy.

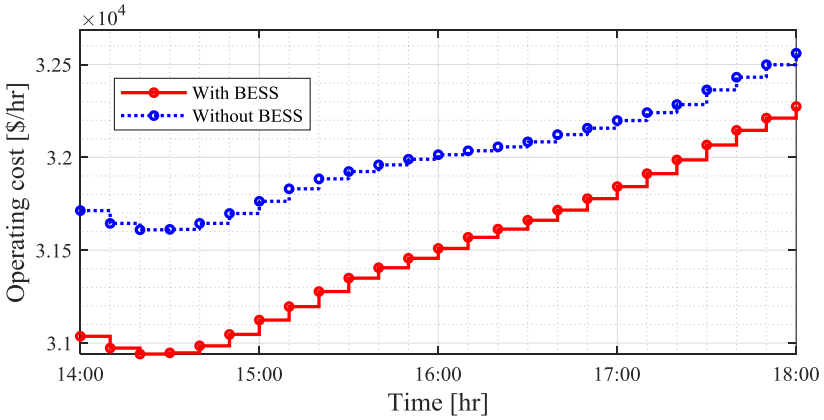

Figure 6.12 Operating costs with and without BESS

For this test system, the computational time required to execute the multi-period SCED model was on average 2.23 [s] for 100 runs. This result further proves the computational efficiency of the present linear SCED model due to the short time required to execute it even for this fair-sized power grid model. Admittedly, this kind of computing times are certainly required in the real-time power system operation at control centers.

6.2. Study cases with the SCOPF model

The SCOPF model developed in Chapter 4 is studied in this subsection, with two VSC-based AC/DC networks are analyzed. The first one corresponds to a relatively simple hybrid power grid with four VSC stations, and the second one is a larger AC/DC grid model formed by seven AC power systems connected through an equal number of VSC stations.

6.2.1. AC/DC system with 4 VSC and 10 generators – Proof of concept

To conceptually corroborate the SCOPF formulation presented in Chapter 4, a VSC-based AC/DC grid formed by four 300-MVA VSC stations, VSC 1 – VSC 4, is studied herein. This hybrid power grid, depicted in Figure 6.13, features three power systems AC 1 – AC 3 with two dispatchable generation units each, and another power grid AC 4 which is a passive grid with no generation of its own. This electrical network contains 10 dispatchable generation units, 16 AC transmission branches, 4 DC lines, thus making up 20 buses in total, 16 of which are of AC and 4 of DC. The four VSC units feature different control strategies: VSC 1 operates with voltage control by exerting voltage regulation E_{ctrl} in DC bus 17 at E^{ref} = 2 [pu]; VSC 2 operates in fixed power control mode P_{set} with P^{ref} = 125 [MW]; VSC 3 is assigned with voltage/power droop control strategy E/P_{ctrl} with DC bus 19 being the voltage-controlled bus E^{ref} = 2 [pu], with P^{ref} = 75 [MW] and droop gain of K_c = 15; while VSC 4 is a passive type converter P_{ass} with ϕ^{ref} = 0 [rad].

The system load data is presented in Table 6.8 for a base power of S_b =100 MVA. Table 6.9 shows the parameters of the transmission lines for the AC/DC grid, while Table 6.10 the parameters and setpoints of all the VSC units comprising the hybrid system, including their corresponding coupling reactors and step-up transformers. On the other hand, the parameters of conventional generation units, including droop and damping constants, are

given in Table 6.11. The PWL technique is applied to nonlinear generation cost functions and transmission losses using *ns* = *ls* =12 segments.

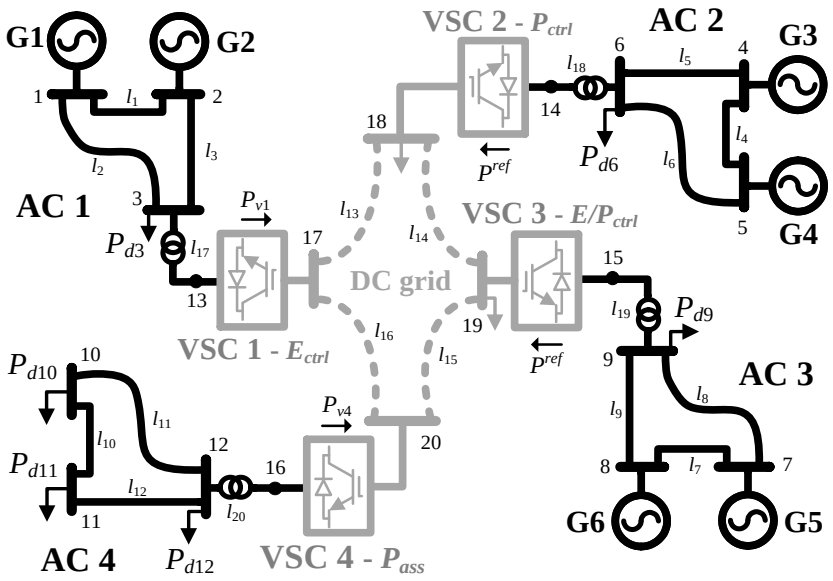

Figure 6.13 AC/DC power grid with four VSC-connected AC systems

Table 6.8 System loads

Bus	Load [MW]	Bus	Load [MW]
3	150	11	40
6	150	12	40
9	150	18	30
10	40	19	30

Table 6.9 Transmission system parameter

AC branches	DC branches
$Z_{1\text{-}2} = Z_{4\text{-}5} = Z_{7\text{-}8} = Z_{10\text{-}11}$=0.03 + j0.15 pu	$r_{17\text{-}18}$ = 0.02085 pu
$Z_{1\text{-}3} = Z_{4\text{-}6} = Z_{7\text{-}9} = Z_{10\text{-}12}$=0.035 + j0.20 pu	$r_{18\text{-}19}$ = 0.0278 pu
$Z_{2\text{-}3} = Z_{5\text{-}6} = Z_{8\text{-}9} = Z_{11\text{-}12}$=0.04 + j0.25 pu	$r_{19\text{-}20}$ = 0.03475pu
$\mathbf{y}_{sh}$= j0.2 pu (all lines); $P_{km}^{\max}$ = 3 pu	$r_{20\text{-}17}$ = 0.0417pu; $P_{jm}^{\max}$ = 3 pu

Table 6.10 Parameters and setpoints of VSC units

VSC 1	VSC 2	VSC 3			VSC 4
E^{ref} [pu]	P^{ref} [pu]	E^{ref} [pu]	P^{ref} [pu]	K_c [pu]	ϕ^{ref} [rad]
2.0	1.25	2.0	0.75	15	0.0
All VSC units: r_{ph} = 5e-4 [pu], x_{ph} = 5e-2 [pu]					
r_{tr}=1.67e-3 pu, x_{tr}= 5e-2 pu, P^{max}=3.0 [pu]					

Table 6.11 Generation units parameters

Gen.	a_i [$/MW^{2}h]	b_i [$/MWh]	c_i [$/h]	P^{min}, P^{max} [MW]	R, D [%]
G1-G2	0.002	7.8	310	10, 300	4, 2
G3-G4	0.004	6.4	60	10, 300	4, 2
G5-G6	0.005	8.0	78	10, 300	4, 2

With the above parameters and operating conditions, the corrective SCOPF algorithm is executed. First, the pre-contingency system conditions are calculated, according to the procedure detailed in Subsection 4.4.1. Subsequently, the post-contingency conditions are obtained for the N-1 contingencies associated with the hybrid grid, see Subsection 4.4.2. The SCOPF results are discussed next, placing emphasis on the generation dispatches and VSC power flows.

- **Pre-contingency OPF**

In carrying out SCOPF studies, the starting point is the calculation of the pre-contingency power system conditions, i.e., the system operating state without contingencies is applied. Under these conditions, neither generators nor VSC units are commanded by droop control responses, implying that converters VSC – E/P_{ctrl} are considered as fixed power converters VSC – P_{ctrl}, as detailed in Subsection 4.4.1. Based on this, the generation dispatch is shown in Table 6.12, and Table 6.13 shows the power flows of AC branches, DC lines, and VSC stations, while nodal prices of both AC and DC nodes are given in Table 6.14. It should be said that for this pre-contingency operating scenario, the entire AC/DC power system losses are 35.84 [MW], with total production costs of 6056.14 [$/hr].

Table 6.12 Pre-contingency generation dispatch

Power generation [MW]					
G1	**G2**	**G3**	**G4**	**G5**	**G6**
72.73	66.66	150.00	140.91	118.76	116.66

Table 6.13 Pre-contingency power flows

AC branch power flows, P_{km} [MW]
P_{13} =75.21, P_{23} =62.31, P_{46} =154.39, P_{56} =128.72,
P_{79} =124.85, P_{89} =105.39, $P_{10\text{-}12}$ = -43.74, $P_{11\text{-}12}$ = -36.96
DC line power flows, P_{jm} [MW]
$P_{17\text{-}18}$ =-63.44, $P_{18\text{-}19}$ =31.04, $P_{19\text{-}20}$ =74.95, $P_{17\text{-}20}$ =-48.18
Power flows - VSC 1, VSC 2, VSC 3, VSC 4 - P_v [MW]
P_{v1}=-14.33, P_{v2} =125.07, P_{v3}=75.02, P_{v4}=-121.67

Table 6.14 Selected pre-contingency nodal prices

AC and DC nodal prices, λ_k[$/MWh]
λ_1 = 8.10, λ_2 = 8.079, λ_4 = 7.566, λ_5 = 7.533,
λ_7 = 9.25, λ_8 = 9.170, λ_{10} = 9.134, λ_{11} = 9.196,
λ_{17} = 8.57, λ_{18} = 8.338, λ_{19} = 8.501, λ_{20} = 8.862

From these results, it can be observed how the power production by G1 and G2 contained in AC 1 is not enough to satisfy its power demand plus losses, which is why this network imports power from the DC grid. That is, the power flow through its pairing converter VSC 1 operating in voltage control mode (VSC – E_{ctrl}) is P_{v1} = -14.33 [MW]. It can be also observed that the generating units in AC 2 produce P_g = 290.91 [MW], i.e., G3 and G4 combined – see Table 6.12. This network is related to a VSC operating in fix power mode which exports to the DC grid a power of P^{ref} = 125 [MW]. However, the total load of AC 2 is only 150 [MW], which means the remainder 15.91 [MW] corresponds to the internal power losses at AC 2. A similar situation occurs in AC 3, which is connected to VSC 3 performing a voltage/power droop control strategy (working in a pre-contingency state as a converter VSC – P_{ctrl}) whose total generation, G5 plus G6, reaches P_g = 235.34 [MW]. In contrast, the total consumption of AC 3 amounts to P_d = 150 [MW] plus power losses, where AC 3 exports P^{ref} = 75 [MW] to the DC grid through VSC 3. It should be noted that, as for AC 4 and DC grid, both lack generation of their own, and so the neccesary power to balance the networks has to be taken from the other converters injecting power into the DC grid. Table 6.14 shows the nodal prices of the VSC-based AC/DC grid. From this, it is appreciated that AC 2 has the smallest locational marginal prices of the entire AC/DC grid, which are about $\lambda \approx 7.6$ [$/MWh], whereas the largest nodal prices occur in AC 3 with a nodal price around $\lambda \approx 9.2$ [$/MWh].

- **Post-contingency SCOPF**

Once the pre-contingency state study has been completed, the next step involves the post-contingency analyses, i.e., the SCOPF model applied to each of the *N*-1 contingencies to be evaluated. For this particular case and the AC/DC system shown in Figure 6.13, this SCOPF analysis considers the following contingencies:

i. **Contingencies no. 1 – no. 16:** disconnection of AC and DC branches, l_1 - l_{16}.
ii. **Contingencies no. 17 – no. 20:** disconnection of converters, VSC 1 - VSC 4.
iii. **Contingencies no. 21 – no. 26:** disconnection of generating units, G1 - G6.

Figure 6.14 shows the relevant results of the SCOPF study in carrying out the 26 contingencies: 16 AC/DC transmission line outages (no. 1 – no. 16), 4 VSC outages (no. 17 – no. 20), and 6 generation unit outages (no. 21 – no. 26), all of them reported in the plots, in the order of appearance listed above in *i* – *iii*.

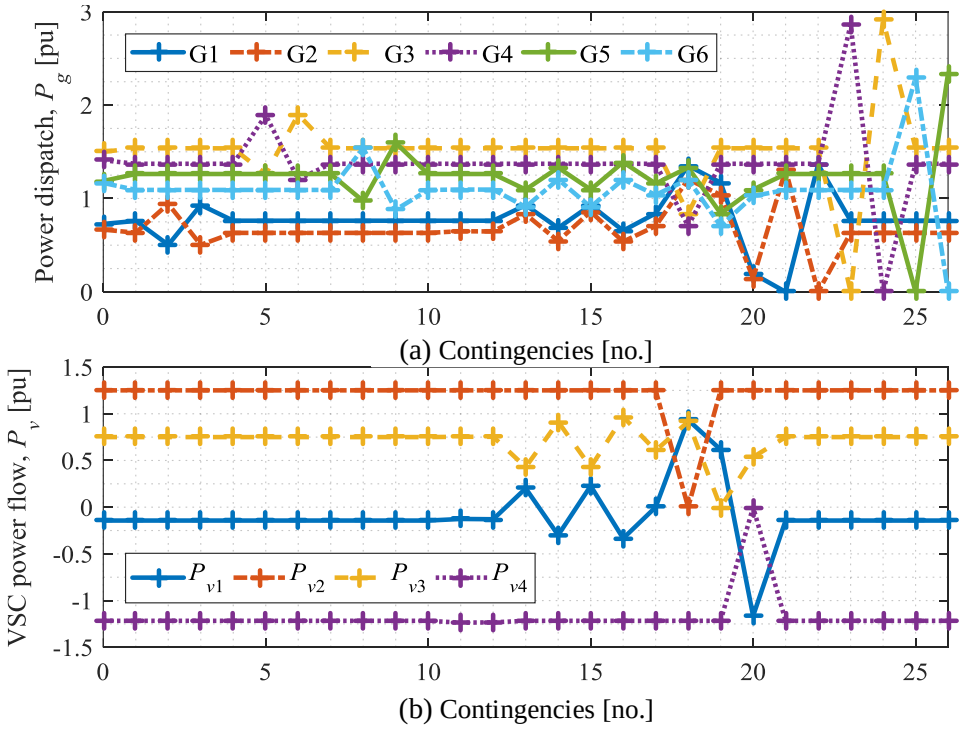

Figure 6.14 Relevant results of the SCOPF study: (a) Power dispatch, (b) VSC power flows

By closely looking at Figure 6.14, some of the most stressing contingencies for the VSC-based AC/DC grid are those related to VSC outages (no. 17 – no. 20). For instance, the contingency no. 20 related to the disconnection of VSC 4 (feeding into a passive grid), causes the disconnection of all loads in AC 4. Due to this, generators G1 and G2, which pertain to network AC 1 connecting to VSC 1 (operating with voltage control), reduce their output power from of P_{g1} = 69 [MW] and P_{g2} = 66 [MW], in pre-contingency conditions, to P_{g1} = 18 [MW] and P_{g2} = 14 [MW], respectively. This happens since VSC 1 operates in voltage control mode, during the contingency the converter adjusts its power flow, moving from an exporting condition to an importing one, as clearly evidenced from Figure 6.14b. A similar situation occurs for VSC 3 since this converter reschedules its power flow from P_{v3} = 75 [MW] to P_{v3} = 53 [MW] due to its droop control strategy.

Other remarkable examples are the disconnection of generating units, which affect the power balance of the VSC-based AC/DC grid. For instance, the outage of G1 (contingency no. 21) provokes an increase in the output power of G2 above P_{g2} = 125 [MW] because both generators belong to AC 1. On the other hand, the disconnection of transmission branches is also assessed in the SCOPF study. For example, the outage of AC branch l_5 in AC 2 (contingency no. 5) causes a redispatch in G4, increasing its power output from P_{g4} = 140 [MW] to P_{g4} = 188 [MW]. Likewise, this contingency provokes a power reduction of G3 moving from P_{g3} = 150 [MW] to P_{g3} = 125 [MW]. It is worth noting that this contingency only provokes power generation and flow changes at AC 2, but it does not cause any changes in the VSC power flows and, by extension, it does not alter the power flows at any other AC system. By the same token, contingencies occurring at AC 3 has minimum effects on AC 2. Another interesting branch disconnection is the outage of the DC line l_{15} (contingency no. 15), which forces the action of the voltage/power droop control of VSC 3, whose power flow varies from P_{v3} = 75 [MW] in pre-contingency conditions to P_{v3} = 40 [MW] after the occurrence of the contingency. More precisely, this power flow variation happens due to the voltage variation at bus no. 19 due to the DC line outage which has a direct connection with this node, i.e., line l_{15}. It is also worth noting the changes in the output powers of G1, G2 in AC 1 and G5, G6 in AC 3, whose related VSC operation strategies are affected by DC bus voltage changes, that is, converters VSC – E_{ctrl} and VSC – E/P_{ctrl}, respectively.

In conclusion, the SCED study permits to appreciate that various events cause a power rescheduling in both generating units and VSC stations, particularly in view of generator and converter outages, which generally impact the whole VSC-based AC/DC grid.

6.2.2. AC/DC system formed by 7 VSC and 70 dispatchable generators

The SCOPF formulation is tested using a larger VSC-based AC/DC system model to demonstrate its applicability to fair-sized hybrid networks. To this end, is employed a power system composed of seven 500-MVA VSC-connected AC sub-systems, as depicted in Figure 6.15, where each AC sub-systems is a replica of the IEEE RTS 24-bus system [94]. Similarly, the DC grid topology corresponds to the IEEE RTS 24-bus system, where the resistance of the DC lines is taken from the resistive part of the AC transmission lines.

This hybrid network is formed by 199 AC buses in total, where 175 of these are in AC and 24 in DC. It also contains 70 generation units, 273 AC branches, 266 of these transmission lines and 7 step-up transformers, and 24 DC lines. The seven 500-MVA VSC units are assumed to be operated with different control strategies. For this SCOPF study, VSC 1 and VSC 6 are assigned with voltage control strategy E_{ctrl}, with E^{ref} = {2, 2} [pu], while VSC 2 and VSC 4 operate with a fixed power control strategy P_{set}, with P^{ref} = {200, 150} [MW]. On the other hand, VSC 3, VSC 5 and VSC 7 are assigned with voltage/power droop control strategy E/P_{ctrl}, where nodes 23, 2, and 3 are the voltage-controlled DC buses, respectively, with E^{ref} = {2, 2, 2} [pu], P^{ref} = {300, 350, 400} [MW], and with equal droop gains of K_c = 2.5 for the three converters. The system load parameters are taken from [94], assuming a base power of S_b = 100 MVA, where each AC system and DC grid has a different demand level, as depicted in Table 6.15. that is, the system load is scaled by a constant factor where P_{dnom} = 2850 [MW] is the total demand of the IEEE RTS 24-bus system. This table also shows the droop constants of generators R and VSC units K_c generators damping factor D. As in previous studies, the PWL technique is applied to the nonlinear generation cost functions and transmission losses using $ns = ls = 12$ linear segments.

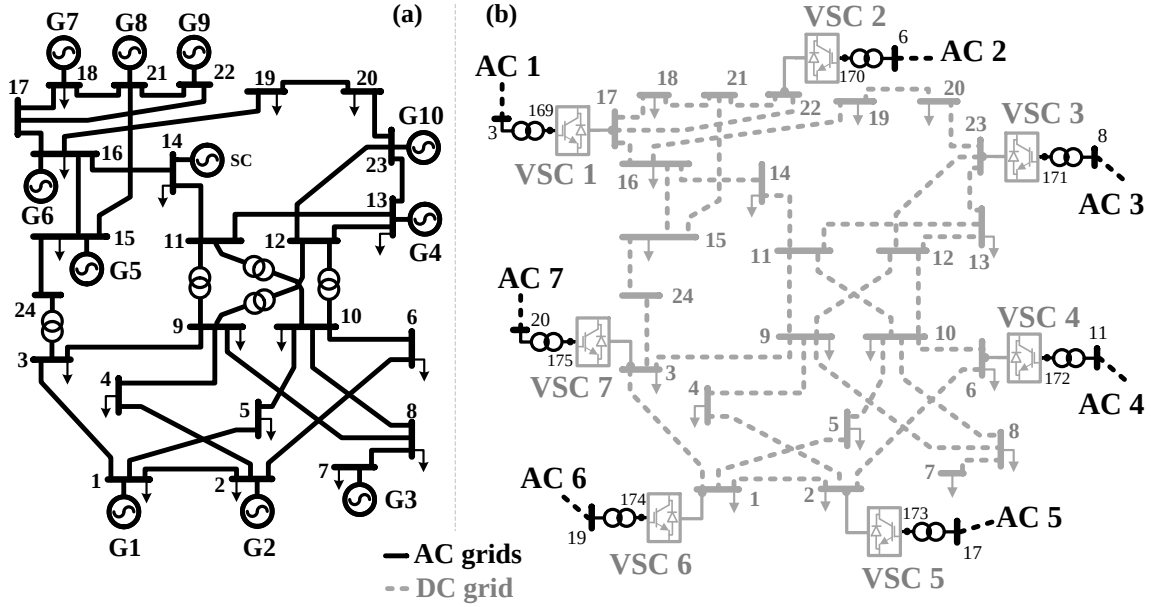

Figure 6.15 Seven-terminal VSC-based AC/DC power grid with 7 AC systems and 70 generators: (a) AC 1 – AC 7; (b) DC grid

Table 6.15 Load level for AC 1 – AC7 and DC grid. Parameters of generators and VSC droop gains

AC 1	**AC 2**	**AC 3**	**AC 4**	**AC 5**
0.50 $x\ P_{dnom}$	0.55 $x\ P_{dnom}$	0.60 $x\ P_{dnom}$	0.65 $x\ P_{dnom}$	0.70 $x\ P_{dnom}$
AC 6	**AC 7**	**DC grid**	**Generators**	**VSC 3, 5, 7**
0.75 $x\ P_{dnom}$	0.80 $x\ P_{dnom}$	0.50 $x\ P_{dnom}$	R=6%, D=2%	K_c = 2.5

To rigorously evaluate the SCOPF formulation, the following 349 events are assessed:

i. **Contingencies no. 1 – no. 238:** disconnection of all 239 AC branches, starting with AC 1 towards AC 7.
ii. **Contingencies no. 239 – no. 272:** disconnection of DC transmission lines.
iii. **Contingencies no. 273 – no. 279:** VSC outages, starting with VSC 1 towards VSC 7.
iv. **Contingencies no. 280 – no. 349:** disconnection of all 70 generating units, starting with those of AC 1 towards those of AC 7.

The SCOPF algorithm is run considering the above parameters, operating conditions, and contingencies. The OPF outcomes are discussed next, mainly focusing on generation unit dispatches and VSC power flows for each contingency. As in the previous SCOPF study case, the post-contingency results depend on the initial conditions given by de pre-contingency analysis.

Figure 6.16(a) shows the power dispatches for the 349 contingencies previously but for selected generation units, that is to say, G7 in AC 1, G8 in AC 2, G10 in AC 3, G7 in AC 4, G8 in AC 5, G10 in AC 6 and G7 in AC 7. As expected, the impact on generation dispatch, P_g, is more noticeable for the outages of DC transmission lines, VSC units, and generators, i.e., from contingency 239 onwards. This is most notorious on AC 1 and AC6, which are connected to the DC grid through VSC 1 and VSC6, respectively, because these converters are exerting DC voltage control. More specifically, this happens in this way because the generation units of power grids coupled to VSC units performing voltage control strategy seek to compensate for any variation in their DC bus voltages over which they exert regulation. Indeed, the DC network demand is met by generation units in AC grids with E_{ctrl} mode, as explained in detail in Subsection 5.2. On the other hand, Figure 6.16(b) presents the power flows of the seven VSC units, P_v, for the 349 contingencies considered. Like in the case of power generations, the disconnections of DC lines, VSC, and generator impact the VSC power flows the most. As expected, this is more perceptible for AC 1 and

AC 6 due to both power grids are coupled to VSC units with DC voltage control, thus directly affecting the power flow in VSC 1, P_{v1}, and VSC 6, P_{v6}.

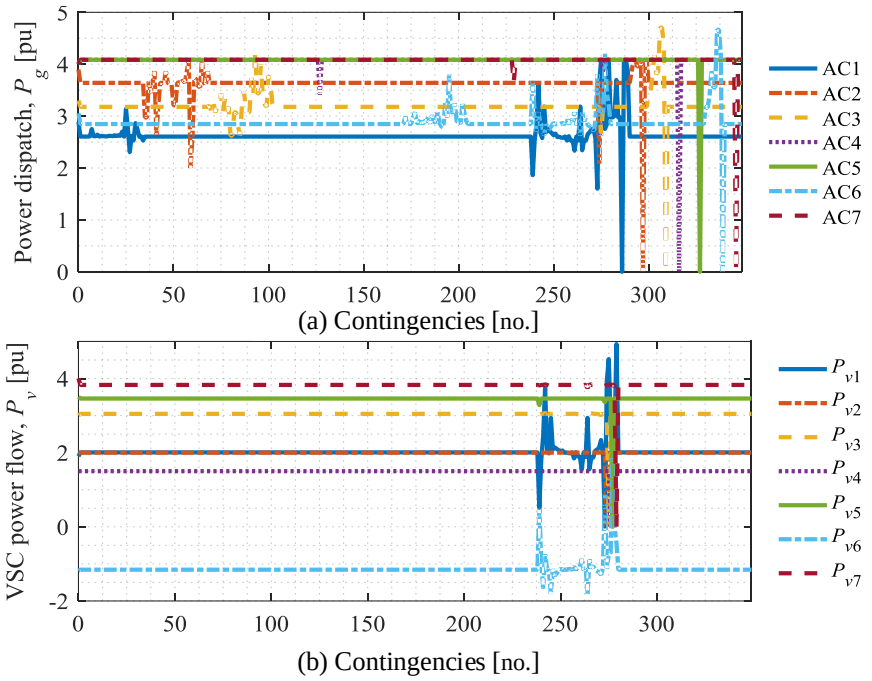

Figure 6.16 Selected results: (a) Generation dispatch: G7 in AC 1, G8 in AC 2, G10 in AC 3, G7 in AC 4, G8 in AC 5, G10 in AC 6, G7 in AC 7; (b) VSC power flows

Figure 6.17(a) presents the marginal price at bus 11 of each power grid forming the AC/DC system, i.e., AC 1 – AC 7 and DC grid. It can be noticed that the most expensive nodal prices are obtained in AC 7, while the most economic process are observed in AC 2 around λ = 5 [$/MWh]. As for the case of AC 7, it can be appreciated that the nodal price is about λ = 20 [$/MWh] for most contingencies, but it reaches approximately λ = 58 [$/MWh] when generation outages occur in this area (contingencies no. 340 to 349). This is due to the fact the AC system is connected to a VSC with voltage/power droop control, which impacts the dispatch of generators that remain on, thus increasing the network nodal marginal prices. Similarly, Figure 6.17(b) shows the system generation cost for the 349 contingencies. It is confirmed anew that some contingencies cause noticeable variations in the system operating costs, especially those related to generation unit disconnections, i.e., from contingency 280 onwards. These kinds of contingencies provoke a redispatch in the remaining generation units, which can produce an increase in generation costs. Notice that the total generation costs remain practically steady about 2.31×10^5[$/h] for

contingencies 1 – 279, but the total production costs are considerably affected for generation outages (contingencies 280 - 349), reaching almost $2.6x10^5$[$/h] approximately.

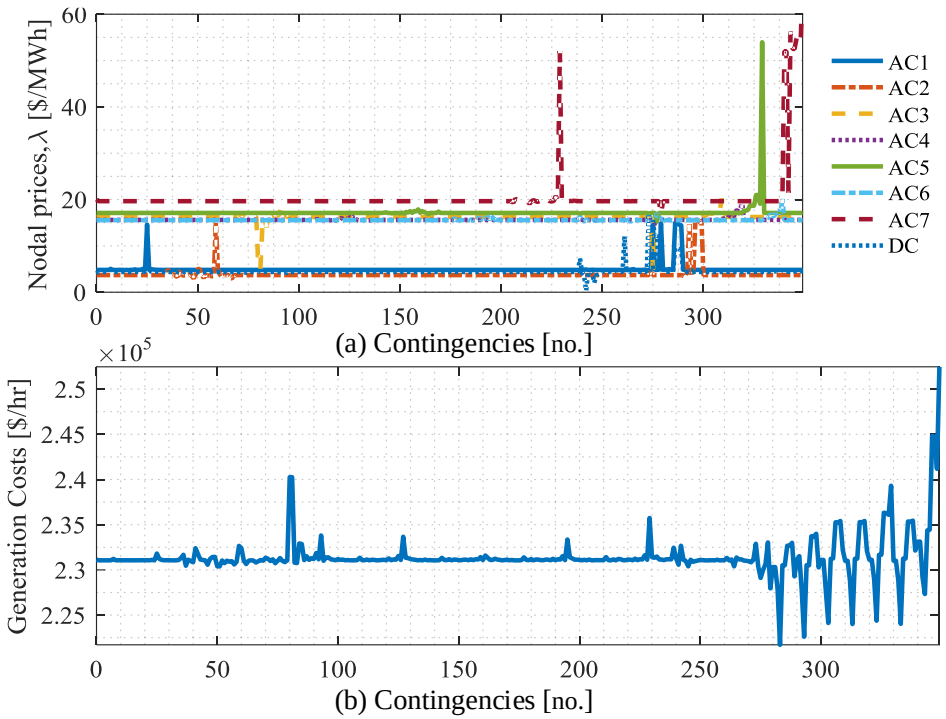

Figure 6.17 Selected results: (a) Nodal prices at bus 11; (b) Total generation costs

For this hybrid AC/DC system model, the computational time required to execute the 349 contingencies was only 82.86 [s], which implies it only took on average 0.24 [s] per event. This aspect confirms further the computational efficiency of the present linear-based SCOPF model useful for fair-sized VSC-based AC/DC grid. The above is very much desirable for the analysis required in different stages of the power system planning and operation at control centers.

6.3. Study cases using the developed UC model

The application of the UC model developed in Chapter 5 is investigated in this subsection, studying two VSC-based hybrid AC/DC power systems. First, to evaluate the developed algorithm, a hybrid power grid comprising four VSC stations is analyzed. Then, a seven-terminal VSC-based AC/DC system with five BESS demonstrates the practicality of the new UC model.

6.3.1. AC/DC grid formed by 4 VSC, 8 generators, 2 BESS – Proof of concept

To conceptually analyze the UC formulation developed in Chapter 5, the VSC-based AC/DC grid comprising four 300-MVA VSC stations depicted in Figure 6.18 is studied for an hourly day-ahead operation horizon. This hybrid network incorporates two storage systems, BESS 1 and BESS 2, operating with an energy time-shifting strategy. Their power ratings are P_b^{max} = {40, 50} [MW] and are connected to buses 12 and 13, respectively. The four VSC units are assigned with different control strategies, where VSC 1 features a voltage control strategy, exerting voltage regulation over DC bus 20. VSC 2 and VSC 3, conversely, operate with fixed power control strategy, and VSC 4 is a passive type converter. Power systems AC 1 and AC 2 contain each three committable generation units, whereas AC 3 contains two generators and one BESS; while AC 4 is a passive grid with no conventional generation of its own, but with one BESS. In summary, this power system is formed by 20 AC buses, 4 DC buses, 8 committable generation units, 22 AC transmission branches, and 4 DC transmission lines. Concerning the spinning reserve, this is taken to be of SR_α = SR_β = 5%, i.e., for area Π, AC 2 and AC 3, recalling the generation-demand balance considerations for VSC-based AC/DC grids provided in Subsection 5.2.

The parameters related to the system load are shown in Table 6.16, with Figure 6.19 showing the normalized load pattern variation for the 24-hour planning horizon of the UC study, the above for each AC system and DC grid comprising the hybrid grid. Table 6.17 provides the parameters of the VSC units, using a base power S_b = 100 MVA. For this UC study case, VSC 1 is assigned with E_{ctrl} mode with E^{ref} = 2 [pu], VSC 2 and VSC 3 are featured by P_{ctrl} mode with P^{ref} = {150, 100} [MW], and VSC 4 operate in P_{ass} mode with ϕ^{ref} = 0 [rad]. Table 6.18 presents the parameters of BESS, including the charging periods, $\mathbb{Z}'_T$, to deploy the energy time-shifting strategy. Table 6.19 shows the parameters of the AC/DC transmission system, whereas Table 6.20 provides the generation unit parameters. The PWL technique is applied to nonlinear generation cost functions and AC/DC power losses, using *ns* = 12 and *ls* = 12 segments, respectively. For this UC study, the planning horizon consists of 24 periods, from 01:00 to 24:00 [hr], $\mathbb{Z}_T$ = {1-24} [hr], using time intervals of 1 hour.

With the previous conditions, the UC algorithm developed in this doctoral thesis is run. The obtained results are discussed next, concentrating on generation unit dispatches and schedules over the planning horizon, VSC power flows, and BESS powers.

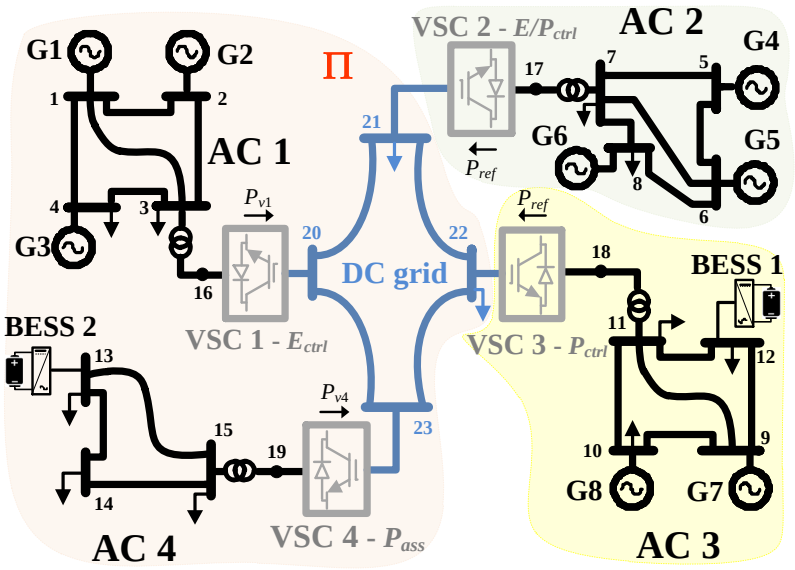

Figure 6.18 Four-terminal VSC-based AC/DC grid with two BESS units

Table 6.16 Systems loads

Bus	Load [MW]	Bus	Load [MW]
3	150	12	100
4	200	13	50
7	100	14	50
8	150	15	50
10	50	21	75
11	50	22	75

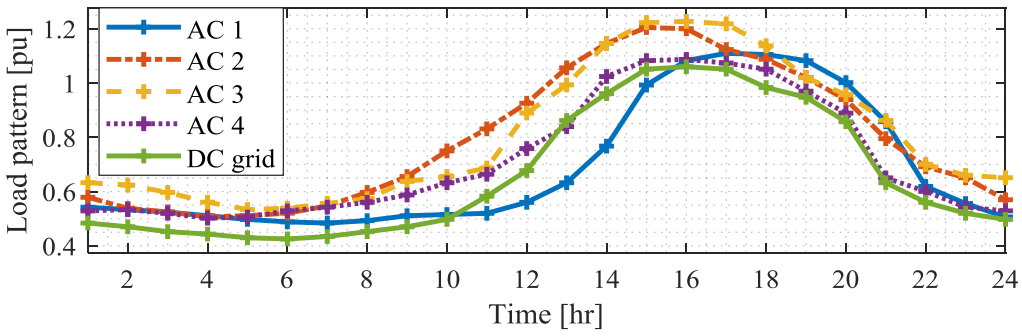

Figure 6.19 Load pattern for the 24-hour UC planning horizon

Table 6.17 Parameters of VSCs

VSC 1 E^{ref} [pu]	VSC 2 P^{ref} [pu]	VSC 3 P^{ref} [pu]	VSC 4 ϕ^{ref} [rad]
2.0	1.50	1.00	0.0
All VSC units: r_{ph} = 5e-4 [pu], x_{ph} = 5e-2 [pu] r_{tr}=1.67e-3 [pu], x_{tr}= 5e-2 [pu], P^{max}=3.0 [pu]			

Table 6.18 Parameters of BESS

BESS	*IC* [$]	W^{min}, W^{max} [MWhr]	P^{min}, P^{max} [MW]	*CR*, *DR* [MW/hr]	$\mathbb{Z}'_T$ [hr]	n_c, $\cdot_B$ [cycles],[pu]
1	4.62E+07	192, 960	-40, 40	15, 30	{1-10, 23-24}	10e3, 0.98
2	5.78E+07	240, 1200	-50, 50	20, 40	{1-10, 23-24}	10e3, 0.98

Table 6.19 Parameters of AC/DC transmission system

AC branches	**DC branches**
$Z_{1\text{-}2} = Z_{5\text{-}6} = Z_{9\text{-}10} = Z_{13\text{-}14}$ = 0.03 + j0.15 pu	$r_{20\text{-}21}$ = 0.02085 pu
$Z_{1\text{-}3} = Z_{5\text{-}7} = Z_{9\text{-}11} = Z_{13\text{-}15}$ = 0.035 + j0.20 pu	$r_{21\text{-}22}$ = 0.0278 pu
$Z_{1\text{-}4} = Z_{3\text{-}4} = Z_{6\text{-}8} = Z_{7\text{-}8} = Z_{9\text{-}12} = Z_{11\text{-}12}$ = 0.01 + j0.10 pu	$r_{22\text{-}23}$ = 0.03475pu
$Z_{2\text{-}3} = Z_{6\text{-}7} = Z_{10\text{-}11} = Z_{14\text{-}15}$ = 0.04+ j0.25 pu	$r_{23\text{-}20}$ = 0.0417pu
$\mathbf{y}_{sh}$= j0.2 pu (all lines); $P_{km}^{\max}$ = 3.3 pu	$P_{jm}^{\max}$ = 3.3 pu

Table 6.20 Parameters of generation units

Gen	a_k [$/MW^{2}h]	b_k [$/MWh]	c_k [$/h]	s^{su}, s^{sd} [$]	P^{min}, P^{max} [MW]	*RU*, *RD* [MW/hr]	*UT*, *DT* [hr]
1, 4	0.004	16.50	900	7e3, 3.5e3	40, 400	250, 250	6, 6
2, 3, 8	0.002	16.75	600	4e3, 750	30, 300	175, 175	5, 5
5, 7	0.005	17.50	300	2e3, 1e3	20, 200	125, 125	4, 4
6	0.003	19.22	100	1e3, 500	10, 100	70, 70	2, 2

The generation dispatch of generation units G1 – G8 is shown in Figure 6.20(a). A remarkable case is G8 in area Π which provides power to the system the whole day, with a minimum power of P_{g8} = 1.6 [pu] at 11:00 [hr] and a maximum dispatch of P_{g8} = 2.2 [pu] at 16:00 [hr]. However, G2 only generates power from 14:00 [hr] to 23:00 [hr], while G3 starts producing power from 11:00 [hr] onwards, reaching maximum values of P_{g2} = 0.8 [pu] at 15:00 [hr] and P_{g3} = 2.3 [pu] at 17:00 [hr], respectively. This situation arises from the fact that the power generation by G2 and G3 is more expensive for the system than if it is generated by G8. Therefore, G2 and G3 only generate power as the load increase over time, according to the consumption pattern of Figure 6.19. Another interesting case is G4, pertaining to AC2 that connects to VSC 2 operating in fixed power control mode. Its

generation output increases from P_{g4} = 2.2 [pu] at 09:00 [hr] to P_{g4} = 3.8 [pu] at 15:00 [hr] as the demand increases, this coinciding with the load consumption increase in AC2, as evidenced in Figure 6.19. Notice that G5 is not committed (zero power production) throughout the planning horizon, thus avoiding a more expensive system to operate.

The power flows through the VSC units are also worth discussing, which are shown in Figure 6.20(b). It can be appreciated how the power flows of VSC 2, P_{v2}, and of VSC 3, P_{v3}, are kept constant through the planning horizon. Certainly, this was expected due to the control strategy of both converters, which are responsible for fixing the power exchange between AC and DC sides in 150 [MW] and 100 [MW], i.e., P_{v2} = 1.5 [pu] and P_{v3}=1.0 [pu]. In sharp contrast, the power flow of VSC 1 varies along the day following a similar pattern to that of the system demand variation. This is so because this power converter is charged with DC voltage control, thus compensating the power variations in area Π, i.e., DC grid and AC 4.

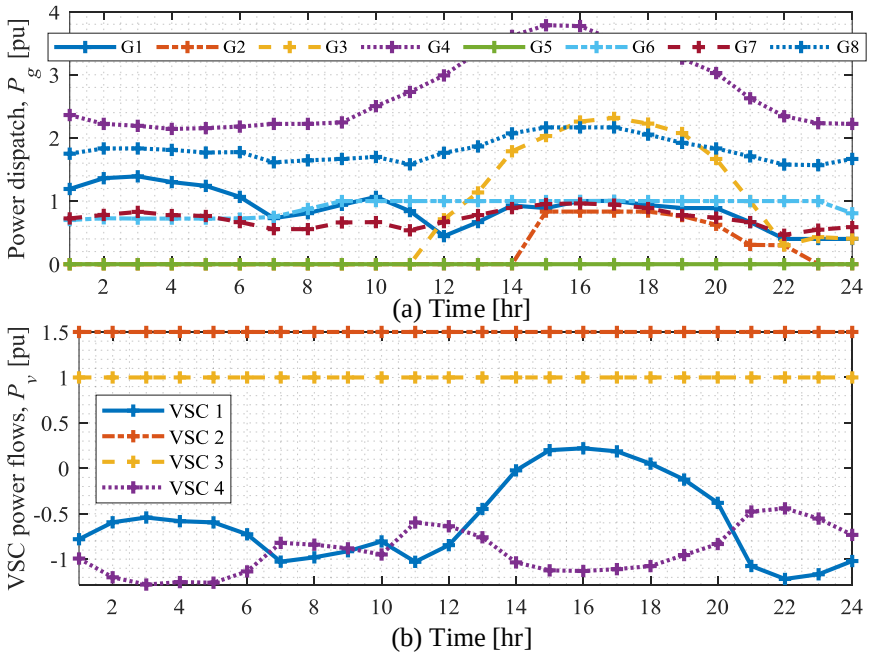

Figure 6.20 (a) Power dispatch of all generation units; (b) VSC power flows

Table 6.21 provides unit commitment schedule of generators, i.e., the on/off statuses for each hour of the day. The UC results can be further corroborated; for instance, G2 was not committed from 1:00 [hr] to 14:00 [hr], as appreciated from the power dispatch of G2 shown in Figure 6.20(a). The same occurs for 23:00 [hr] and 24:00 [hr], where the dispatch

of G2 is zero because it was turned-off by the system's schedule. Another example is G3, whose dispatch level reported in Figure 6.20(a) is zero from 1:00 [hr] to 11:00 [hr], thus coinciding with the off status for the same periods. In summary, it can be appreciated from Table 6.21 how the more expensive generation units are not committed during peak demand hours, which is precisely where BESS units are injecting power to the grid, as explained next.

Table 6.21 Startups and shutdowns of generating units

Unit	**24-hour unit commitment**																							
	1	2	3	4	5	6	7	8	9	10	11	12	13	14	15	16	17	18	19	20	21	22	23	24
G1	1	1	1	1	1	1	1	1	1	1	1	1	1	1	1	1	1	1	1	1	1	1	1	1
G2	0	0	0	0	0	0	0	0	0	0	0	0	0	0	1	1	1	1	1	1	1	1	0	0
G3	0	0	0	0	0	0	0	0	0	0	0	1	1	1	1	1	1	1	1	1	1	1	1	1
G4	1	1	1	1	1	1	1	1	1	1	1	1	1	1	1	1	1	1	1	1	1	1	1	1
G5	0	0	0	0	0	0	0	0	0	0	0	0	0	0	0	0	0	0	0	0	0	0	0	0
G6	1	1	1	1	1	1	1	1	1	1	1	1	1	1	1	1	1	1	1	1	1	1	1	1
G7	1	1	1	1	1	1	1	1	1	1	1	1	1	1	1	1	1	1	1	1	1	1	1	1
G8	1	1	1	1	1	1	1	1	1	1	1	1	1	1	1	1	1	1	1	1	1	1	1	1

Figure 6.21 provides the BESS power injections for the day-ahead planning horizon. As expected, the BESS do operate following the proposed energy time-shifting strategy, i.e., by charging in low demand periods and discharging in peak demand hours, as it was modeled in (5.20) of Subsection5.3. Interestingly, it can be seen how in the first discharge period, at 11:00 [hr], the power injections by both BESS only reach $P_{b1} = 0.3$ [pu] and $P_{b2} = 0.4$ [pu], respectively, which are smaller than their maximum discharge powers, $P_{b1}^{max} = 0.4$ [pu] and $P_{b2}^{max} = 0.5$ [pu]. The reason for this situation is that BESS units are imposed discharging rates *DR*. Another aspect worth remarking is the relationship that exist between the power injection by BESS 2, P_{b2}, and the power flow through VSC 4, P_{v4}, where it is observed how BESS 2 supports the load in AC 4 by reducing the power importation of AC 4 during the discharge periods of this BESS. The above can be confirmed by looking at the power flow of VSC 4 in Figure 6.20(b) due to it does not precisely follow the load pattern variation of AC 4 because of the power demand directly supplied by BESS 2.

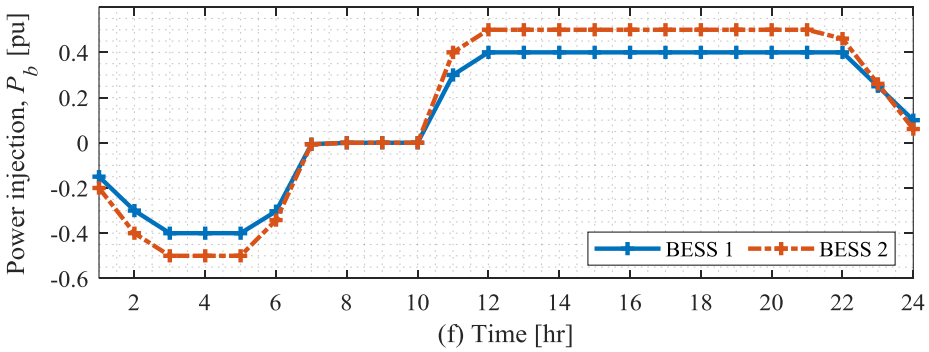

Figure 6.21 BESS power injection

6.3.2. AC/DC system formed by 7 VSC, 70 generators and 5 BESS

The applicability of the developed UC formulation is confirmed using a large-scale VSC-based AC/DC power grid model. This electrical network consists of seven 400-MVA VSC stations, VSC 1 – VSC 7, interfacing seven AC sub-systems with the DC grid, as depicted in Figure 6.22, with each AC power grid containing 10 committable generation units. This AC/DC grid carries the same transmission structure that the one employed in Subsection 6.2.2 to assess the SCOPF algorithm. But now it incorporates five BESS operating with an energy time-shifting strategy, BESS 1 – BESS 5, carrying the power ratings of P_b^{max} = {40, 50, 60, 80, 90} [MW], which are connected to bus 11 in power systems AC 1, 2, 5, 7 and in bus 13 in the DC grid, respectively. The seven VSC units are assigned with the following control strategies: (i) VSC 1, 4, and 7 are responsible of DC voltage control E_{ctrl} by exerting regulation in the DC buses 17, 6, and 3, at E^{ref} = {2.0, 2.0, 2.0} [pu], respectively; (ii) while converters VSC 2, 3, 5, and 6 operate with fixed power control strategies P_{ctrl} with P^{ref} = {150, 100, -150, -300} [MW]. The per-unit DC line resistances are taken from the IEEE RTS 24-bus system [94], by considering that the AC resistances are divided by 4, i.e., $r_{dc} = 0.25 r_{ac}$, whereas the nodal DC loads are assumed to be 40 [%] of the AC loads, i.e., $P_{dc} = 0.4 P_{ac}$.

The parameters related to the system load are taken from [95], for a base power of S_b = 100 MVA, while Figure 6.23 depicts the load pattern variation for the 24-hour operation planning horizon of the UC, for both the DC grid and the seven AC sub-systems. Table 6.22 shows the parameters of the VSC units together with their operating modes, whereas Table 6.23 presents the BESS parameters including the discharge periods, $\mathbb{Z}'_T$, for the day-ahead planning horizon, and Table 6.24 provides the parameters of generation units. In this

case, *ns* = *ls* = 12 linear segments are also considered for the application of the PWL technique is applied to the nonlinear generation cost functions and transmission losses. The planning horizon consists of 24 periods, from 01:00 to 24:00 [hr], $\mathbb{Z}_T$ = {1-24} [hr], using time intervals of 1 hour.

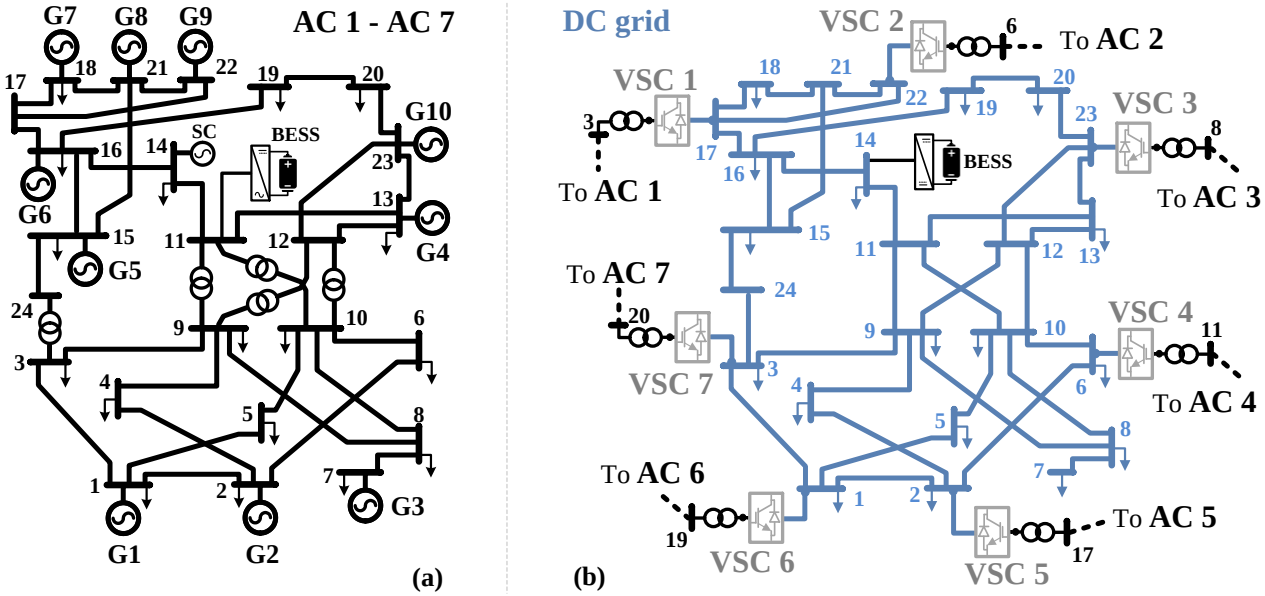

Figure 6.22 Seven-terminal VSC-based HVDC power system with 70 generation units and 5 BESS: (a) AC grids; (b) DC grid

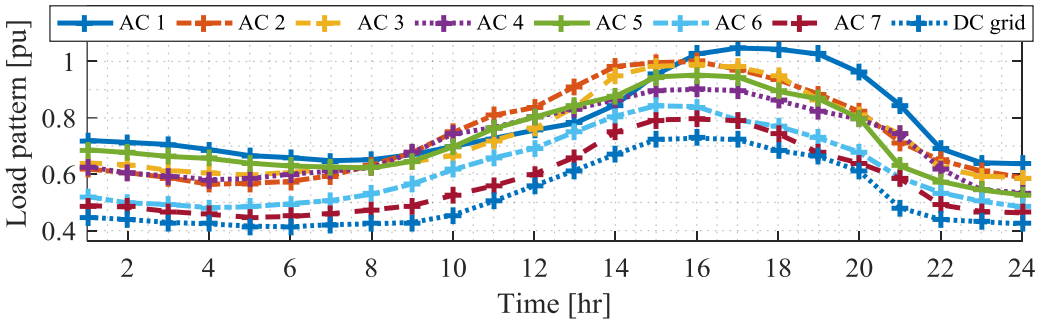

Figure 6.23 Load pattern for the seven-terminal VSC-HVDC test system

Table 6.22 Parameters of VSC stations

VSC 1	VSC 2	VSC 3	VSC 4	VSC 5	VSC 6	VSC 7
E^{ref} [pu]	P^{ref} [pu]	P^{ref} [pu]	E^{ref} [pu]	P^{ref} [pu]	P^{ref} [pu]	E^{ref} [pu]
2.0	1.50	1.00	2.0	-1.50	-3.0	2.0
VSC units: r_{ph}+jx_{ph} = 0.375e-3+j0.0375 [pu]						
r_{tr}+jx_{tr} = 1.25e-3 + j0.0375 [pu], P^{max} = 4.0 [pu]						

Table 6.23 Parameters of BESS

BESS	Grid	Bus	IC [$]	W^{min}, W^{max} [MWhr]	P^{min}, P^{max} [MW]	CR, DR [MW/hr]	$\mathbb{Z}'_T$ [hr]
1	**AC 1**	11	46.2e6	192, 960	-40, 40	10, 30	{1-9, 22-24}
2	**AC 2**	11	57.75e6	240, 1200	-50, 50	20, 35	{1-10, 23-24}
3	**AC 5**	11	69.30e6	288, 1440	-60, 60	24, 44	{1-8, 22-24}
4	**AC 7**	11	92.40e6	384, 1920	-80, 80	35, 50	{1-9, 23-24}
5	**DC**	14	103.95e6	432, 2160	-90, 90	24, 60	{1-8, 22-24}
All BESS facilities: (n_c =10e3 cycles; η_B = 0.98)							

Table 6.24 Parameters of generation units

Gen	a_k [$/MW^{2}h]	b_k [$/MWh]	c_k [$/h]	s^{su}, s^{sd} [$]	P^{min}, P^{max} [MW]	RU, RD [MW/hr]	UT, DT [hr]
1, 2	0.014142	16.0811	212.307	1430, 715	62, 192	120, 120	8, 4
3	0.052672	43.6615	781.521	1725, 862.5	75, 300	300, 300	8, 8
4	0.00717	48.5804	832.757	3056, 1528	206.85, 591	240, 240	12, 10
5	0.008342	12.3883	382.239	500, 250	66.25, 215	215, 215	6, 5
6	0.008342	12.3883	382.239	312, 156	66.25, 215	155, 155	8, 8
7, 8	0.000213	4.4231	395.375	2500, 1250	100, 400	280, 280	1, 1
9	0.00001	0.0001	100.00	100.0, 50.0	0.0, 300	300, 300	1, 1
10	0.004895	11.8495	665.109	2800, 1400	248.5, 660	420, 420	8, 8

The UC algorithm is run considering the previous parameters and operating conditions. Next, the obtained results are discussed, focusing on generation unit dispatches over the operating horizon, VSC power flows, and BESS powers. Figure 6.24(a) presents the calculated output powers of selected generation units for the case when BESS are not in operation, that is, the power produced by the 10 generators of AC 1. On the contrary, Figure 6.24(b) shows the power outputs by the same generators when the BESS are supporting the power system operation while pursuing the energy time-shifting strategy. Very interesting observations can be made from these results, though maybe the most striking situation is what happens with G4. When the BESS are not considered in the power grid, G4 is set to inject a power from 15:00 [hr] onwards, reaching P_{g4} = 5.5 [pu] at 17:00 [hr]. However, when the BESS are included in the system, G4 does not inject power at any moment, i.e., P_{g4} = 0 [pu] for all time periods. This means that G4 is not committed because the UC determines an off status for the 24-hour planning horizon. With this key example, it is shown how the incorporation of BESS reduce the generation dispatch of the more expensive generators, thus helping reduce the overall system operating costs as well.

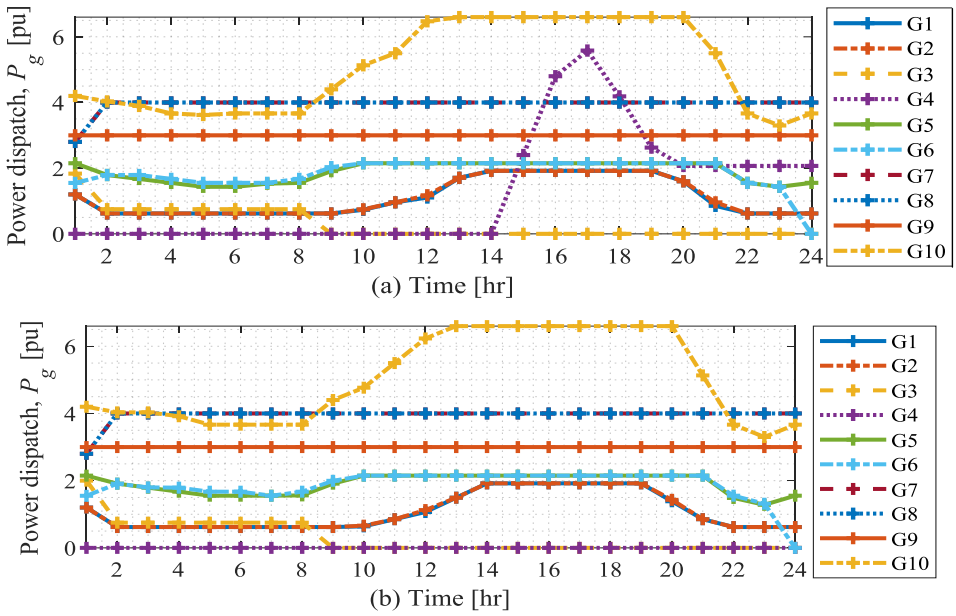

Figure 6.24 UC results for generators in AC 1: (a) without BESS; (b) with BESS

On the other hand, Figure 6.25 shows the BESS operation related to their power delivery towards the electrical network, as established by the corresponding energy time-shifting strategy. In this sense, BESS 3 is the first storage equipment to reach its maximum output power P_{b3} = 0.6 [pu] at 10:00 [hr], whereas BESS 5 is the last device arriving at its maximum power P_{b5} = 0.9 [pu] at 15:00 [hr]. As in the previous case study, it is worth noting that when BESS transit from the charging periods to the discharging ones, these devices do not reach their maximum discharge powers immediately. On the contrary, all BESS begin to discharge at reduced powers due to the discharge rate imposed on the BESS units. Just as important, it is observed anew the relationship between the BESS power injections and generation unit dispatches, where the output power of conventional units is displaced by BESS power injections. In this regard, a remarkable case in point is BESS 1, which reaches its maximum power injection, P_{b1} = 0.4 [pu], from 11:00 [hr] to 21:00 [hr], which coincide with the periods where G4 in AC 1 is not scheduled (off), i.e., P_{g4} = 0 [pu], see Figure 6.24(b). In contrast, when BESS 1 does not operate, G4 is committed from 14:00 [hr] to 24:00 [hr], reaching a maximum dispatch of P_{g4} = 5.5 [pu] at 17:00 [hr], see Figure 6.24(a). The above reaffirms further the fact that BESS avoids a more expensive system operation.

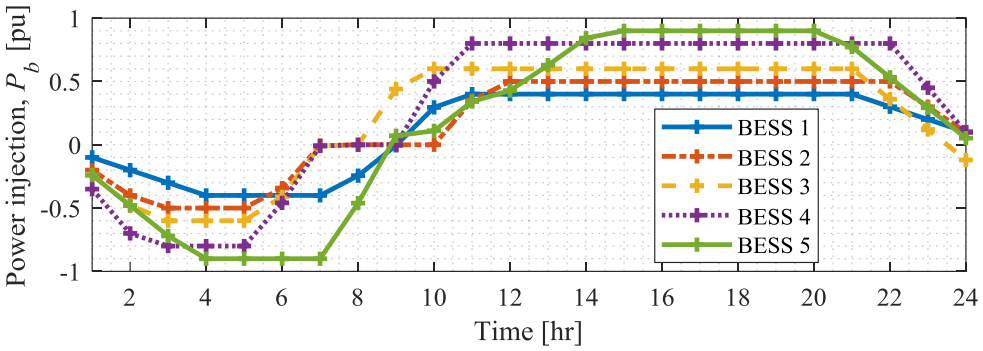

Figure 6.25 Power injections by the BESS for the UC study

Figure 6.26 shows the VSC power flows for both cases, without and with BESS incorporated in the power system, all this for the entire UC planning horizon. It can be clearly observed how incorporating BESS changes the power flows in the VSC stations. A case in point is BESS 5, which locally supplies the load in the DC grid, thus reducing the power flows through VSC 1, VSC 4, and VSC 7, from 10:00 [hr] to 22:00 [hr]. For instance, VSC 1 reduces its maximum power flow from P_{v1} = 2.6 [pu] when there are no BESS units in the power system, to approximately P_{v1} = 2.2 [pu] around 16:00 [hr], when BESS are operating. To a greater or lesser extent, this specific case shows the impact of BESS facilities in the operation of the AC/DC network.

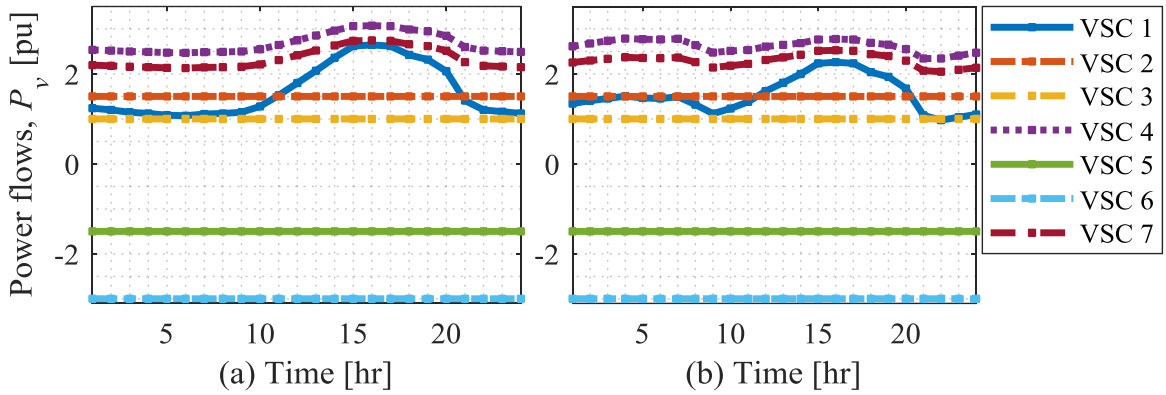

Figure 6.26 VSC power flows: (a) without BESS; (b) with BESS

Chapter 7

7. Conclusions and future research work

New modeling concepts for economic operation problems related to SCED, SCOPF and UC for VSC-based AC/DC power systems were presented in this doctoral thesis, ones considering the inclusion of BESS with two different operating strategies and PV plants. Initially, Chapter 1 presented the literature review of the SCED, SCOPF, and UC problems, also placing emphasis on the modeling of BESS and PV plants for these kinds of power system optimization models. Secondly, Chapter 2 provided the models of all power system components useful for creating VSC-based AC/DC power grid models, which are employed in the rest of chapters. Chapter 3 addressed the SCED model for AC grids with BESS acting with a load-following strategy, whereas Chapter 4 presented the SCOPF model of hybrid AC/DC grids considering the power rescheduling related to droop control response of VSC stations and generation units. Chapter 5, on the other hand, described the UC model for VSC-based AC/DC networks considering BESS operating with energy time-shifting strategy. Finally, case studies were presented in Chapter 6 including the main results associated with the proposed optimization models useful for the three tools employed in the analysis of the power system economic operation. In this sense, this chapter presents the main conclusions of this research. Also, research lines are pointed out as a suggestion for future developments in the economic operation area of electrical grids, especially for the economic operation of AC/DC power systems.

7.1. Conclusions

Nowadays, electrical power systems face several key challenges mainly driven by both the rapid growth in the global population and the increased penetration of renewable generation sources. This situation is leading power networks to operate close to its allowed limits. Due to this, several power systems around the world are being upgraded by the inclusion of VSC-HVDC lines into the traditional AC systems because of the technical benefits inherent

to this transmission technology. By the same token, other vanguard technologies have been gaining attention in modern power grids. This is the case of BESS are also experiencing a massive integration into power grids thanks to its flexible characteristics of charge/discharge operations. In this doctoral thesis, particularly in Chapter 1, the advantages of VSC-based hybrid AC/DC systems are discussed, such as the improvement in reliability, the possibility of creating multi-terminal AC/DC systems, and the reduction of power losses in long transmission systems. Similarly, the benefits obtained by the incorporation of BESS are addressed, such as the possibility of reducing the system operation costs, all this in the framework of the economic operation of AC/DC systems.

Economic operation studies for conventional power systems are carried out by control centers aimed to guarantee the power supply to all loads at a minimum cost, while fulfilling the physical constraints of the transmission network and power plants. In this sense, similar requirements exist for VSC-based AC/DC systems, but with a higher degree of complexity in the mathematical models, thus increasing inevitably the computational times required to execute these analyses. In this respect, it is necessary to adequately handle these computing time issues, whereby the representation of AC/DC systems through linear models is more than suitable to address the economic operation studies for this complex hybrid power networks. As discussed in Chapter 2, with the consideration of nonlinear generation cost curves and transmission losses in the linear optimization modeling framework, it is expected more precision in the outcomes of the economic operation studies, this being precisely one of the main hypotheses formulated for this doctoral thesis.

All the fundamental power equipment models employed in this work were presented in Chapter 2. First, basic principles of the steady-state modeling of AC systems were described, and this was followed by the modeling of AC transmission systems using shift factors. The basic operating principles of VSC devices and nonlinear modeling of these power electronic devices were also presented in this chapter, where the linear modeling of VSC units along with four state-of-the-art control strategies was discussed in this part of the thesis work. In this sense, the nonlinear and linear models of DC systems was also paid attention, placing emphasis on the modeling of comprehensive VSC-based AC/DC models through shift factors, and to complete the modeling, the application of the PWL technique to linearize the effects of the AC/DC power losses, thermal generation units, and PV plants

was also discussed in detail. Just as important, in this chapter the modeling of BESS with load-following and energy time-shifting strategies was given a great deal of attention. All aspects considered, all these fundamentals served as the starting point for the development of the SCED, SCOPF, and UC models addressed in subsequent chapters.

In this sense, Chapter 3 focused on describing a novel, generalized SCED model considering BESS featuring a load-following strategy and PV plants. The developed model is completely featured by linear programming, where the nonlinear cost functions of generation units and AC transmission losses are considered through the PWL method. This SCED framework proposed in this doctoral thesis allows to calculate the generation dispatch for the conventional generation units, where the BESS power generation governed by load-following strategy are also obtained. The outcomes obtained with the study cases enabled the corroboration of the initial hypothesis where BESS featuring a load-following strategy helps the power system reducing the operating costs and relaxing the ramp requirements of thermal generations, aspects that were verified later in Chapter 6 which presents the case studies associated with the introduced SCED model.

Chapter 4, on the other hand, concentrates on describing an advanced corrective SCOPF model for VSC-based hybrid AC/DC power systems, where voltage/power droop control of generation units and VSC devices are both considered. The developed method is entirely based on a linear programming optimization framework. The nonlinear characteristics of AC/DC transmission losses and generation cost curves are also considered by the application of the PWL technique. The SCOPF method presented in this thesis enables the obtention of power generation dispatches and VSC power flows in view of N-1 contingency analysis, where generation/load disconnections, VSC outages, or AC/DC branches contingencies can be assessed with the developed formulation. Indeed, the proposed SCOPF algorithm is comprehensive and flexible; it enables the accommodation of several VSC stations with different state-of-the-art control strategies. In this regard, the results obtained with the study cases confirm the initial hypothesis that the inclusion of voltage/power droop control of power plants and VSC stations improves the network response as a corrective action after a contingency, an aspect that was confirmed later in Chapter 6 through study cases.

The last economic operation model developed in this thesis was presented in Chapter 5, which describes an innovative UC model for VSC-based AC/DC systems. BESS operating with an energy time-shifting strategy were considered in the UC formulation, where the charge and discharge periods are defined according to the load pattern of the power system. The developed model is featured by a mixed-integer linear programming framework. Just like in the case of SCED and SCOPF models, this UC model incorporates the nonlinear generation cost functions and the AC/DC transmission losses through the application of the PWL technique, where shift factors were employed to represent the transmission grid. This new UC model enabled the determination of the on/off statuses of the committable generation units, along with the power scheduled for each generator for the day ahead. Likewise, the UC model permits to suitably calculate the BESS powers (injection/absorption) for the same planning horizon. The results obtained with the case studies allowed to confirm the initial hypothesis formulated in this thesis. That is to say, the inclusion of BESS with energy time-shifting strategy reduces the operation of the more expensive generation units of the power system. This aspect was verified in Chapter 6 through the evaluation of two study cases.

The case studies evaluated in this thesis were presented in Chapter 6. Initially, two case studies related to the SCED model were presented. The first SCED case was a modified version of the IEEE RTS 24-bus test system to conceptually analyze the developed model. The second case study corresponded to a modified version of the IEEE 300-bus test system to show the applicability of the SCED model to fair-sized power grids. The results obtained showed how the BESS integration reduces the system operating costs, with a total reduction, over the operating horizon, of 2.3% in the first case and 2.9 % in the second case. Here, it was also discussed that, when BESS are included in the system, there is a reduction in the ramping requirements of conventional generation units. Subsequently, two test systems related to the corrective SCOPF model were evaluated. The first case study corresponded to a small four-terminal VSC-based AC/DC system, while in the second case a larger hybrid power system formed by seven-terminal VSC-HVDC transmission grid was analyzed. The results obtained for these test systems confirmed the SCOPF applicability; it was shown that the voltage/power droop control of generation units and VSC provide a corrective action in post-contingency states. Finally, two case studies related to the

developed UC formulation including BESS units were analyzed in Chapter 6 to show its usefulness. The obtained results permitted to show how the BESS incorporation obeys the energy time-shifting strategy, charging in low demand periods and discharging in the peak demand conditions, which stimulate a high competition level of energy trading in the hybrid network.

Having finalized this doctoral project, it is important to verify if the four hypotheses initially formulated in Chapter 1, Section 1.3, were fulfilled. This is stated below,

i. The inclusion of linearized generation cost curves and power losses does improve the efficiency of the optimization models, also producing accurate results.

ii. When the operation of the network includes BESS with a load-following strategy, the SCED yields smaller operation costs, compared with the case when the power grid does not include BESS. This aspect was corroborated in Subsection 6.1.

iii. The consideration of voltage/power droop controls for VSC stations and generation units allowed the AC/DC system to respond adequately against N-1 contingencies, especially to those altering the balance between generation and load. This aspect was corroborated in Subsection 6.2.

iv. As discussed in Subsection 6.3, when BESS operate with an energy time-shifting strategy, the operation costs of the AC/DC systems are reduced compared to when the hybrid power does not contain BESS units.

It can be finally concluded that the application of linear models to economic operation optimization problems for hybrid AC/DC power systems is very attractive. The formulations developed of SCED, SCOPF and UC were implemented in a generalized manner, thus enabling the modeling of complex power systems, with a variety of operating conditions. The tools developed in this doctoral thesis may be of actual interest for TSO dealing with the economic operation of modern hybrid power grids.

7.2. Future research work

The applicability of the SCED, SCOPF, and UC models put forward in this research work has been demonstrated by using the algorithms to solve fair-sized power networks. It should be expected that due to the increased installation of VSC-HVDC lines and BESS,

some additional requirements may arise in the context of the planning and operation of hybrid AC/DC grids. For instance:

- The development of Generation Expansion Planning (GEP) models for VSC-based hybrid grids, considering BESS and PV plants. This aspect goes in line with the need for counting on appropriate tools to determine optimal investments in generation assets, especially considering massive penetrations of renewable generation sources.
- The development of Transmission Expansion Planning (TEP) models for VSC-based hybrid grids, including BESS, considering HVDC lines and renewable sources. This is so because of the need for adequately assessing the investment in transmission assets as it is the backbone for the adequate growth of AC/DC power systems.
- Due to the close relationship between the commissioning of new power plants and transmission lines, another timely future research topic would be a joint Generation/Transmission Expansion Planning model (GTEP) for hybrid power grids, considering the BESS charge/discharge operations related to practical control strategies.

References

[1] Acha, E., Roncero-Sánchez, P., de la Villa-Jaen, A., Castro, L. M., & Kazemtabrizi, B. (2019). *VSC-FACTS-HVDC: Analysis, modelling and simulation in power grids*. John Wiley & Sons.

[2] Alassi, A., Bañales, S., Ellabban, O., Adam, G., & MacIver, C. (2019). HVDC transmission: Technology review, market trends and future outlook. *Renewable and Sustainable Energy Reviews*, 112, 530-554.

[3] Wang, W., Li, G., & Guo, J. (2022). Large-scale renewable energy transmission by HVDC: Challenges and proposals. *Engineering*.

[4] Luo, X., Wang, J., Dooner, M., & Clarke, J. (2015). Overview of current development in electrical energy storage technologies and the application potential in power system operation. *Applied energy*, *137*, 511-536.

[5] Argyrou, M. C., Christodoulides, P., & Kalogirou, S. A. (2018). Energy storage for electricity generation and related processes: Technologies appraisal and grid scale applications. *Renewable and Sustainable Energy Reviews*, *94*, 804-821.

[6] Farivar, G. G., Manalastas, W., Tafti, H. D., Ceballos, S., Sánchez-Ruiz, A., Lovell, E. C., ... & Pou, J. (2022). Grid-connected energy storage systems: state-of-the-art and emerging technologies. *Proceedings of the IEEE*.

[7] Al-Shetwi, A. Q., Hannan, M. A., Jern, K. P., Mansur, M., & Mahlia, T. M. I. (2020). Grid-connected renewable energy sources: Review of the recent integration requirements and control methods. *Journal of Cleaner Production*, *253*, 119831.

[8] Ulbig, A., Borsche, T. S., & Andersson, G. (2014). Impact of low rotational inertia on power system stability and operation. *IFAC Proceedings Volumes*, *47*(3), 7290-7297.

[9] American Council on Renewable Energy – ACORE (2016), "Beyond Renewable Integration: The Energy Storage Value Proposition", ACORE – Washington DC 20006, 202.393.0001, 1-36.

[10] Cole, W. J., & Frazier, A. (2019). *Cost projections for utility-scale battery storage* (No. NREL/TP-6A20-73222). National Renewable Energy Lab. (NREL), Golden, CO (United States).

[11] Chen, H. (Ed.). (2016). *Power grid operation in a market environment: economic efficiency and risk mitigation*. John Wiley & Sons.

[12] Ma, Y., Hao, Y., Zhao, S., & Bi, H. (2017). Security constrained economic dispatch of wind-integrated power system considering optimal system state selection. *IET Generation, Transmission & Distribution*, *11*(1), 27-36.

[13] Safdarian, F., Mohammadi, A., Kargarian, A., & Falahati, B. (2020, February). Partitioning analysis in temporal decomposition for security-constrained economic dispatch. In *2020 IEEE Texas Power and Energy Conference (TPEC)* (pp. 1-6). IEEE.

[14] Safdarian, F., & Kargarian, A. (2019). Time decomposition strategy for security-constrained economic dispatch. *IET Generation, Transmission & Distribution*, *13*(22), 5129-5138.

[15] Zare, M., Narimani, M. R., Malekpour, M., Azizipanah-Abarghooee, R., & Terzija, V. (2021). Reserve constrained dynamic economic dispatch in multi-area power systems: An improved fireworks algorithm. *International Journal of Electrical Power & Energy Systems*, *126*, 106579.

[16] Yu, Y., & Luh, P. (2018). Scalable corrective security-constrained economic dispatch considering conflicting contingencies. *International Journal of Electrical Power & Energy Systems*, *98*, 269-278.

[17] Liu, Y., Ferris, M. C., & Zhao, F. (2014). Computational study of security constrained economic dispatch with multi-stage rescheduling. *IEEE Transactions on Power Systems*, *30*(2), 920-929.

[18] Javadi, M., Amraee, T., & Capitanescu, F. (2019). Look ahead dynamic security-constrained economic dispatch considering frequency stability and smart loads. *International Journal of Electrical Power & Energy Systems*, *108*, 240-251.

[19] Yang, Q., Ding, T., Ma, W., Zhang, H., Jia, Z., Tian, W., & Cao, Y. (2017, November). Decentralized security-constrained economic dispatch for global energy Internet and practice in northeast Asia. In *2017 IEEE Conference on Energy Internet and Energy System Integration (EI2)* (pp. 1-6). IEEE.

[20] Lu, X., Chan, K. W., Xia, S., Zhou, B., & Luo, X. (2018). Security-constrained multiperiod economic dispatch with renewable energy utilizing distributionally robust optimization. *IEEE Transactions on Sustainable Energy*, *10*(2), 768-779.

[21] Zhang, G., McCalley, J., & Wang, Q. (2019). An AGC dynamics-constrained economic dispatch model. *IEEE Transactions on Power Systems*, *34*(5), 3931-3940.

[22] Garcia, M., & Baldick, R. (2019). Approximating economic dispatch by linearizing transmission losses. *IEEE Transactions on Power Systems*, *35*(2), 1009-1022.

[23] Pöschel-LØvengreen, S., & Mancarella, P. (2018, June). Frequency response constrained economic dispatch with consideration of generation contingency size. In *2018 Power Systems Computation Conference (PSCC)* (pp. 1-7). IEEE.

[24] Dehghani Filabadi, M., & Pirooz Azad, S. (2020). Robust optimisation framework for SCED problem in mixed AC-HVDC power systems with wind uncertainty. *IET Renewable Power Generation*, *14*(14), 2563-2572.

[25] Van Horn, K. E., Domínguez-García, A. D., & Sauer, P. W. (2015). Measurement-based real-time security-constrained economic dispatch. *IEEE Transactions on Power Systems*, *31*(5), 3548-3560.

[26] Li, G., Zhang, R., Jiang, T., Chen, H., Bai, L., & Li, X. (2017). Security-constrained bi-level economic dispatch model for integrated natural gas and electricity systems considering wind power and power-to-gas process. *Applied energy*, *194*, 696-704.

[27] Dehghani Filabadi, M., & Pirooz Azad, S. (2020). Robust optimisation framework for SCED problem in mixed AC-HVDC power systems with wind uncertainty. *IET Renewable Power Generation*, *14*(14), 2563-2572.

[28] Gu, N., Wang, H., Zhang, J., & Wu, C. (2021). Bridging chance-constrained and robust optimization in an emission-aware economic dispatch with energy storage. *IEEE Transactions on Power Systems*, *37*(2), 1078-1090.

[29] Cheng, J., Chen, R. L. Y., Najm, H. N., Pinar, A., Safta, C., & Watson, J. P. (2018). Chance-constrained economic dispatch with renewable energy and storage. *Computational Optimization and Applications*, *70*(2), 479-502.

[30] Xing, H., Lin, Z., Fu, M., & F. Hobbs, B. (2017). Distributed algorithm for dynamic economic power dispatch with energy storage in smart grids. *IET Control Theory & Applications*, *11*(11), 1813-1821.

[31] Gil-González, W., Montoya, O. D., Holguín, E., Garces, A., & Grisales-Noreña, L. F. (2019). Economic dispatch of energy storage systems in dc microgrids employing a semidefinite programming model. *Journal of Energy Storage*, *21*, 1-8.

[32] Gbadamosi, S. L., & Nwulu, N. I. (2021). A comparative analysis of generation and transmission expansion planning models for power loss minimization. *Sustainable Energy, Grids and Networks*, *26*, 100456.

[33] Feng, W., Tjernberg, L. B., Mannikoff, A., & Bergman, A. (2013). A new approach for benefit evaluation of multiterminal VSC–HVDC using a proposed mixed AC/DC optimal power flow. *IEEE Transactions on Power Delivery*, *29*(1), 432-443.

[34] Capitanescu, F., Ramos, J. M., Panciatici, P., Kirschen, D., Marcolini, A. M., Platbrood, L., & Wehenkel, L. (2011). State-of-the-art, challenges, and future trends in security constrained optimal power flow. *Electric power systems research*, *81*(8), 1731-1741.

[35] Dvorkin, Y., Henneaux, P., Kirschen, D. S., & Pandžić, H. (2016). Optimizing primary response in preventive security-constrained optimal power flow. *IEEE Systems Journal*, *12*(1), 414-423.

[36] Velay, M., Vinyals, M., Besanger, Y., & Retière, N. (2019). Fully distributed security constrained optimal power flow with primary frequency control. *International Journal of Electrical Power & Energy Systems*, *110*, 536-547.

[37] Avramidis, I. I., Capitanescu, F., Karagiannopoulos, S., & Vrettos, E. (2020). A novel approximation of security-constrained optimal power flow with incorporation of generator frequency and voltage control response. *IEEE Transactions on Power Systems*, *36*(3), 2438-2447.

[38] Sharifzadeh, H., & Amjady, N. (2016). Stochastic security-constrained optimal power flow incorporating preventive and corrective actions. *International Transactions on Electrical Energy Systems*, *26*(11), 2337-2352.

[39] Roald, L., Vrakopoulou, M., Oldewurtel, F., & Andersson, G. (2015). Risk-based optimal power flow with probabilistic guarantees. *International journal of electrical power & energy systems*, *72*, 66-74.

[40] Mohammadi, J., Hug, G., & Kar, S. (2016). Agent-based distributed security constrained optimal power flow. *IEEE Transactions on Smart Grid*, *9*(2), 1118-1130.

[41] Cao, J., Du, W., & Wang, H. F. (2015). An improved corrective security constrained OPF with distributed energy storage. *IEEE Transactions on Power Systems*, *31*(2), 1537-1545.

[42] Wu, X., & Conejo, A. J. (2019). Security-constrained ACOPF: Incorporating worst contingencies and discrete controllers. *IEEE Transactions on Power Systems*, *35*(3), 1936-1945.

[43] Hinojosa, V. H. (2020). Comparing corrective and preventive security-constrained DCOPF problems using linear shift-factors. *Energies*, *13*(3), 516.

[44] Ardakani, A. J., & Bouffard, F. (2013). Identification of umbrella constraints in DC-based security-constrained optimal power flow. *IEEE Transactions on Power Systems*, *28*(4), 3924-3934.

[45] Xu, Y., Hu, J., Gu, W., Su, W., & Liu, W. (2016). Real-time distributed control of battery energy storage systems for security constrained DC-OPF. *IEEE Transactions on Smart Grid*, *9*(3), 1580-1589.

[46] Correa-Posada, C. M., & Sánchez-Martín, P. (2014). Security-constrained optimal power and natural-gas flow. *IEEE Transactions on Power Systems*, *29*(4), 1780-1787.

[47] Wiget, R., Vrakopoulou, M., & Andersson, G. (2014, August). Probabilistic security constrained optimal power flow for a mixed HVAC and HVDC grid with stochastic infeed. In *2014 Power Systems Computation Conference* (pp. 1-7). IEEE.

[48] Sennewald, T., Sass, F., & Westermann, D. (2017). A preventive security constrained optimal power flow for mixed AC-HVDC-systems.

[49] Cao, J., Du, W., & Wang, H. F. (2015). An improved corrective security constrained OPF for meshed AC/DC grids with multi-terminal VSC-HVDC. *IEEE Transactions on Power Systems*, *31*(1), 485-495.

[50] Meng, K., Zhang, W., Li, Y., Dong, Z. Y., Xu, Z., Wong, K. P., & Zheng, Y. (2017). Hierarchical SCOPF considering wind energy integration through multiterminal VSC-HVDC grids. *IEEE Transactions on Power Systems*, *32*(6), 4211-4221.

[51] Li, Y., & Li, Y. (2019). Security-constrained multi-objective optimal power flow for a hybrid AC/VSC-MTDC system with lasso-based contingency filtering. *IEEE Access*, *8*, 6801-6811.

[52] Zhang, H., Vittal, V., Heydt, G. T., & Quintero, J. (2011). A mixed-integer linear programming approach for multi-stage security-constrained transmission expansion planning. *IEEE Transactions on Power Systems*, *27*(2), 1125-1133.

[53] Anjos, M. F., & Conejo, A. J. (2017). Unit commitment in electric energy systems. *Foundations and Trends® in Electric Energy Systems*, *1*(4), 220-310.

[54] Morales-España, G., Latorre, J. M., & Ramos, A. (2013). Tight and compact MILP formulation for the thermal unit commitment problem. *IEEE Transactions on Power Systems*, *28*(4), 4897-4908.

[55] Howlader, H. O. R., Adewuyi, O. B., Hong, Y. Y., Mandal, P., Mohamed Hemeida, A., & Senjyu, T. (2019). Energy storage system analysis review for optimal unit commitment. *Energies*, *13*(1), 158.

[56] Pozo, D., Contreras, J., & Sauma, E. E. (2014). Unit commitment with ideal and generic energy storage units. *IEEE Transactions on Power Systems*, *29*(6), 2974-2984.

[57] Tejada-Arango, D. A., Sánchez-Martın, P., & Ramos, A. (2017). Security constrained unit commitment using line outage distribution factors. *IEEE Transactions on power systems*, *33*(1), 329-337.

[58] Bahrami, S., & Wong, V. W. (2017). Security-constrained unit commitment for ac-dc grids with generation and load uncertainty. *IEEE Transactions on Power Systems*, *33*(3), 2717-2732.

[59] Zhou, B., Ai, X., Fang, J., Yao, W., Zuo, W., Chen, Z., & Wen, J. (2019). Data-adaptive robust unit commitment in the hybrid AC/DC power system. *Applied Energy*, *254*, 113784.

[60] Isuru, M., Hotz, M., Gooi, H. B., & Utschick, W. (2020). Network-constrained thermal unit commitment for hybrid AC/DC transmission grids under wind power uncertainty. *Applied Energy*, *258*, 114031.

[61] Fu, Y., Wang, C., Tian, W., & Shahidehpour, M. (2015). Integration of large-scale offshore wind energy via VSC-HVDC in day-ahead scheduling. *IEEE Transactions on Sustainable Energy*, *7*(2), 535-545.

[62] Li, N., Uckun, C., Constantinescu, E. M., Birge, J. R., Hedman, K. W., & Botterud, A. (2015). Flexible operation of batteries in power system scheduling with renewable energy. *IEEE Transactions on Sustainable Energy*, *7*(2), 685-696.

[63] Luburić, Z., & Pandžić, H. (2019). FACTS devices and energy storage in unit commitment. *International Journal of Electrical Power & Energy Systems*, *104*, 311-325.

[64] Ahmadi, A., Nezhad, A. E., & Hredzak, B. (2018). Security-constrained unit commitment in presence of lithium-ion battery storage units using information-gap decision theory. *IEEE Transactions on Industrial Informatics*, *15*(1), 148-157.

[65] Wen, Y., Guo, C., Pandžić, H., & Kirschen, D. S. (2015). Enhanced security-constrained unit commitment with emerging utility-scale energy storage. *IEEE Transactions on power Systems*, *31*(1), 652-662.

[66] Jiang, S., Gao, S., Pan, G., Zhao, X., Liu, Y., Guo, Y., & Wang, S. (2020). A novel robust security constrained unit commitment model considering HVDC regulation. *Applied Energy*, *278*, 115652.

[67] Li, L., Huan, J., Zhou, Y., & Chen, Z. (2019, May). Security Constrained Unit Commitment Model for AC/DC Interconnected System. In *2019 IEEE Innovative Smart Grid Technologies-Asia (ISGT Asia)* (pp. 520-524). IEEE.

[68] Lotfjou, A., Shahidehpour, M., Fu, Y., & Li, Z. (2009). Security-constrained unit commitment with AC/DC transmission systems. *IEEE Transactions on power systems*, *25*(1), 531-542.

[69] Zhou, M., Zhai, J., Li, G., & Ren, J. (2017). Distributed dispatch approach for bulk AC/DC hybrid systems with high wind power penetration. *IEEE Transactions on Power Systems*, *33*(3), 3325-3336.

[70] Guerrero-Mestre, V., Dvorkin, Y., Fernández-Blanco, R., Ortega-Vázquez, M. A., & Contreras, J. (2018). Incorporating energy storage into probabilistic security-constrained unit commitment. *IET Generation, Transmission & Distribution*, *12*(18), 4206-4215.

[71] Álvarez, G. E., Marcovecchio, M. G., & Aguirre, P. A. (2018). Security-constrained unit commitment problem including thermal and pumped storage units: An MILP formulation by the application of linear approximations techniques. *Electric Power Systems Research*, *154*, 67-74.

[72] Ahmadi, A., Nezhad, A. E., Siano, P., Hredzak, B., & Saha, S. (2019). Information-gap decision theory for robust security-constrained unit commitment of joint

renewable energy and gridable vehicles. *IEEE Transactions on Industrial Informatics*, *16*(5), 3064-3075.

[73] Jiang, M., Guo, Q., Sun, H., & Ge, H. (2020). Short-Term Voltage Stability-Constrained Unit Commitment for Receiving-End Grid With Multi-Infeed HVDCs. *IEEE Transactions on Power Systems*, *36*(3), 2603-2613.

[74] Zhang, N., Wu, S., An, H., & Zhu, X. (2020). Security-Constraint Unit Commitment for AC/DC Transmission Systems with Voltage Stability Constraint. *Journal of Electrical Engineering & Technology*, *15*(6), 2459-2469.

[75] Kërçi, T., Giraldo, J., & Milano, F. (2020). Analysis of the impact of sub-hourly unit commitment on power system dynamics. *International Journal of Electrical Power & Energy Systems*, *119*, 105819.

[76] Mirzaei, M. A., Yazdankhah, A. S., & Mohammadi-Ivatloo, B. (2019). Stochastic security-constrained operation of wind and hydrogen energy storage systems integrated with price-based demand response. *International Journal of Hydrogen Energy*, *44*(27), 14217-14227.

[77] Grainger, J. J., & Stevenson, W. D. (1994). Power Systems Analysis McGraw-Hill. *New York*.

[78] Wood, A. J., Wollenberg, B. F., & Sheblé, G. B. (2013). *Power generation, operation, and control (2nd edition)*. John Wiley & Sons.

[79] Saadat, H. (2009). Power system analysis, (2nd). *McGraw-Hill Higher Education*.

[80] Elgerd, O.I. (1982) Electric Energy Systems Theory: An introduction. *McGraw-Hill: New York, NY, USA*.

[81] González-Cabrera, N., Castro, L. M., Gutiérrez-Alcaraz, G., & Tovar-Hernández, J. H. (2021). Alternative approach for efficient OPF calculations in hybrid AC/DC power grids with VSC-HVDC systems based on shift factors. *International Journal of Electrical Power & Energy Systems*, *124*, 106395.

[82] Yazdani, A., & Iravani, R. (2010). *Voltage-sourced converters in power systems: modeling, control, and applications*. John Wiley & Sons.

[83] Castro, L. M. (2016). Modelling of multi-terminal VSC-HVDC links for power flows and dynamic simulations of AC/DC power networks. Doctoral dissertation, PhD Thesis, Tampere university of technology, Finland, 2016.
Available at: https://tutcris. tut. fi/portal/en/publications/modelling-of-multiterminal-vschvdc-links-for-power-flowsand-dynamic-simulations-of-acdc-power-networks (a5fad7ff-c96f-4460-8f32-4394fc19328f). html).

[84] Álvarez-Romero, G., Castro, L. M., & Roncero-Sánchez, P. (2020). Effective sensitivity-based method for N-1 contingency analysis of VSC-based MTDC power

grids considering power generation droop speed controls. *International Journal of Electrical Power & Energy Systems*, *122*, 106175.

[85] Guzmán-Feria, J. S., Castro, L. M., González-Cabrera, N., & Tovar-Hernández, J. H. (2021). Security constrained OPF for AC/DC systems with power rescheduling by power plants and VSC stations. *Sustainable Energy, Grids and Networks*, 27, 100517.

[86] Guzmán-Feria, J. S., Castro, L. M., Tovar-Hernández, J. H., González-Cabrera, N., & Gutiérrez-Alcaraz, G. (2022). Unit commitment for multi-terminal VSC-connected AC systems including BESS facilities with energy time-shifting strategy. *International Journal of Electrical Power & Energy Systems*, 134, 107367.

[87] Castro, L. M., Acha, E., & Rodriguez-Rodriguez, J. R. (2018). Efficient method for the real-time contingency analysis of meshed HVDC power grids fed by VSC stations. *IET Generation, Transmission & Distribution*, *12*(13), 3158-3166.

[88] Bradley, S. P., Hax, A. C., & Magnanti, T. L. (1977). *Applied mathematical programming*. Addison-Wesley.

[89] Cheng, D., Mather, B. A., Seguin, R., Hambrick, J., & Broadwater, R. P. (2015). Photovoltaic (PV) impact assessment for very high penetration levels. *IEEE Journal of photovoltaics*, *6*(1), 295-300.

[90] Castro, L. M., Rodríguez-Rodríguez, J. R., & Martin-del-Campo, C. (2020). Modelling of PV systems as distributed energy resources for steady-state power flow studies. *International Journal of Electrical Power & Energy Systems*, *115*, 105505.

[91] Guerra, O. J. (2021). Beyond short-duration energy storage. *Nature Energy*, *6*(5), 460-461.

[92] Kundur, P. S., & Malik, O. P. (2022). *Power system stability and control*. McGraw-Hill Education.

[93] Castro, L. M., González-Cabrera, N., Hernández-Amador, L. E., & Guzmán-Feria, J. S. (2022). Innovative Unit Commitment Modeling Approach Considering Multi-infeed VSC-HVDC Links. *Electric Power Components and Systems*, 916-930.

[94] Grigg, C., Wong, P., Albrecht, P., Allan, R., Bhavaraju, M., Billinton, R., ... & Singh, C. (1999). The IEEE reliability test system-1996. A report prepared by the reliability test system task force of the application of probability methods subcommittee. *IEEE Transactions on power systems*, *14*(3), 1010-1020.

[95] Peyghami, S., Davari, P., Fotuhi-Firuzabad, M., & Blaabjerg, F. (2019). Standard test systems for modern power system analysis: An overview. *IEEE Industrial Electronics Magazine*, *13*(4), 86-105.